The Development of a Biofuels Engine Testing Facility

by

Duncan Palmer

Thesis submitted in fulfilment of the requirements for the Degree
of

MASTER OF SCIENCE IN ENGINEERING
(CHEMICAL ENGINEERING)
in the Department of Process Engineering
at Stellenbosch University

Supervised by
Leon Lorenzen (Process Engineering)
Johan van der Spuy (Mechanical and Mechatronic Engineering)

DECEMBER 2008

Declaration

By submitting this thesis electronically, I declare that the entirety of the work contained therein is my own, original work, that I am the owner of the copyright thereof (unless to the extent explicitly otherwise stated) and that I have not previously in its entirety or in part submitted it for obtaining any qualification.

Date: 22 December 2008

Copyright © 2008 Stellenbosch University
All rights reserved

Abstract

This report covers the development of a biofuels engine testing facility at Stellenbosch University. The motivation for the project was three fold: a) a desire to establish biofuels and engine testing know-how; b) to test the performance characteristics of biodiesel; and c) make a facility available for future research. The two main conclusions drawn from the initial test results are: 1) the test cell is fully operational and 2) biodiesel can be substituted for mineral diesel. To the author's knowledge this is the first biofuel specific engine testing facility in South Africa.

After a literature study the test cell was realised in three phases.

- Firstly, the hardware layout was designed and the necessary equipment was sourced from respectable suppliers including the judicious use of good qaulity second hand components to minimize capital cost.
- The test cell was then instrumented with new sensors. Key components among these are the K-type thermocouples, barometric pressure, humidity, oil pressure and an Allen-Bradley programmable controller to serve as a data acquisition card. Two software programs were chosen, ETA for the control of the test cell and RSLogix to program the programmable logic controller (PLC).
- The complete system was then integrated, debugged and validated.

The design methods and procedures have been documented throughout the project along with user manuals to facilitate further research.

To determine the difference in combustion parameters between biodiesel and mineral diesel an autonomous power curve test was conducted. This revealed little difference in terms of performance between the two fuels, although biodiesel had on average a marginal 0.4% decrease in power over mineral diesel. The fuel consumption for pure biodiesel was found to be higher, which is as expected as it is has a lower calorific value than mineral diesel.

As a final validation, an energy balance was conducted. Here the calculated calorific value of biodiesel was compared to the results from a calorie bomb test, and the two results were found to be within 2% of each of other.

Opsomming

Hierdie tesis handel oor die ontwikkeling van ‘n biobrandstof-enjintoetsfasiliteit by die Universiteit van Stellenbosch. Die motivering agter die projek was drieledig: a) ‘n behoefte aan kennis rakende biobrandstof en enjin proefneming; b) die toets van biobrandstof uitvoerbaarheid; c) die beskikbaarstelling van ‘n fasiliteit vir toekomstige navorsing. Twee hoof gevolgtrekkings kan van die aanvanklike toetsresultate gemaak word: 1) die toetssel is volledige bedryfbaar en 2) mineraaldiesel kan met biodiesel vervang word. Volgens die outeur se kennis is dit die eerste biobrandstof-enjintoetsfasiliteit in Suid Afrika.

Na ‘n literatuuroorsig was die toetssel in drie fases ontwikkel:

- Eerstens was die hardeware uitleg ontwerp en die nodige toerusting van die onderskeie verskaffers bekom terwyl goeie kwaliteit tweehandse komponente oordeelkundig gebruik is om kapitaalkoste te sny.
- Die toetssel was daarna toegerus met instrumentasie sensors. Die hoofkomponente was die K-tipe termokoppels, barometriese druk, humiditeits-en olie-druk sensors en ‘n Allen-Bradley programmeerbare beheerder wat het gedien het as ‘n data-insamelingskaart. Twee sagteware programme was gebruik, ETA vir die beheer van die toetssel en RSLogic vir die programmering van die programmeerbare logiese beheerder (PLC).
- Die volledige sisteem was daarna geïntegreer, foute gekorrigeer en die sisteem gevalideer.

Die ontwerps metode agter die ontwerp en prosedures is voordurent gedokumenteer asook handleidings om toekomstige navorsing moontlik te maak.

‘n Selfregulerende werkverrigtingskurwe toets was bewerkstellig om die verskil tussen biodiesel en mineraaldiesel verbrandingsparameters vas te stel. ‘n Klein verskil in terme van werkverrigting was waargeneem tussen die twee brandstowwe, met biodiesel wat ‘n gemiddelde afname van 0.4% in werkverrigting teen oor mineraaldiesel vertoon het. Die brandstofverbruik vir suiwer biodiesel was hoër, soos wat verwag sal word aangesien dit ‘n laer kaloriese waarde het in vergelyking met mineraaldiesel.

‘n Energiebalans was uitgevoer as finale validasie. Hiermee was die berekende kaloriesewaarde van biodiesel vergelyk met die resultate van ‘n kalorie-bomtoets. ‘n 2% verskil in die resultate is verkry.

Thank you to my two study leaders; Prof Leon Lorenzen and Mr Johan van der Spuy and a special thanks to my father for the unending support and answers to my questions

My family, I love them dearly.

Table of Contents

Declaration i
Abstract ii
Opsomming iii
Table of Contents v
List of Figures viii
List of Abbreviations xi
1. Introduction 1
2. Literature review 5
2.1 Biodiesel production 5
2.1.1 Raw materials 5
2.1.2 Transesterfication 6
2.1.3 Separation and washing 7
2.2 Properties of biodiesel 9
2.2.1 Density 9
2.2.2 Cetane number 9
2.2.3 Flash point 10
2.2.4 Kinematic viscosity 11
2.2.5 Sulphur content 13
2.2.6 Cold flow properties 14
2.3 Biodiesel combustion parameters 15
2.4 Overview of test cells in general 16
2.4.1 Vibration and Noise 16
2.4.2 Electrical design 18
2.4.3 Ventilation and air handling 18
2.4.4 Test cell building and control room design 19
2.4.5 Water cooling and exhaust systems 21
2.5 Dynamometer and coupling 22
2.6 Sensors 24
2.6.1 Oxygen 24
2.6.2 Cylinder, manifold and ambient pressure 25
2.6.3 Engine speed and crankshaft angle 26

2.6.4 Temperature 26
2.7 Data collection and processing 27
2.8 Summary 27
3. Mechanical design and system integration 29
3.1 Test cell layout 29
3.2 Engine and fuel supply 32
3.3 Engine oil: pressure and temperature 34
3.4 Water supply and engine coolant 37
3.4.1 Water supply 37
3.4.2 Closed loop engine coolant system 39
3.5 Dynamometer and fuel balance operation 40
3.5.1 Dynamometer operation 40
3.5.2 AVL operation 44
3.5.3 Calibration of AVL and D360 45
3.6 Ventilation 46
3.7 Wiring, sensors and electronics 48
3.7.1 Emergency stop and fuel relay 49
3.7.2 Glow plug and starter relays 51
3.7.3 Rack controller 53
3.7.4 Water temperature controller 55
3.7.5 Ambient Measurements and AVL 57
3.7.6 Schenck D360 controller 59
3.7.7 Wall mounted junction box 60
3.7.8 19” Cabinet 61
3.8 Software and automation 62
3.8.1 ETA 62
3.8.2 PLC ladder program 66
3.8.3 Test program 67
3.8.4 Backups and storing data 68
3.9 Summary 68
4. Fuel testing and results 69
4.1 Test fuel properties 69
4.2 Problem solving and commissioning 70

4.2.1 Engine over heating 70
4.2.2 Perceived anomaly in the power curve 72
4.2.3 Commissioning 73
4.3 Automated test and repeatability 73
4.4 Performance curves 76
4.5 Fuel consumption 78
4.6 Energy balance 80
4.8 Summary 81
5. Conclusions and recommendations 83
References 85
Appendix A: Research methodology mind map 89
Appendix B: Gantry crane calculations 90
Appendix C: Dynamometer calibration arms 94
Appendix D: Servo Specifications 96
Appendix E: PLC pin connections 97
Appendix F: Löbro shaft catalogue pages 98
Appendix G: Calibrated channels in ETA 100
Appendix H: IN and OUT ladder logic for the PLC 103
Appendix I: Water temperature controller flow diagram and ladder logic 106
Appendix J: Performance curves; ULSD1, ULSD2, B5, B10, B15 and B50 109
Appendix K: Wiring diagrams 111
Appendix L: Fuel and water supply schematics with pictures 112
Appendix M: Energy balance calculations 114
Appendix N: Raw data tables of test results 119
Appendix O: Press articles 120
Appendix P: BTF Corporate logo 125

List of Figures

Figure 1-1: Project Constraints 2
Figure 2-1: Sample showing biodiesel on top and glycerol at the bottom 8
Figure 2-2: Biodiesel sample on left hand side and mineral diesel on the right 8
Figure 2-3: Cetane values (Mittelbach and Remschmidt, 2005) 10
Figure 2-4: Axis of engine vibration 16
Figure 2-5: Shared control room 20
Figure 2-6: Separate control room entry 20
Figure 3-1: Test bed and dynamometer 30
Figure 3-2: Test cell layout 31
Figure 3-3: Completed test bed 31
Figure 3-4: Toyota 2C turbo diesel 32
Figure 3-5: Fuel supply schematic 33
Figure 3-6: Exhaust system 34
Figure 3-7: Oil pressure transducer adaptor 35
Figure 3-8: Oil pressure transducer connected to braided hose 35
Figure 3-9: Oil pressure braided hose with adapter 36
Figure 3-10: Sump plug with thermocouple 37
Figure 3-11: Water supply layout 38
Figure 3-12: 3-way valve actuator 39
Figure 3-13: Dynamometer operating quadrants (Martyr and Plint, 2007) 41
Figure 3-14: Dynamometer-CV coupling (see Figure 3-16 for complete coupling) 42
Figure 3-15: Engine-CV coupling (see Figure 3-16 for complete coupling) 42
Figure 3-16: Cardan shaft coupling (Figure 3-17 shows the closed protective housing) 43
Figure 3-17: Shaft protector made from 16mm thick steel pipe 43
Figure 3-18: AVL internal view of the vessel and electronics 44
Figure 3-19: Test cell air flow showing air flow past the engine 47
Figure 3-20: 18" Spot fan for additional air movement 47
Figure 3-21: Allen-Bradley Micrologix PLC on the left with the 5 expansion modules on the right 49
Figure 3-22: Emergency stop opened displaying contactors 50

Figure 3-23: Emergency stop wiring diagram 50
Figure 3-24: Glow plug relay 51
Figure 3-25: Starter wiring diagram 52
Figure 3-26: Glow plug wiring diagram 52
Figure 3-27: Rack servo 53
Figure 3-28: JR servo wiring (Venter, 2005) 54
Figure 3-29: PWM module to modulate a 0-10 V output voltage 54
Figure 3-30: Rack servo wiring diagram 55
Figure 3-31: Actuator internal wiring (Honeywell, 2006) 56
Figure 3-32: 3-way valve actuator wiring diagram 56
Figure 3-33: Ambient pressure sensors; barometric pressure on the left, humidity probe above right and the thermocouple 57
Figure 3-34: Ambient sensor's enclosure 58
Figure 3-35: 4 Channel analogue inputs 59
Figure 3-36: Dynamometer wiring diagram 60
Figure 3-37: Junction box 60
Figure 3-38: Thermocouple wiring 61
Figure 3-39: 19" Cabinet 62
Figure 3-40: ETA's user interface, labelled for explanations 64
Figure 4-1: Damaged coolant outlet pipe limiting flow 71
Figure 4-2: Redesigned coolant outlet pipe 71
Figure 4-3: Anomaly in power curve 72
Figure 4-4: Test with preloads showing the anomaly in the power curve is not introduced by the test cell but rather an engine characteristic 73
Figure 4-5: Automated test successfully executed 74
Figure 4-6: ULSD Performance curves showing repeatability 75
Figure 4-7: AVL results showing ULSD fuel consumption 75
Figure 4-8: Power curves of ULSD, biodiesel and its blends 76
Figure 4-9: Torque curve for ULSD, biodiesel and its blends 77
Figure 4-10: B100 performance curve 77
Figure 4-11: Fuel consumption curves for ULSD, biodiesel and its blends 79
Figure 4-12: Energy consumption in kg/kWh 79
Figure B-1: Picture of the gantry crane with a hoist and beam trolley 90

Figure B-2: I-beam moment of inertia 91
Figure C-1: Calibration arm drawing 94
Figure C-2: Dynamometer calibration setup 95
Figure J-1: ULSD1 Performance curve 109
Figure J-2: ULSD2 Performance curve 109
Figure J-3: B5 Performance curve 109
Figure J-4: B10 Performance curve 110
Figure J-5: B15 Performance curve 110
Figure J-6: B50 Performance curve 110
Figure M-1: Standard orifice plate setup as used in to determine the flow rate (Crowe et al., 2001) 114
Figure M-2: Flow coefficient K and Re_d/K versus the Reynolds number (Crowe et al., 2001) 115

List of Abbreviations

A	Ampere
A/D	Analogue to digital
AC	Alternating current
AVL	Company manufacturing testing equipment
BSFC	Brake specific fuel consumption
BTF	Biofuel test facility
CCTV	Closed circuit television
CI	Compression ignition
CFPP	Cold-filter plugging point
CO	Carbon monoxide
CP	Cloud point
CV	Constant velocity
D/A	Digital to analogue
DC	Direct current
ECU	Engine control unit
EGR	Exhaust gas recirculation
EMC	Electromagnetic coupling
ETA	Engine test automation software
FAME	Fatty acid methyl ester
FFA	Free fatty acid
g	Gravitational constant
GPa	Giga Pascal
GUI	Graphical user interface
HC	Hydro carbon
kg	Kilogram
kW	Kilowatt
MPa	Mega Pascal
NC	Normally closed
Nm	Newton meter
NO	Normally open
NO_x	Nitrogen oxides

OEM	Original equipment manufacturer
Pa	Pascal
PLC	Programmable logic controller
PM	Particulate matter
PP	Pour point
PPM	Parts per million
PWM	Pulse width modulation
RME	Rapeseed methyl ester
RPM	Revolutions per minute
s	Second
TDC	Top dead centre
ULSD	Ultra low sulphur diesel
VO	Vegetable oil

1. Introduction

The use of biodiesel blends are becoming more prevalent as there is greater awareness about the environmental impact effects, depleting mineral oil reserves and dependency on the oil supply. Biodiesel can be manufactured from various raw materials such as fish or vegetable oil. The production of biodiesel from the various raw materials lends itself to small, localised plants making quality control, testing and distribution difficult. The chemical composition of biodiesel can be tested in a laboratory, though more in depth research is required to determine the combustion parameters.

An autonomous test cell has been developed to test the combustion properties of biodiesel. The design was completed in three phases: hardware (dynamometer and test bed); electronics (PLC and sensors) and software to control the test cell. From the test results conclusions are drawn about the differences between mineral diesel and biodiesel as well assessing the accuracy of the test cell.

Three specifications need be considered when a new test cell is being commissioned, namely the operational, functional and detailed functional specification. The operational specification describes what the test cell is going to be used for, the functional specification describes what it consists of and its purpose while the detailed functional specification describes how it fits together and works as a unit (Martyr and Plint, 2007). The following points describe the objective specifications for the biofuels testing facility:

- The primary function is to provide an autonomous test cell which can be used for both research and future education.
- The secondary function is to test the performance characteristics of locally manufactured biodiesel and biodiesel:diesel blends.

The three major constraints for most projects are applicable here. These are: quality, time and cost, shown in Figure 1-1. These constraints are interlinked, that is one cannot change without affecting the other, and the importance of each is project dependant. For the biofuels testing facility (BTF), cost is the most important factor as

there is a fixed budget while, secondly, the project has to be completed within a time frame of 2 years. Since two of the constraints are fixed the third constraint, quality, can be expected to vary (Martyr and Plint, 2007). To optimise the quality of the final product within the two given constraints used equipment from reputable suppliers was sourced. This could however increase future maintenance costs.

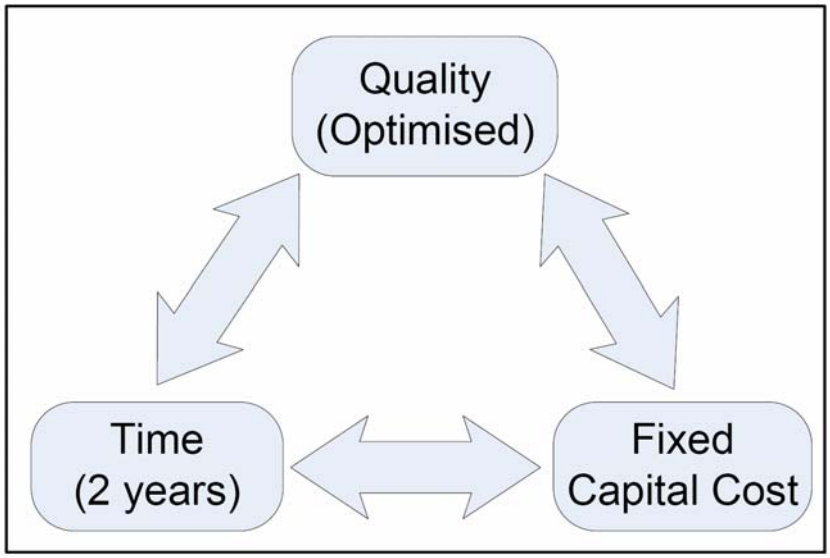

Figure 1-1: Project Constraints

The following steps were followed to develop the test cell;

- A literature study was conducted.
- The hardware was designed and implemented.
- The software purchased and programmed.
- The automated test procedure was coded.
- The documentation for future operators was written.

A mind map showing these fives steps and their breakdown is shown in Appendix A. Despite the literature study being at the start of the project report constant references and updates where made for the duration of the project. The first stage was to select the correct hardware, purchase and install it and then verify that each component functioned. This is not ideal as it would be better to verify the system integration with the addition of each component, but this was not possible until the software was installed. When the hardware was completed the software was installed and each system checked individually. The system was then integrated and

manual test runs were executed after which it was automated. Problems that occurred during the automated run were addressed, the test cell commissioned, various tests performed and finally a user manual compiled.

This thesis layout is as follows:

Chapter 1: This introduction

Chapter 2: Literature review

The literature study is divided into two sections; biodiesel and the test facility. The important characteristics for biodiesel in terms of combustion are dependant on the manufacturing process as this determines the quality, the chemical composition of biodiesel and the combustion parameters. Types of sensors, data acquisition systems, test cell layout and ventilation for test cells were researched.

Chapter 3: Mechanical design and system integration

This is the core chapter as it discusses the development of the test cell. The following hardware aspects are covered; test cell layout, fuel and coolant systems, ventilation, calibration, wiring, sensors and electronics. This chapter concludes with a discussion of the two software packages, the coded programs and the manipulation of the data.

Chapter 4: Fuel testing and results

The results from the biodiesel analysis are discussed, followed by the problems that were encountered during testing and how they were solved. Results from the automated engine test are used to check repeatability of measurements and thus, determine whether the test cell meets the specifications. From the performance and fuel consumption graphs the differences between mineral diesel, biodiesel and its blends can be determined.

Chapter 6: Conclusions and recommendations

In this chapter conclusions are drawn and recommendations are suggested.

During the project term several press articles were released in various newspapers and publications, they have been included in Appendix O. The corporate logo that was designed is shown in Appendix P.

2. Literature review

2.1 Biodiesel production

In order to understand the properties of biodiesel and how they affect the performance of an internal combustion engine, a brief background on biodiesel production and its combustion properties is given.

2.1.1 Raw materials

There are approximately 350 oil bearing crops that can be used for biodiesel production, of which only a handful can be considered as a viable replacement for mineral diesel because the others are not produced in sufficient quantities. These are: sunflower, safflower, soybean, cotton seed, rapeseed (also known as canola) and peanut oils (Dermibas, 2005). South Africa consumed 11.56 billion litres of diesel in 2007 (www.sapia.co.za, 2008). The exact volume of biodiesel produced in South Africa is not known, but worldwide it is estimated to be 7.9 billion litres in 2007, substantially less than what is needed, both locally and worldwide (www.planetark.org, 2008). It is impossible to replace all mineral oil with vegetable oil (VO) as there is not enough land or water to grow the needed crops, however, a partial replacement of say 10%, could reduce a country's dependency on mineral imports and stimulate its economy through work creation.

A further problem is that the food market is in direct competition with the fuel market, with the fuel market willing to pay a premium for the oil. This leads to an increase in price and shortage issues for food consumers. As vegetable oils are freely available as fuel replacements, the market must be controlled to ensure fairness to the food industry and to meet the required mineral replacements.

Other sources for biodiesel production are used cooking oils and animal derived fats (lard and tallow). Used cooking oils previously considered a waste by-product are now sought after by both the animal feed and biodiesel manufacturers. The used oil contains food particles that must be filtered out and possibly water contamination. A more important contamination is the free fatty acids (FFA) contained in the oil

because these cannot be converted to biodiesel with the use of an alkali catalyst (Dermibas, 2005). This limits the number of available processes when used cooking oil is considered, but it still provides a low cost raw material for the manufacturing of biodiesel.

Oil production from sources such as algae and sewage are currently being investigated, because these alternative sources, unlike crops, are not limited by agricultural capacity, have high yields and may contribute to the raw materials needed along with the conventional feedstock's (Kiong, 2006).

2.1.2 Transesterfication

Transesterfication is one of the most common chemical processes by which vegetable oil is converted to biodiesel. Vegetable oils are typically made of triglycerides, which when reacted with alcohol in the presence of a catalyst create an alcohol ester and glycerol. The reaction is shown in Equation 1 (van Gerpen, 2005).

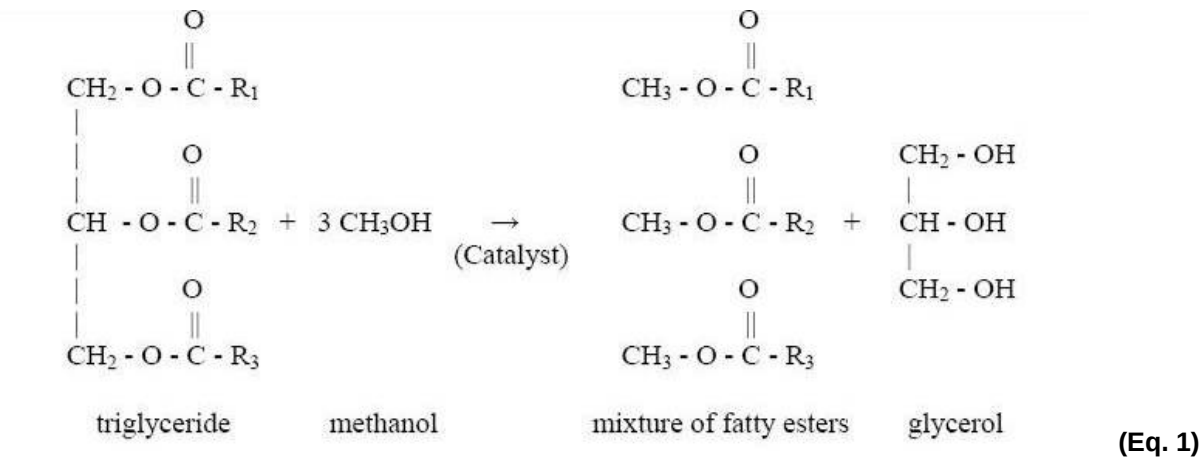

(Eq. 1)

The most common reactant is methanol (Dermibas, 2006) with sodium or potassium hydroxide (NaOH and KOH) as the catalyst respectively. The most important variable to ensure maximum methyl ester production is the molar ratio of methanol:VO, which should be 6:1 for optimum results (Felizardo et al., 2005). The oil, alcohol and excess catalyst are combined in the reactor and then heated to reduce the reaction time. Excess catalyst can be used because it is recovered at the end of the process and fed back into the system.

Several types of transesterification processes exist: batch; continuous; ultra- and high shear; and ultrasonic reactors. The batch reactors are typically used by the individual or small companies who are producing biodiesel for own use and require a fixed amount of fuel. The continuous reactors are for uninterrupted biodiesel manufacturing, producing higher volumes than the batch reactors but having a higher capital cost. The remaining reactors are variations on the continuous reactor where detail design depends on: space available; oil to be processed; time; cost; manpower and quality of biodiesel required.

2.1.3 Separation and washing

Two liquid phases are produced by a successful transesterfication reaction: glycerol (crude glycerine) and biodiesel (Figure 2-1). The free glycerol has a higher density than the biodiesel and can be removed through settling or centrifugation. Most of the catalyst will also be removed in this step as the alkaline catalysts are more soluble in the polar glycerol phase (van Gerpen, 2005). Some dissolved glycerol will remain in the biodiesel after the decanting process, but can be removed during the water washing phase. In Figure 2-2 samples of pure biodiesel are shown on the left and ultra low sulphur diesel on the right.

If not completely removed, glycerol can plug filters, damage the injector pump and settle out in storage tanks. The remaining dissolved glycerol can be removed by repeated washing steps, using either water or a 0.5% HCl solution. The remaining methanol (or catalyst) will also be removed during the washing phase, which also raises the flash point of the biodiesel. A proposed more elegant removal of the dissolved glycerol and partial glycerides is to convert them to a triglyceride (Klok and Verveer, 1990), which allows for easy separation. This is done by adding extra alkaline catalyst to the biodiesel and heating the mixture from 80 to 100°C, also distilling off the excess methanol. After removing traces of soap and methyl esters, the triglycerides can be reintroduced to the reactor with the new oils.

Figure 2-1: Sample showing biodiesel on top and glycerol at the bottom

Figure 2-2: Biodiesel sample on left hand side and mineral diesel on the right

2.2 Properties of biodiesel

As biodiesel is a replacement fuel for mineral diesel, it has similar properties, although there are some minor differences. The standards to which biodiesel must comply are country dependant. The following section considers the most applicable properties of biodiesel affecting combustion and the difference in reference standards.

2.2.1 Density

Density is the mass of fluid per unit volume, given in kg/m^3. Biodiesel generally has a density of 860-900 kg/m^3 which complies with the fatty acid methyl ester (FAME) standard (Dermibas, 2005) where mineral diesel has a density of 820-845 kg/m^3 at 15°C. This slight difference will not be significanct if the temperature remains relatively high as biodiesel has a low cloud point (see Section 2.2.6). The fuel injected into the combustion chamber is measured on a volumetric basis, thus the amount of fuel (or energy) injected per cycle will increase with increasing fuel density, negatively affecting the fuel consumption.

2.2.2 Cetane number

The cetane number is a measure of the ignition quality and relates to the delay time between fuel being injected into the combustion chamber and igniting (Dermibas, 2005). A higher cetane value indicates a shorter time between injection and ignition which improves cold starting and smoothness of the engine. A shorter ignition time will lead to a more complete combustion, reducing the exhaust emissions, engine deposits and knocking. On average biodiesel has an equivalent or higher cetane value than mineral diesel as indicated in Figure 2-3.

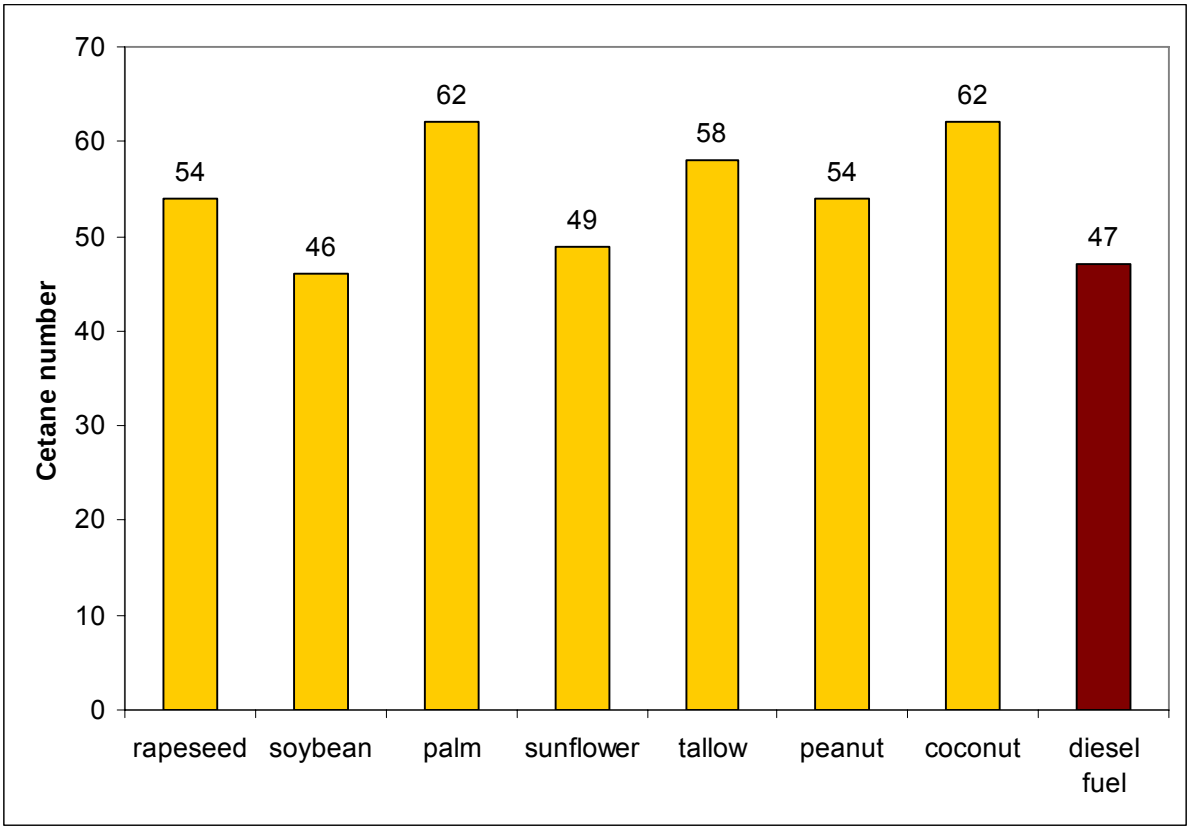

Figure 2-3: Cetane values (Mittelbach and Remschmidt, 2005)

Longer fatty acid carbon chains and more saturated molecules increase the cetane number while the number of double bonds decrease it. When the fuel is injected into the cylinder, it is subjected to a gradual increase in pressure and temperature during which various chemical reactions take place, such as producing aromatics which offers an explanation as to why unsaturated esters tend to have a lower cetane value. A higher cetane value can be obtained by choosing a feedstock with a high proportion of medium or long saturated fatty acids, this however negatively affects the viscosity and cold temperature properties (Mittelbach and Remschmidt, 2005; Dermibas, 2005).

2.2.3 Flash point

The flash point of a fuel is the stage at which the vapour will combust when exposed to a spark or flame. Biodiesel typically has a flash point of 150°C or higher while mineral diesel is around 70°C (www.biodieselsa.co.za, 2007) and this is a good measure of how safely a fuel can be transported, stored and used. Biodiesel's flash

point is more than double that of mineral diesel making it useful for applications that would otherwise be unsuitable for diesel. The standards to which biodiesel and mineral diesel must comply to in Europe are the EN ISO 3679 and EN ISO 2719, respectively. Properties such as the flash point are determined using the same basic principles although the methods differ for mineral and biodiesel (Mittelbach and Remschmidt, 2005).

2.2.4 Kinematic viscosity

The measure of a fluid's resistance to flow under gravity is called the kinematic viscosity (www.britannica.com, 2008). This is one of the most important parameters of biodiesel in terms of engine operation because it affects both the combustion process and the injector pumps. Incorrect viscosity can cause mechanical damage to the injector pump, poor fuel atomization when injected into the cylinder and will eventually lead to the coking of the injector tips. This coking may eventually cause the engine to lose power or component failure.

The viscosity standards for diesel (both regular and low sulphur diesel), stipulate values between 2.2 to 5.3 mm^2/s (Standards South Africa, 2002). From Table 2-1 it can be seen that most countries require biodiesel to be between 3.5 and 5.0 mm^2/s, America is the most lenient and requires the viscosity to be between 1.9 and 6 mm^2/s (Felizardo et al., 2005; www.shaval.co.za, 2007). Excluding America, biodiesel and mineral diesel meet similar standards and can thus be interchanged without any noticeable changes in performance or damage to the engine.

Table 2-1: Biodiesel properties (www.shaval.co.za, 2007)

		Austria	Czech Republic	France	Germany	Italy	Sweden	USA	Europe
Specifications		**ON C1191**	**CSN 65 6507**	**Journal office**	**DIN V 51606**	**UNI 10635**	**SS 155436**	**ASTM 6751-02**	**EN 14214:2005**
Applies to		FAME	RME	VOME	FAME	VOME	VOME	FAMAE	FAME
Density 15°C	**g/cm³**	0.85-0.89	0.87-0.89	0.87-0.90	0.875-0.90	0.86-0.90	0.87-0.90	0.87-0.89	0.86-0.90
Viscosity 40°C	**mm²/s**	3.5-5.0	3.5-5.0	3.5-5.0	3.5-5.0	3.5-5.0	3.5-5.0	1.9-6.0	3.5-5.0
Distillatioin	**% @ °C**			95%, 360°C		95%, 360°C		95%, 360°C	
Flashpoint	**°C**	100 min	110 min	100 min	110 min	100 min	100 min	100 min	120 min
CFPP	**°C**	summer 0 winter -15	-5		summer 0 spr/aut -10 winter -20		-5		* country specific
Pourpoint	**°C**			-10 max			sum 0 max win -15 max		
Sulphur	**%mass**	0.02 max	0.02 max		0.01 max	0.01 max	0.001 max	0.0015 max	10 max
CCR 100%	**%mass**	0.05 max	0.05 max		0.05 max			0.05 max	
Ramsbottom 10% dist resid	**%mass**			0.3 max	0.3 max	0.5 max		0.1 max	0.3 max
Oxid ash	**%mass**						0.01 max	0.01 max	
Water	**mg/kg**		500 max	200 max	300 max	700 max	300 max	500 max	500 max
Total contamination	**mg/kg**		24 max		20 max		20 max		24 max
Cu corrosion max	**3h/50°C**								6 hrs min
Oxidation stability	**hrs;110°C**								
Cetane No.		49 min	48 min	49 min	49 min		48 min	45 min	51 min
Acid value	**mgKOH/g**								0.05 max
Neutral No.	**mgKOH/g**	0.8 max	0.5 max	0.5 max	0.5 max	0.5 max	0.5 max	0.6 max	0.8 max
Methanol	**%mass**	0.2 max		0.1 max	0.3Max	0.2 max	0.2 max		0.2 max
Ester content	**%mass**			96.5 min		98 min	98 min		96.5 min
Monoglyceride	**%mass**			0.8 max	0.8 max	0.8 max	0.8 max		0.8 max
Diglyceride	**%mass**			0.2 max	0.4 max	0.2 max	0.1 max		0.2 max
Triglyceride	**%mass**			0.2 max	0.4 max	0.1 max	0.1 max		0.2 max
Free Glycerol	**%mass**	0.02 max	0.02 max	0.02 max	0.02 max	0.02 max	0.05 max	0.02 max	0.02 max
Total Glycerol	**%mass**	0.24 max	0.24 max	0.25 max	0.25 max			0.24 max	0.25 max
Iodine No.		120 max		115 max	115 max		125 max		120 max
Phosphorus	**mg/kg**	20 max	20 max	10 max	10 max	10 max	10 max	10 max	10 max
Alkalinity	**mg/kg**		10 max	5 max	5 max			10 max	

Biodiesel's viscosity is inversely related to temperature, increasing as it gets colder while the viscosity of mineral diesel varies less over the normal temperature range. This is a negative characteristic as in colder countries an additive must be used, resulting in a higher monetary and environmental cost. The major viscosity increase in biodiesel starts below around 5°C and solids will form soon after dropping below 0°C. This can be reduced by blending it with mineral diesel. See Table 2-2 and Table 2-3, respectively.

Table 2-2: Viscosities of biodiesel and mineral diesel (Knothe and Steidley, 2006)

Temperature (°C)	Fuel	
	Biodiesel	Petrodiesel
40	4.15	2.90
35	4.64	3.25
30	5.15	3.64
25	5.76	4.08
20	6.43	4.55
15	37.52	5.31
10	8.67	6.21
5	10.47	7.23
0	11.75	8.58
-5	n/a	10.81
-10	n/a	n/a
LTVR	2.83	2.96

Table 2-3: Viscosities of blends with low-sulphur diesel (Knothe and Steidley, 2006)

Temperature (°C)	Commercial biodiesel (%)								
	10	20	30	40	50	60	70	80	90
40	2.95	3.07	3.15	3.26	3.38	3.53	3.64	3.77	3.94
35	3.35	3.44	3.53	3.64	3.77	3.97	4.09	4.25	4.4
30	3.74	3.82	3.94	4.05	4.22	4.44	4.57	4.72	4.89
25	4.15	4.30	4.39	4.52	4.76	4.94	5.09	5.27	5.48
20	4.68	4.85	4.92	5.08	5.24	5.49	5.66	5.9	6.11
15	5.37	5.54	5.69	5.88	6.11	6.36	6.57	6.84	7.13
10	6.23	6.44	6.61	6.82	7.00	7.35	7.67	8	8.17
5	7.47	7.66	7.78	8.01	8.33	8.70	8.97	9.35	9.97
0	8.63	8.84	9.15	9.46	9.67	10.14	10.54	11.04	11.1
-5	10.77	11.04	11.23	11.63	12.04	n/a	n/a	n/a	n/a
-10	n/a	n/a	n/a	n/a	n/a	-	-	-	-
LTVR	2.93	2.88	2.91	2.90	2.86	2.87	2.90	2.93	2.83

2.2.5 Sulphur content

Sulphur acts as a lubricating agent, although in certain countries new mineral diesel regulations stipulate that the sulphur content may not exceed 50ppm. This has led to a reduction in sulphur dioxide and particulate matter emissions and lubricity of the fuel. Low sulphur fuel reduces human and environmental impact and increases the life of the catalytic converter, although extra lubricating agents are required to prevent damage to the injector pump and reduce engine wear. Biodiesel has traditionally been perceived as being sulphur free, but this only holds true for fatty acid methyl esters produced without the use of sulphuric acid and for fresh vegetable oils (Mittelbach and Remschmidt, 2005). In reality there are traces of sulphur, around 31ppm for most types of biodiesel produced around the world (Waina et al., 2005).

Biodiesel has an advantage over mineral diesel in that it has an inherent high lubricity, because of its chemical structure and oxygen content, eliminating the need for additives (www.biodiesel.org, 2007) while maintaining the benefit of low sulphur content.

2.2.6 Cold flow properties

The cloud point (CP) is the temperature at which visible crystals start to form and the pour point (PP) is the temperature when the fluid starts to gel (or is no longer viscous). Biodiesel has a higher CP and PP than mineral diesel, which must be taken into account in countries with colder climates. The cold flow properties of biodiesel derived from some common vegetable oils are compared with mineral diesel in Table 2-4. The cold-filter plugging point (CFPP) is the point at which the fluid fails to pass through a standardized filter in a given amount of time under set conditions.

Table 2-4: Cold flow properties (Mittelbach and Remschmidt, 2005)

	Diesel fuel	Rapeseed	Olive	Sunflower	Soybean	Coconut	Palm	Tallow
CP [°C]	-15	-2	-2	-1	0	12	13	14
PP [°C]	-33	-9	-6	-3	-2	-	-	12
CFPP [°C]	-18	-15	-9	-3	-2	8	1	13

Cold flow parameters do not influence the combustion process but affect the injector pumps and the vehicle fuelling system. To improve these properties, additives such as those used in the petroleum industry, can be used. Another option to improve the cold properties in low temperature environments is to mix biodiesel and mineral diesel, which eliminates the need for expensive additives and has a reduced influence on combustion.

Through extensive vehicle modification this problem can be solved mechanically by placing a heater in the fuel tank, fuel line or filter and a parallel electric heater system. The modifications however have a high capital cost, because a basic conversion system in the United Kingdom costs around R7,700 (www.smartveg.com, 2008). This initial purchase price is approximately 8% of the purchase price of a

small diesel (model and manufacturer dependant), excluding the shipment and fitting cost. The reliability may also be affected due to the modifications of the fuelling and cooling systems without original equipment manufacturer (OEM) parts.

2.3 Biodiesel combustion parameters

When biodiesel is injected, the spray penetration and pattern are the first in a sequence of parameters to be affected in a standard diesel compression ignition (CI) engine. The primary factors affecting the spray are the spray angle, volatility, surface tension and viscosity. The spray angle of biodiesel is narrowed to about half that of diesel (Li et al., 2006) and the higher viscosity and surface tension combined with a lower volatility lead to reduced atomisation. Poor atomisation causes larger droplet formation and a longer ignition delay but can be improved by higher injection pressures, assistant swirl and a smaller orifice diameter. The researched literature and forums gave no indication that the higher injection pressures of newer fuelling systems were affected with the use of biodiesel. This is to be expected because biodiesels properties are similar to those of diesel, if it is within specification.

Apart from being a renewable energy source, biodiesel is a cleaner burning fuel than mineral diesel as it results in lower emissions. One possible exception is that nitrogen oxides (NO_x) emissions are in some cases adversely affected, which can be attributed to the small advance in fuel injection timing needed due to the different biodiesel combustion characteristics (McCormick et al., 2005). The literature differs widely with regards to NO_x emissions though the general trend is that there is a slight increase in NO_x emissions with respect to mineral diesel. Although in some cases a NO_x reduction is reported (Desantes et al., 1999). Carbon monoxide, (CO), hydro carbons (HC) and smoke are also reduced, with the latter being reduced as a result of the additional oxygen content in biodiesel (Tsolakis et al., 2007).

The power developed by an engine running on biodiesel is similar to that of mineral diesel, while the exhaust gas and lubricating oil temperatures are lower (Tsolakis et al., 2007) with no reported problems of hot or cold starting. The thermal efficiency remains similar, although the brake specific fuel consumption (BSFC) increases

because of the lower calorific value of the biodiesel. Blending of biodiesel with mineral diesel, such as B20 (20% biodiesel + 80% mineral diesel) can reduce emissions without affecting the fuel combustion or injection properties.

It can be concluded that biodiesel can be substituted for mineral diesel without any negative engine combustion effects.

2.4 Overview of test cells in general

The following sections present a brief overview of the main considerations when designing and building an engine test cell. An engine test cell is a room dedicated for the operating and testing of engines on a test bed which can be instrumented and data recorded. This is given as background study as the current project utilizes existing buildings, water supply and ventilation systems, which have to be taken into account when installing and commissioning the equipment.

2.4.1 Vibration and Noise

In the test cell most of the noise and vibration comes from the engine itself with secondary sources such as pumps and ventilation fans also contributing to these effects. The engine is considered to have six degrees of vibration about the axis' running through the centre of gravity, as shown in Figure 2-4 (Martyr and Plint, 2007).

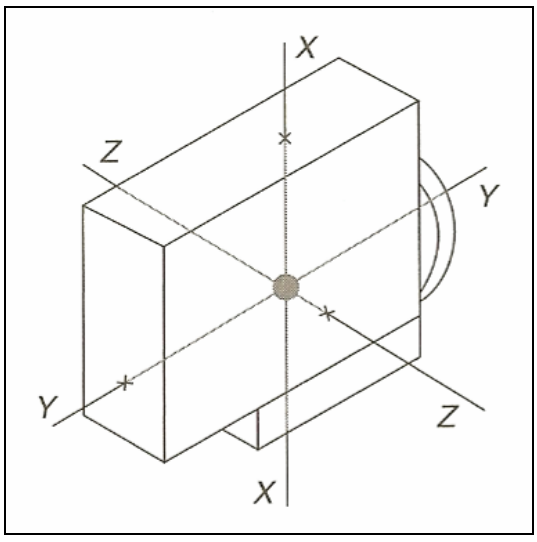

Figure 2-4: Axis of engine vibration

There are only three modes that need to be taken into consideration when designing for vibration, according to Martyr and Plint (2007):

- Vertical X-axis oscillations due to unbalanced forces
- Y-axis rotation due to cyclic variations in torque
- Unbalanced forces in different transverse planes because of rotation about the Z-axis

When designing the test bed and engine mounts, the following have to be considered, bearing in mind the three modes stated above: the force to be attenuated; the natural frequency range of the engine; the load distribution of the engine; the vibration amplitudes; higher frequency structure borne noise; transient forces and the effect of the environment (Martyr and Plint, 2007). It can be assumed that the engine manufacturer took these into consideration when designing the engine mountings. The approach adopted here is to use the engine manufacturers standard mounts, replicating the vehicle setup as closely as possible. The test bed can be mounted on a seismic block or sprung steel frame to reduce vibration. The seismic block, whether on isolated, resilient matting or air spring foundation is expensive and requires a pit to be dug for the block. This type of test bed is expensive and increases the complexity of the test cell and mounting of the engine. The most common test bed, and the one used in this design, is a steel frame mounted on spring-rubber supports or air springs.

Noise in a test cell can be problematic when anechoic testing is required. There are two types of anechoic cells: semi-anechoic with reflective floors and insulated walls to simulate a vehicle on the road or a full anechoic cell in which all surfaces are sound absorbent. Anechoic cells are expensive, require specialist design and are normally only used during engine development. Noise however, must still be attenuated to permissible levels as there will inevitably be an operator on duty and there may be more than one test cell in the vicinity. The facility under development used a double glass pane control room to isolate the operator from the cell noise. Along with vibration, noise can also be used for fault finding and alarm monitoring but this would have to be based on statistical data obtained through many hours of testing.

2.4.2 Electrical design

The electrical system is the life line of the test cell as it is used to control the tests, monitor alarms and sample data. The physical environment in which the electronics operate can vary widely in test cells, anywhere from -30°C to 45°C with relative humidity ranging from 0-100%. Thus the electronics either have to be certified for the given conditions or installed in such a way that they are protected from these conditions. Electromagnetic coupling (EMC) and cross signal interference must be considered, especially for the signal carrying cables. For example, a 3–phase power supply cable running into the control room could readily interfere with a poorly designed 4-20mA signal cable running parallel with it. Correct earthing of cables and shields not only reduce interference, but are also safety requirements.

2.4.3 Ventilation and air handling

An engine on a test bed can be seen as a large heater from which all the waste energy has to be removed, using water or air. Approximately one third of the power developed by the engine is removed by the engine coolant, another third is converted to shaft work and the remaining third has to be removed by the ventilation system. Sufficient air flow in a test cell is therefore important to prevent temperature build-up which may affect engine operation.

The rate at which air (at standard atmospheric pressure and temperature) has to be removed from the test cell with a constant temperature rise is calculated using Equation 2. Auxiliary equipment such as the fans, lights and instrumentation generate additional heat, which, however small in comparison with the engine, also has to be removed and accounted for in the design.

$$\dot{m} = \frac{P}{C_p \Delta t} \qquad \textbf{(Eq. 2)}$$

From Equation 2 it can be seen that the mass flow is directly proportional to power (engine + auxiliaries), and inversely proportional to the change in temperature. The specific heat for air is approximately, C_p=1005 J.kg^{-1}.K^{-1}, roughly four times less than

that of water. The air flow should be designed for maximum rated engine power, usually obtained from the specifications.

2.4.4 Test cell building and control room design

The layout and detail design of the test cell building and the associated control room was not required for this project as an available test cell was used. The control room allows the operator monitor a test being performed from a safe area within close proximity to the test cell. The key aspects are however discussed.

The size and layout of the test cell is determined by the type of tests that are going to be performed. For example, an engine test cell requires less floor space than a test cell which houses the complete drive train. When designing the test cell layout there must be enough space for personnel to move around freely, preventing potential accidents resulted from working in confined spaces. Two typical cell layouts are shown in Figure 2-5 and Figure 2-6 (Martyr and Plint, 2007). As can be seen the cells have large doors through which the equipment and engines can be brought in, typically with a roof crane or pallet system.

The advantage of the shared control room is that it requires less floor space and thus less expensive. The disadvantage is the operators may interfere with each other during testing and if works need to be done on the control room, both test cells become inoperable.

The control room is typically located next to the test cell with a window for visual monitoring, although the use of close circuit television (CCTV) cameras can make windows obsolete and allows relocation of the control room. A window has several disadvantages: it compromises fire rating, has negative sound attenuation characteristics and reduces the usable space in the test cell (Martyr and Plint, 2007). The sound that does pass through the window can serve as an audible alarm for an experienced operator as they will be able to detect a failure by the change in the engine noise. The instrumentation is located in the control room, with the primary equipment being the operators focus centre and secondary equipment displayed

away from the operator's field of view. An emergency stop button should be installed that is clearly marked and easily within reach of the operator. A control room that is well laid out will be intuitive and allow for smooth and safe operation.

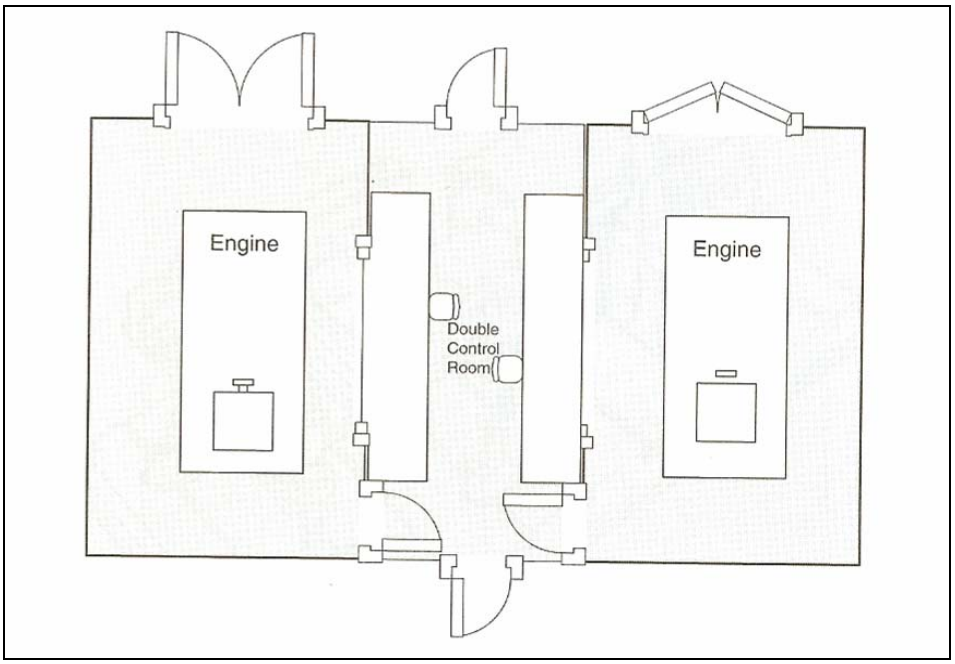

Figure 2-5: Shared control room

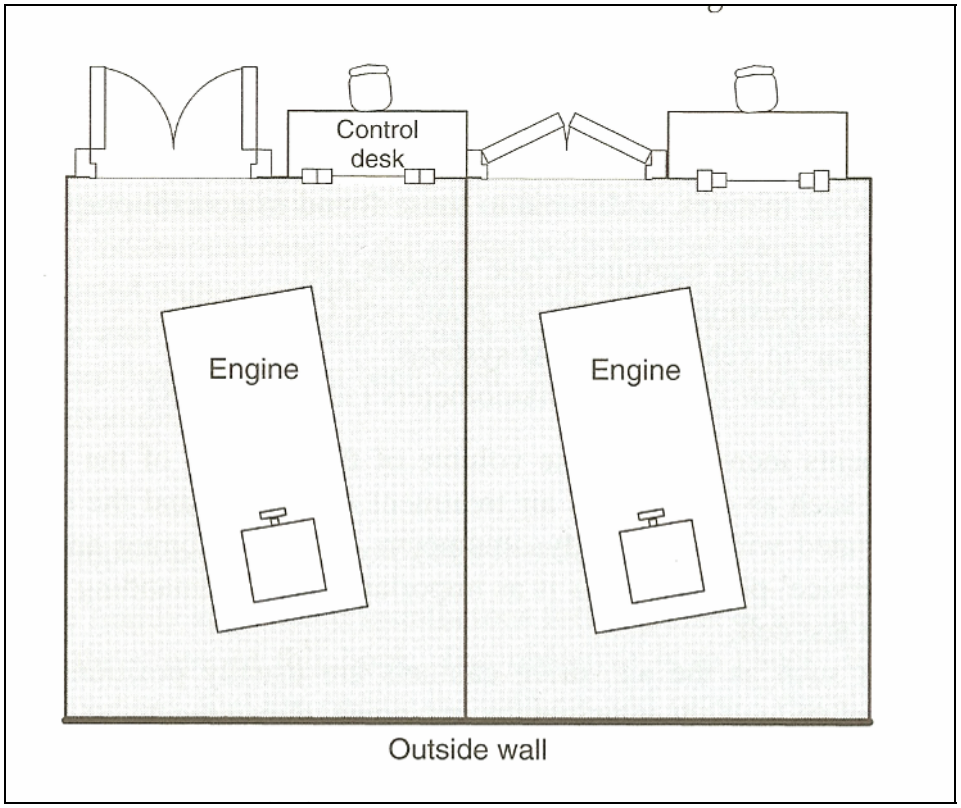

Figure 2-6: Separate control room entry

Test cell aspects such as the doors, floors, wall, roof and lighting must be suitable for the application. The doors have to be sound and fire proof while still allowing easy access to the test cell. To control fume leakage the test cell may be at a reduced pressure and opening a large door may be impossible or dangerous due to the pressure differential. The floors and sub floor should be strong enough to handle the load as well as the induced vibration. The coating of the floor should not become slippery or react with the spilled fluids. Walls and roofing have be to fire proof, strong enough to carry loads such as the crane and have suitable sound damping material. Lighting is normally a last consideration when designing a test cell, although it is important to provide good lighting for working purposes. The lights may also interfere with the mounting of equipment and or the roof mounted crane. Prior design and consideration is therefore essential.

2.4.5 Water cooling and exhaust systems

Water is an almost ideal cooling fluid as it has a high specific heat value, low viscosity, relatively low corrosivity and is freely available (Martyr and Plint, 2007). The required flow rates can be calculated similarly to that of air if the heat to be transferred and the change in temperature is known. Additives such as ethylene glycol (antifreeze) can be added to the water to improve the operating temperature range of the cooling system and inhibit corrosion, although the specific heat value will be reduced. Water quality is as important as the ability to transfer heat since it will cause engine and dynamometer failure if the specifications of cleanliness are not met. All solids must be removed and if there is hard water (high concentration of calcium carbonate) the temperature must be kept below 70°C. Soft water (water containing few or no magnesium or calcium irons) can cause corrosion and can be as harmful as hard water. The water quality and flow rate specifications for equipment should be obtained from the manufacture.

The exhaust system layout is important for emissions testing and correct engine operation. Ideally it should mimic that of the vehicle in operation. This is problematic as each engine has a different layout and has to be located near a scavenge duct. The exhaust system, especially from turbo-charged engines, runs at high

temperatures compared to the surroundings and adds a large heat load on the ventilating system. If comparative testing is to be done, using a standard exhaust is less important unless it contains a catalytic converter or is required by the engine control unit (ECU). For this project a custom exhaust was manufactured as the engine has neither a catalytic converter nor ECU. There are three possible exhaust layouts: a closed coupled system in which the exhaust is vented outside, a scavenge duct for each cell or a common scavenge duct for multiple test cells. The common scavenge duct is most prevalent for multiple cell installations as it requires one fan and exhaust termination. The exhaust must be located away from the air inlet to prevent recirculation and terminated with the correct cowl.

The water quality in the test cell is important because it must not be a cause for engine failure (especially during endurance testing) and it may influence the pumps or sensors on the engine, giving rise to false data. Similarly, the accuracy of the measurements could be affected if an original exhaust system is not used as it may lead to erroneous readings as well as resonant vibrations and reliability problems.

The follow guidelines should be followed when designing the duct (Martyr and Plint, 2007):

- The duct should be made of stainless steel to prevent corrosion.
- Soot deposits and staining condensate should not affect maintenance.
- Exhaust backpressure should not be affected by an increase in air flow rate.
- The air flow must be sufficient to maintain an acceptable duct temperature, this can however, cause an undesired drop in temperature in the test cell on a cold day.

2.5 Dynamometer and coupling

The dynamometer is mounted on the test bed with the controller in the control room. The data from the dynamometer are recorded and stored on the provided PC. The dynamometer provides an external load that allows the engine to operate under controlled load. The early dynamometer's used a mechanical brake mechanism to

dissipate the power, hence the name “brake horsepower” (Ferguson and Kirkpatrick, 2001). Due to the fact that these relied on friction to dissipate power, they overheated and had a limited power rating.

There are several different types of dynamometers, chiefly; water brake, eddy current, direct current (DC) and alternating current (AC). The water brake dynamometer dissipates power through shearing water by means of a vaned rotor and is controlled by the amount of water in the casing. These dynamometers are inexpensive although they are difficult to control, require a cooler to maintain the water temperature and are not suitable for dynamic testing due to there slow response. The direct current dynamometer has traditionally been the most flexible but at a high cost, recently being replaced by the AC dynamometer. The electrical dynamometers are easier to control and the power generated can be used to power auxiliary equipment or routed back into the electrical supply grid.

Depending on the desired application, it may be necessary for the dynamometer to act as a generator and transmit power back into the engine. This would simulate a vehicle going downhill with the throttle in the closed position. When this is the desired result, an AC or DC dynamometer is generally used, although an eddy current dynamometer can be configured with an electric motor to yield the desired results. The water brake dynamometer is also limited to horizontal operation, whereas a closed loop unit like the eddy current and AC/DC dynamometers can operate at any given angle. Testing at angles is typically used in the marine industry or to simulate an ascending or descending off road vehicle.

There are five major types of couplings used for connecting the engine to the dynamometer (Martyr and Plint, 2007):

- Quill shaft with internal flanges and rigid couplings:
  These are used when the drive and the driven machine are permanently coupled as they are vibration and misalignment intolerant.
- Quill shaft with toothed or gear type coupling:
  The geared couplings are inherently stiff, suitable for high speed and power and allow for a small amount of misalignment. They, however,

require lubrication to prevent wear and once tooth to tooth seizure takes place the shaft failure may be rapid and catastrophic.

- Cardan shaft:
  Cardan shafts are the most commonly used shafts and consist of two universal or constant velocity (CV) joints connected with a solid shaft. They are prone to give trouble when fretting of the needle roller bearings occurs.
- Multiple membrane couplings:
  They are used for high speeds, are stiff and tolerate a moderate degree of misalignment and axial displacement.
- Elastomeric couplings:
  There are a wide number of designs on the market to suite different applications, but the basic principle is an interchangeable elastic element that can be changed to vary the torsional stiffness, thereby eliminating problems with critical speeds and torsional vibration.

For this biofuel test facility a cardan shaft will be used as it is an inexpensive standard engine test setup. As the engine will not be changed on a regular basis the problem of alignment can be addressed once in the initial setup and the shaft will be designed to handle the speed and torque of a particular engine.

2.6 Sensors

The following sensors are used to measure engine parameters, both for the ECU and testing purposes.

2.6.1 Oxygen

A lambda sensor placed in the exhaust can be used to measure the amount of oxygen in the exhaust gas. The lambda sensor determines the amount on unburned oxygen in the exhaust, from this it can be determined whether the engine is running lean or not. This input is then used by the ECU to balance the fuel-air mixture. This sensor is constructed from solid zirconium oxide (ZrO_3) electrolyte stabilised with

yttrium oxide (Y_2O_3) and is in the shape of a thimble. Porous platinum is used to coat the inner and outer surfaces which form interior and exterior electrodes.

Negative oxygen ions are produced on the electrodes by means of an electrochemical reaction, which then gives rise to a voltage across the electrolyte. The voltage produced is dependant on the flow of oxygen ions, which is proportional to the oxygen partial pressure at the electrodes. This voltage can be sampled and the oxygen content calculated.

2.6.2 Cylinder, manifold and ambient pressure

In-cylinder pressure is measured with a piezo-electric pressure transducer and a high speed sampling device. Since the transducer is in contact with the combustion flame the older types needed cooling. There are however newer transducers on the market for which this is no longer required. In diesel engines it is possible to replace one of the glow plugs with a transducer, which eliminates the need to drill and tap the cylinder head, although this may conceivably have adverse effects on the starting of the engine. Spark plugs combined with a pressure transducer are available for petrol engines but are expensive and have a limited life, therefore drilling the cylinder head is the best option.

The manifold pressure gives an indication whether the engine is under load or not. For a turbo-charged engine, high pressures equals high load and vice versa. These data are then used by the ECU to make the necessary adjustments. A diaphragm sensor, which consists of a rubber diaphragm with strain gauge (in Wheatstone bridge layout) attached, is used in such cases. The deflection of the diaphragm causes the resistance in the strain gauge to vary, from which the pressure can be determined. In this design no cylinder or manifold pressures are measured, although a high speed data acquisition unit is provided should transducers be fitted at a later stage.

A digital barometer and humidity sensor are used to record the ambient pressure and relative humidity should a climate controlled test cell not be available. All engine

performance tests must be carried out at standard atmospheric pressure (101,325 kPa) to ensure consistency, but because the ambient pressure changes day to day and a climate controlled test cell is not economically viable, the use of a correction factor is a viable cheaper solution. The correction factor is discussed in section 3.8.1.

2.6.3 Engine speed and crankshaft angle

The engine speed and crankshaft angle can be determined at any of the following places; crankshaft, camshaft, distributor shaft or on the output shaft. Electronic sensors are the most popular and employ magnetic or optical detection, with magnetic detection being the more robust of the two.

Magnetic sensors operate on the Hall Effect which is the electromagnetic force acting on electrons in metals and semiconductors (Ferguson and Kirkpatrick, 2001). When current is passed through a semiconductor and a magnet is placed close by, a voltage is induced in the direction of current flow. The voltage is proportional to the magnetic flux, therefore the change in voltage can be measured and the speed is determined by the frequency of this change in voltage. Top dead centre (TDC) or crankshaft angle can be determined by using a different notch in the Hall Effect sensor or by placing a notch in the fly wheel and noting the change in voltage as it passes.

2.6.4 Temperature

The inlet air, coolant inlet and outlet, exhaust and oil temperatures can be measured with thermocouples. Depending on the temperature to be measured, K and J type thermocouples are the most common thermocouples available. J types operate in a smaller range, approximately to 150°C while K types operate up to 1500°C. As the K type spans a larger range it is less accurate, although for general engine testing the accuracy difference is not of concern. When ordering thermocouples the following can be specified: type, probe length, type of cable (PVC, screened or fibre glass), wire length and a probe diameter of 1.6 or 3 mm.

For this test cell the 3 mm diameter K-type probe is used as there are relatively few, if any, rapidly fluctuating temperatures and is more robust. The screened cable is used in high interference and heat environments but is prone to breaking due to flexing. Through careful layout the PVC or fibre glass cables can be used, reducing the cost of the thermocouples.

2.7 Data collection and processing

The outdated method of recording data with a pen and paper on the appropriate form has not been completely eliminated as it is still used when facilities and budgets are limited, but the PC has automated this process in virtually all cases. Signals from analogue components are captured with the use of an analogue to digital (A/D) card as well as signals being sent to analogue card via a digital to analogue (D/A) card, enabling completely autonomous control. The most likely information to be recorded is torque, speed, fuel consumption, fluid temperatures and pressures.

After the test is completed the data will be contained in a file format specific to that software package. This generally does not allow the user to access and manipulate the data. The simplest solution is to import it into Microsoft Excel® or a similar program and manipulate the data into desired form or generate easy to read graphs. Data can also be imported into statistical packages to determine trends, means or variances. The data is now in such a form that it can be submitted in a report or reviewed to determine results of the test.

2.8 Summary

Biodiesel can be produced from a variety of raw materials, such as sunflower and canola oil, but the availability of the oils is limited so only a partial replacement of mineral diesel would be possible. The raw oils are converted to biodiesel through a transesterification reaction which results in two liquid phases. The glycerol is removed through settling and the remaining biodiesel is then washed to remove any dissolved glycerol. Relevant chemical properties, such as density and kinematic viscosity are discussed along with the relevant standards and their influence on the engine and combustion.

A brief overview of the main considerations when designing a test cell is given. Vibration and noise are not problematic, expect in the case of anechoic testing as they would influence the data set. The types of test cells and control room layouts were presented although an existing facility was used. Other design considerations, such as electrics, ventilation and air handling, water cooling, exhaust systems, dynamometers and sensors were also discussed.

3. Mechanical design and system integration

This chapter details the organization, layout, design, equipment and software of the test cell. Initially the test cell layout is discussed along with the engine and fuel supply. Thereafter the water cooling system is discussed followed by the operation of the dynamometer and the fuel balance. This chapter has been laid out in such a way that an operator can use it as a reference manual for each piece of equipment and where it fits into the global system.

3.1 Test cell layout

It was decided that the test cell hardware was to be housed in one of the unused existing test cells because the cells already have a water supply and ventilation system. Rooms 166 and 169 in the Mechanical and Mechatronic Engineering building were chosen as the control room and test cell as Room 169 is the only test cell with a dedicated control room.

This section gives a system layout and explains where each piece of equipment is mounted. Detailed explanations of the equipment and how they work are provided in later sections of this chapter, but a paragraph and discussion are first given to orientate the reader.

Figure 3-1 shows the first skeletal components, the test bed and the dynamometer. The test cell layout is shown in Figure 3-2 and a photograph of the completed test bed in Figure 3-3. In Figure 3-3 it can be seen the engine, tube-in-shell heat exchanger and dynamometer are bolted to the test bed with an 18” spot fan on either side providing air movement to prevent localised temperature build ups. The water supply inlets are located in the centre of the test cell on opposing sides. The AVL fuel balance, fuel pump and fuel filter are mounted 1m above the floor in the corner nearest the access hole. Most of the equipment required special brackets to be made in order to secure it to the wall or test bed. This was done in the departmental workshop. A gantry crane was manufactured (Appendix B) for in-cell lifting and is stored in the corner opposite the access hole so that it does not interfere with

movement in the test cell. The ventilation system is located 2.5m off the floor and is bolted to the wall inside the test cell, while the extraction duct is outside the cell with the vents approximately 3.5m from the floor.

Figure 3-1: Test bed and dynamometer

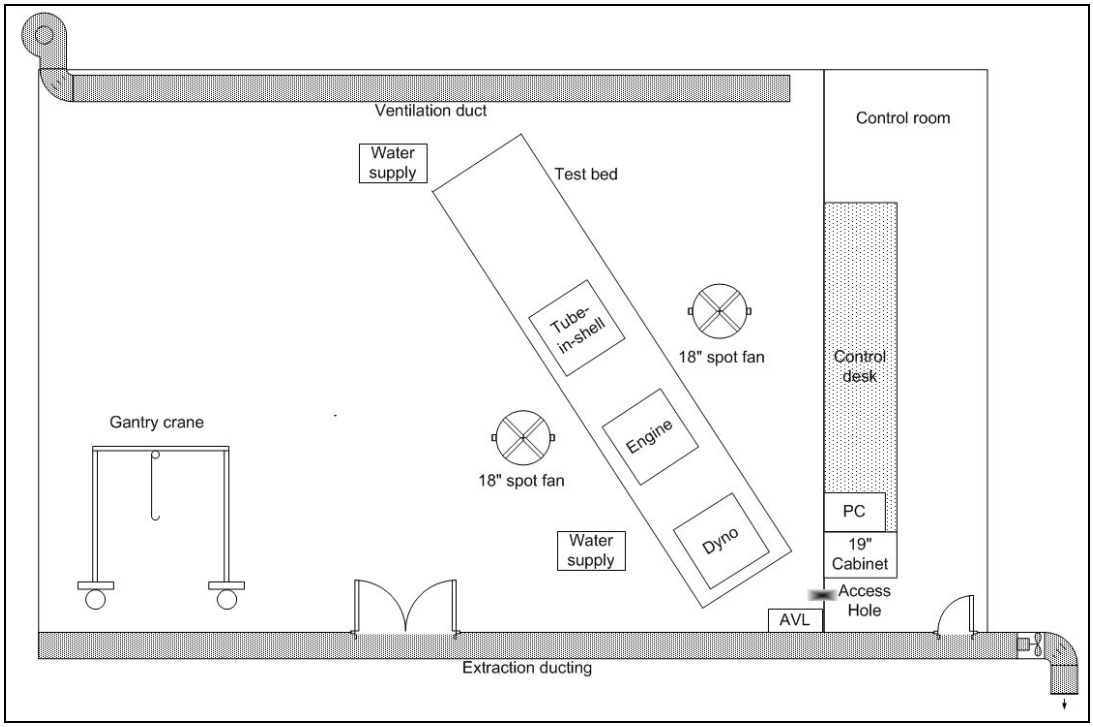

Figure 3-2: Test cell layout

Figure 3-3: Completed test bed

All the wiring between the control room and the test cell passes through the access hole (behind the dynamometer in Figure 3-3) located near the door of the control room. In the control room a 19” cabinet houses the PLC, dynamometer controller,

Honeywell temperature controller and the AVL fuel balance controller. A standard PC serves as the operators test cell interface.

3.2 Engine and fuel supply

An imported low cost second hand 2 litre Toyota 2C turbo diesel engine (Figure 3-4) was purchased and mounted on the adjustable engine stands with standard Toyota engine mounts. This is a 65kW, 176Nm engine that uses a mechanical injection pump with no ECU. It was chosen because of its price and commissioning simplicity.

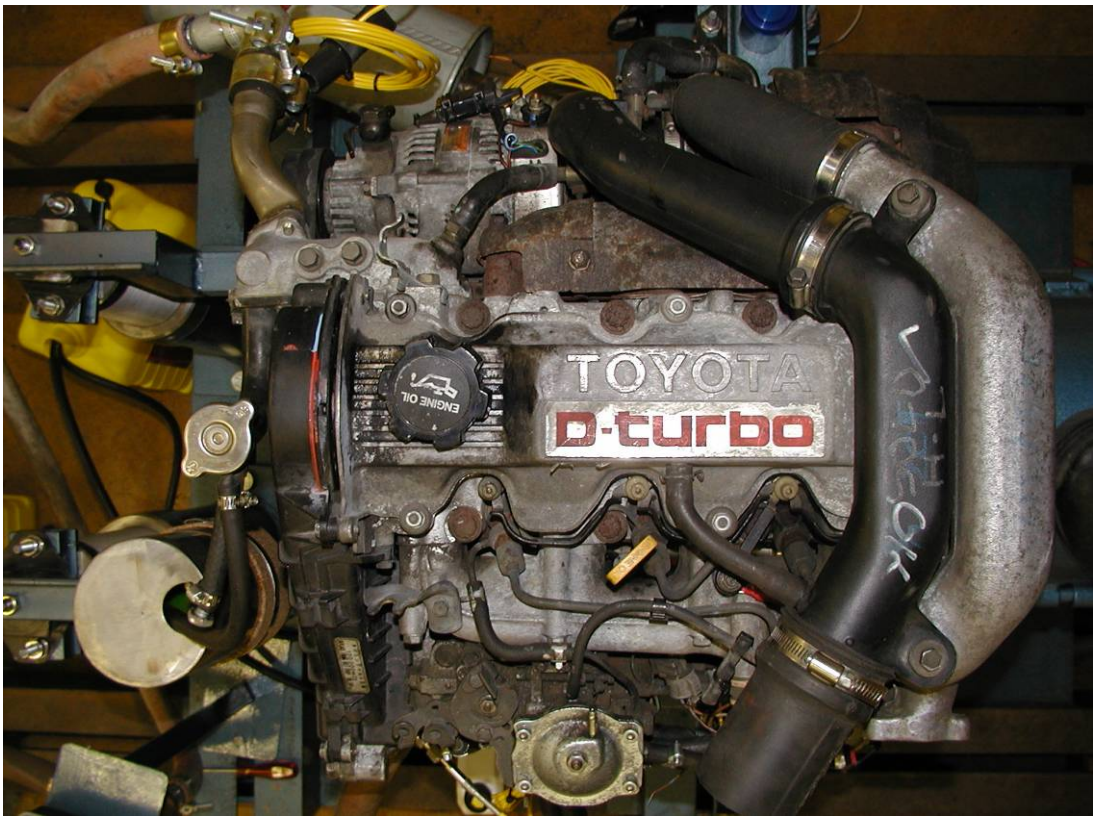

Figure 3-4: Toyota 2C turbo diesel

As different blends of biodiesel are to be tested, a large fuel tank is not needed so the biodiesel and its blends are stored in small portable fuel containers as any one test will not require more than 10l of fuel. The fuel is pumped into the AVL fuel balance via a filter using a Bosch fuel pump. The fuel pump relay is wired in parallel with the fill valve so that when the controller opens the valve, the pump will switch on and fill the AVL. An inline primer bulb was fitted to allow manual bleeding when the fuel is changed. The return fuel from the engine is returned back into the AVL. Figure

3-5 shows the schematic while in Appendix M the symbols have been replaced with photos.

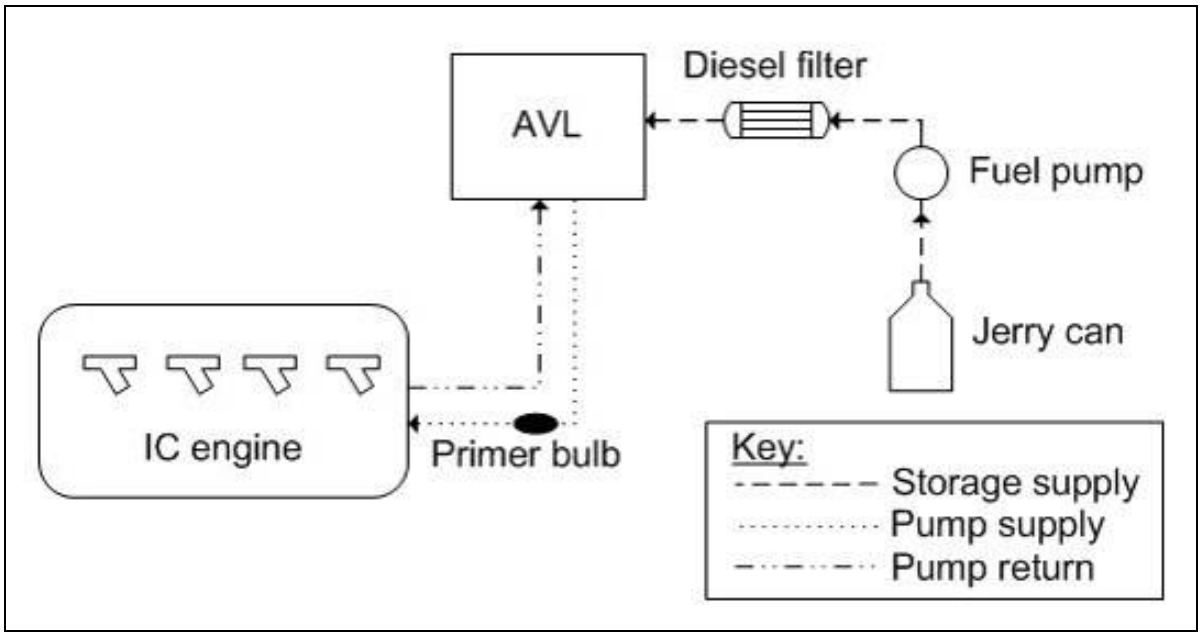

Figure 3-5: Fuel supply schematic

An exhaust system was manufactured in-house from 50mm stainless steel pipe and a standard Toyota diesel vehicle silencer (from the 2.4D series) and configured to vent directly into the extraction duct. This layout is not always suitable as ideally the exhaust should be the same as that on the vehicle, especially when there is a catalytic converter in the system and emissions are being measured. At present only reference testing is being done so the original exhaust system was not required, but it should be added in future research. Figure 3-6 shows the bottom half of the exhaust system and silencer and that the exhaust is terminated in the extraction duct (out of picture).

Figure 3-6: Exhaust system

3.3 Engine oil: pressure and temperature

A Wika Ecotronic 0-10 bar pressure transducer is used to measure oil pressure. The original motor oil light switch connects to the oil system with a 1/8” BSPF male connector. This switch was modified from a 1/8 BSPF male to 1/4 BSP male adapter (Figure 3-7), allowing a 1 m braided hose and pressure transducer to be connected (Figure 3-8 and Figure 3-9). The hose is required to reduce the temperature of the oil as the pressure transducer operates up to 85°C while the engine oil temperature can reach 110°C.

Figure 3-7: Oil pressure transducer adaptor

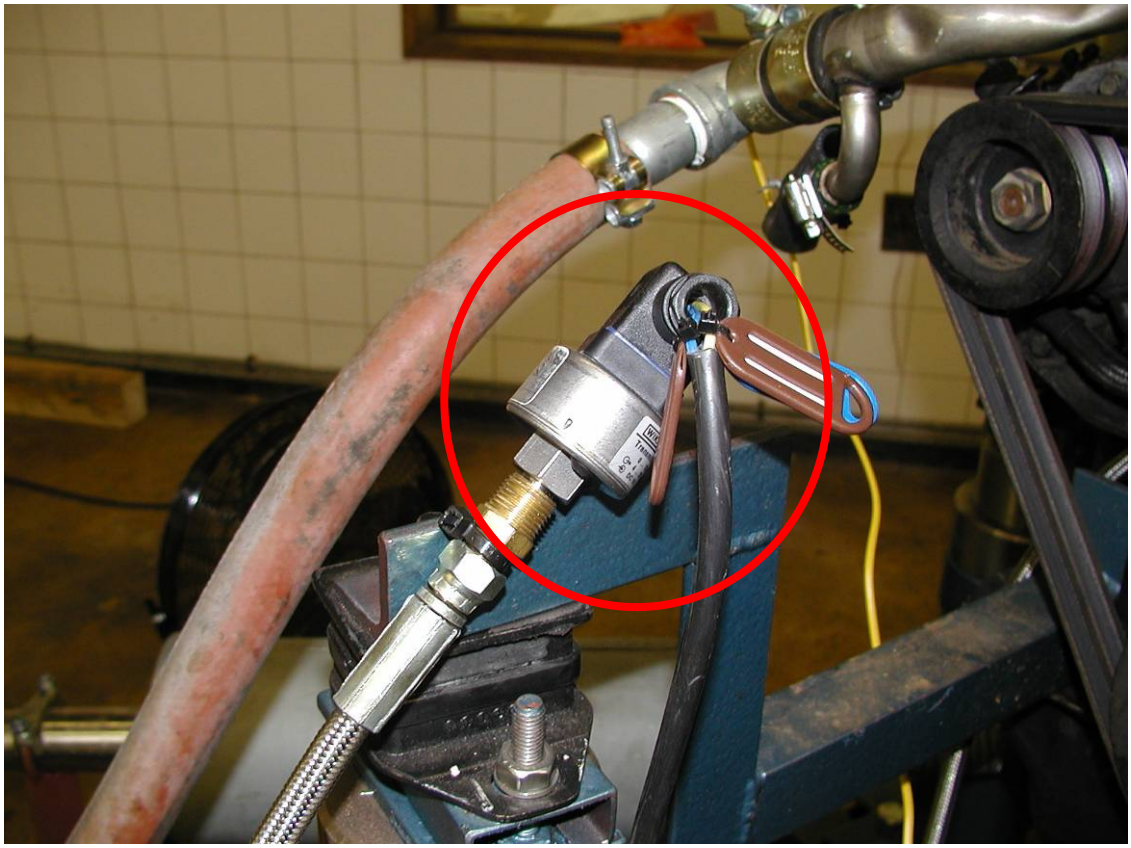

Figure 3-8: Oil pressure transducer connected to braided hose

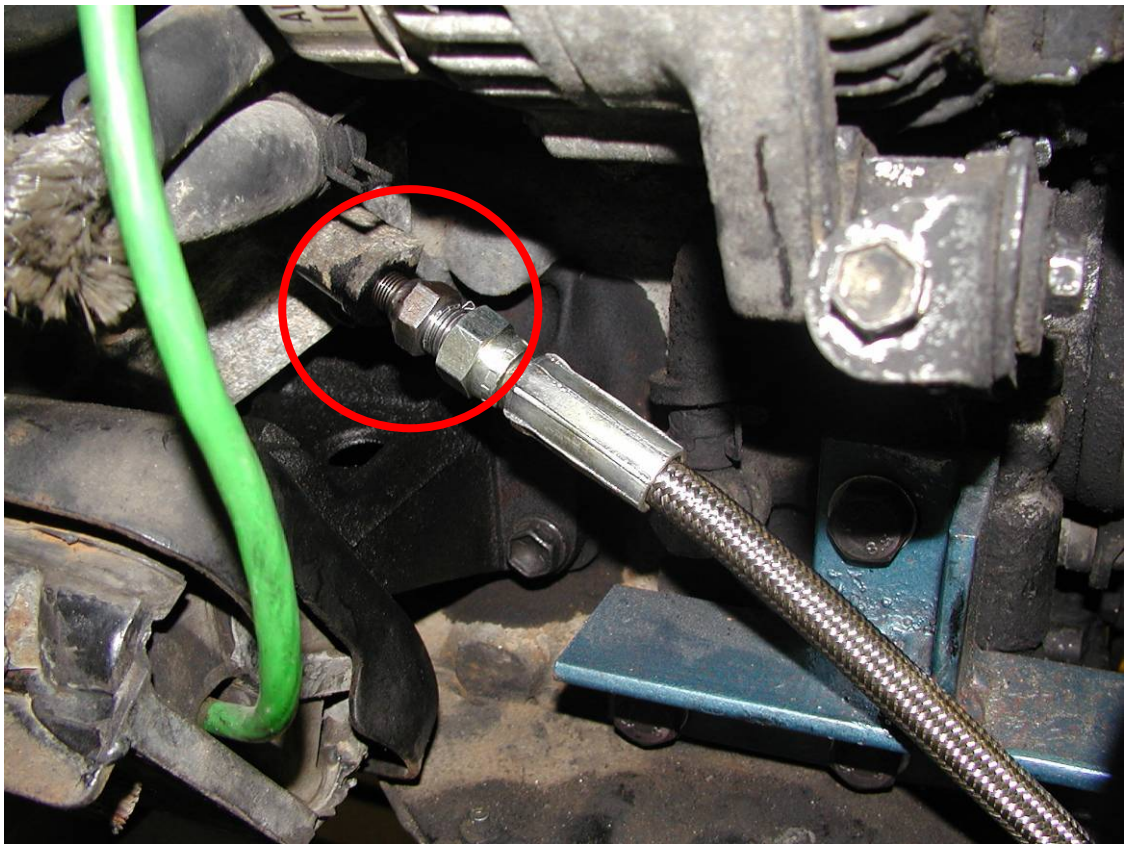

Figure 3-9: Oil pressure braided hose with adapter

A thermocouple is used to measure the oil temperature. The sump plug was drilled out and welded to a compression fitting so that the thermocouple can be placed in the engine oil. Figure 3-10 shows the thermocouple mounted in the sump plug.

Figure 3-10: Sump plug with thermocouple

3.4 Water supply and engine coolant

The water supply to the test cell and dynamometer and the coolant system are explained in this section.

3.4.1 Water supply

Water provides cooling for the engine and is the working fluid for the dynamometer. The water supply is a closed loop system to prevent wastage and to maintain a stable water temperature. The water supply consists of an underground storage tank to which the warm water is returned. From there is it is passed through a chiller (an evaporative cooling system) and then pumped via a PLC controlled centrifugal pump up to the holding tank on the roof of the Mechanical and Mechatronic Engineering

building. The water is then gravity fed to the inlet supplies in the test cell. This arrangement ensures that water supplied to the test cell is at a constant pressure of approximately 2 bar. Connectors and gate valves allow the flow in and out of the test cell and are located under protective covers. Figure 3-11 gives a schematic layout of the water supply.

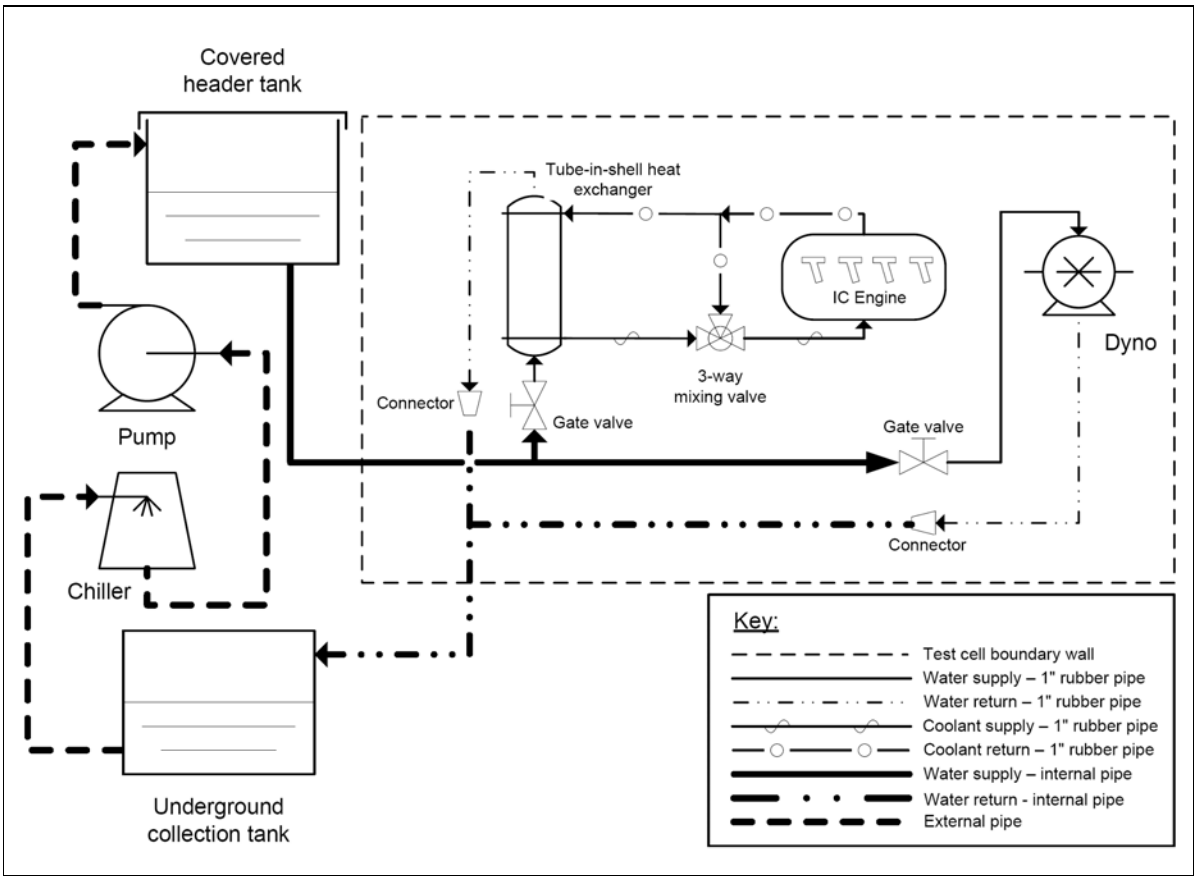

Figure 3-11: Water supply layout

In Appendix L is a similar schematic to that of Figure 3-11 where the symbols have been replaced with photographs. A centrifugal pump pumps the water to the header tank and is controlled by means of level switches. When the tank level is low the pump will operate until the upper limit is reached. There is a safety overflow should the pump fail to switch off. A Searle Bush chiller is used to cool the water. The engine coolant system is explained in the following section (see coolant supply and coolant return in Figure 3-11).

3.4.2 Closed loop engine coolant system

The test cell water supply cannot be used to cool the engine directly as it contains impurities and antifreeze cannot be added. To overcome this a separate closed loop system is created with a tube-in-shell heat exchanger, as shown in Figure 3-11. A closed loop system allows antifreeze to be added and enables the temperate of the engine coolant to the controlled. A radiator is not suitable for a hot test cell environment since it will not provide sufficient cooling due to the difficulty of moving large volumes of air through it. The volume of the coolant in the closed loop system is more than that on the standard radiator, so a larger radiator reservoir bottle was made to accommodate the water expansion.

In the closed loop system the inlet coolant temperature is kept at a constant 65°C to mimic the situation found in the case of water coming from a radiator. This is done by using a 3-way mixing valve that is controlled by the PLC. Without this valve the temperature would be around 20°C because of the large capacity heat exchanger and will not allow the engine to heat up quickly. The 3-way valve is shown in Figure 3-12 and its operation is discussed in section 3.7.4 as part of the discussion under controllers.

Figure 3-12: 3-way valve actuator

3.5 Dynamometer and fuel balance operation

A Schenck D360 water brake dynamometer is used to dissipate the engine load and an AVL fuel balance provides an accurate fuel consumption measurement. The operating and calibration procedure for this equipment is discussed in this section.

3.5.1 Dynamometer operation

The water brake dynamometer is used to dissipate work by transferring the energy to the water by means of a vaned rotor. The torque is controlled by varying the amount of water in the casing by means of a servo actuated valve. The heated water must continuously be removed and cooled before being pumped up to the header tank. The water is fed directly into the dynamometer, but because the pressure in the system is high, a gate valve was placed before the dynamometer to reduce the flow. The maximum inlet pressure for the dynamometer is 0.6 bar with a 1.6 m^3/s minimum flow rate (Schenck Pegasus GmbH, 2001). The flow through the gate valve is set by running the engine at full power and closing the gate valve until water outlet temperature is at 50°C, after which the handle is removed to prevent tampering. This setup optimises the dynamometer control because it allows the control value to be used over a wide part of its range.

There are four quadrants in which a dynamometer can operate: rotating clockwise producing or absorbing torque and rotating counter clockwise producing or absorbing torque. Figure 3-13 gives a diagrammatical layout of these four quadrants. Most water brakes can only operate in the first quadrant. Eddy current dynamometers can operate in the first two quadrants, while AC/DC dynamometers can be used in all four quadrants. Since a water brake is being used, only first quadrant operation is possible. This simplifies the control system since no power can be returned to the engine.

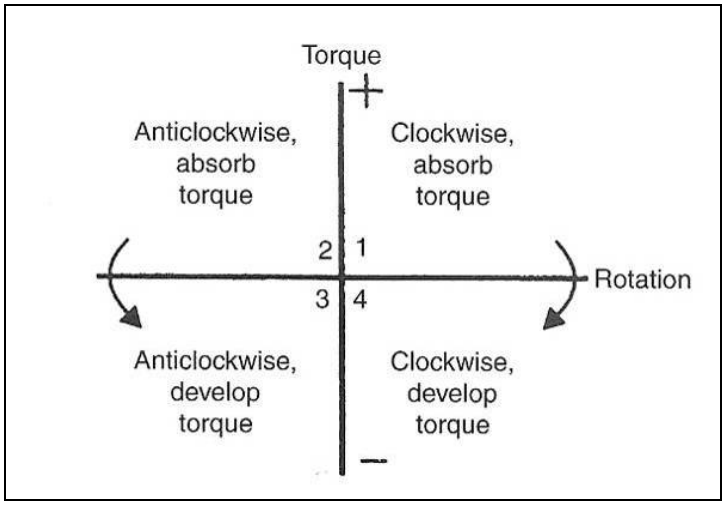

Figure 3-13: Dynamometer operating quadrants (Martyr and Plint, 2007)

A Cardan Shaft is used to connect the engine to the dynamometer. To reduce cost, an available shaft from a Löbro catalogue was reverse engineered. The desired properties of the couplings are determined by the engine parameters (speed and torque), and the dimensions of the CV joint and shaft were obtained accordingly. A Löbro Type 104 shaft was selected and the relevant catalogue pages are displayed in Appendix F. The CV joint and side shaft from a VW Microbus were chosen as they had suitable dimensions, although the shaft was 1mm thicker that the one specified in the catalogue. Holes where then drilled and tapped in the dynamometer and a spigot manufactured to connect the CV joint to the engine. The joints were then greased and bolted in place (see Figure 3-14, Figure 3-15 and Figure 3-16). A strong protective shaft housing was added to contain the shaft in the event of a failure. The protective housing was built from 16mm steel pipe (Figure 3-17).

The Cardan Shaft setup is an inexpensive for low speed applications. The disadvantage with this system is that there is no rubber coupling to absorb torque spikes and vibrations.

Figure 3-14: Dynamometer-CV coupling (see Figure 3-16 for complete coupling)

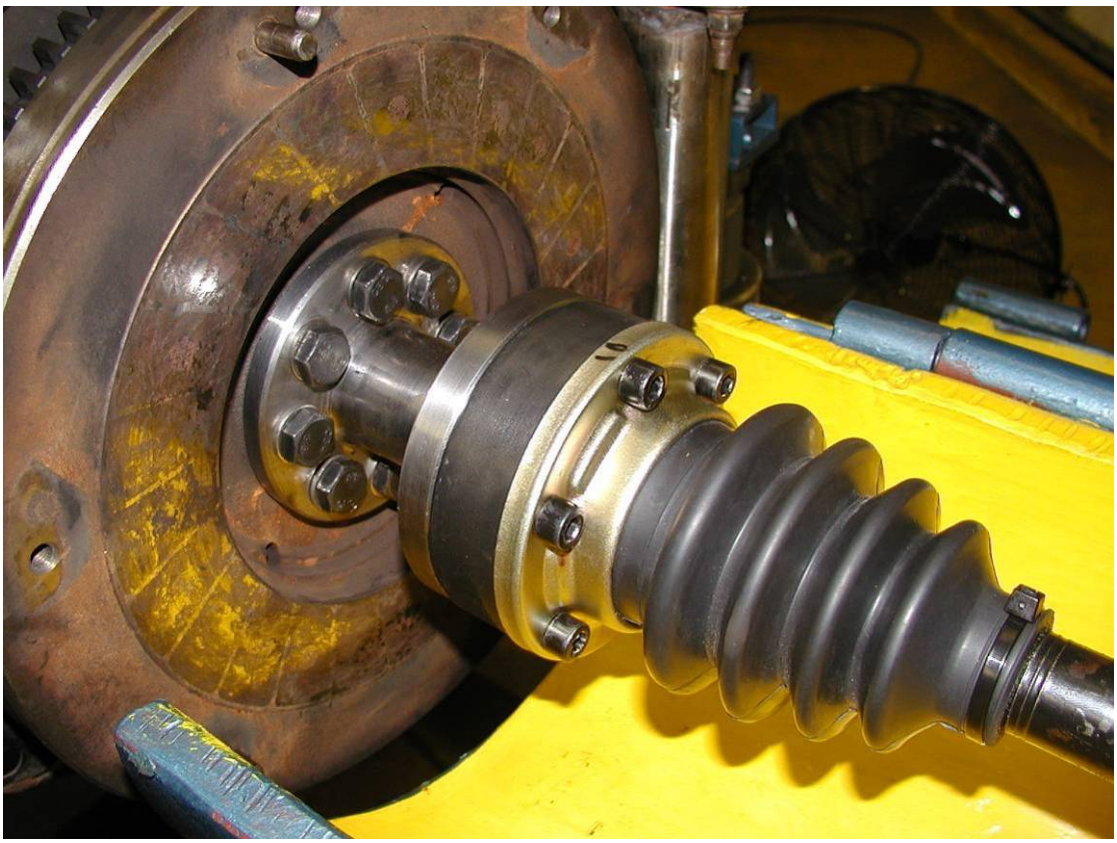

Figure 3-15: Engine-CV coupling (see Figure 3-16 for complete coupling)

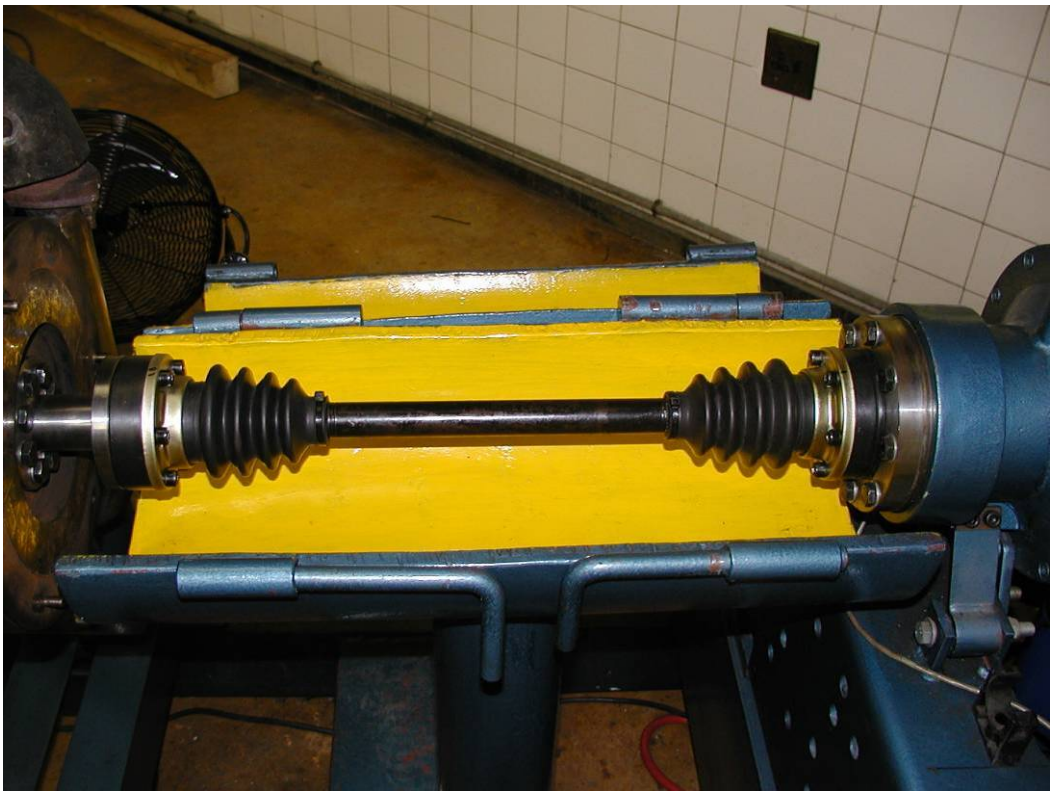

Figure 3-16: Cardan shaft coupling (Figure 3-17 shows the closed protective housing)

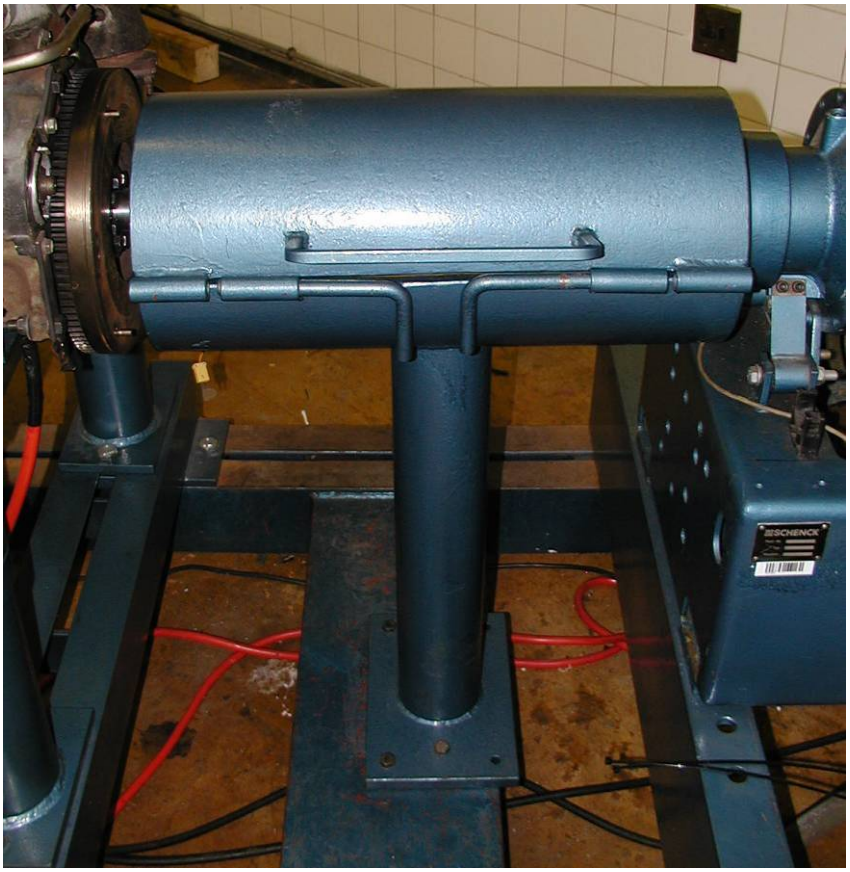

Figure 3-17: Shaft protector made from 16mm thick steel pipe

3.5.2 AVL operation

The AVL 7030 is a dynamic fuel balance that is used to measure the fuel consumption on a mass basis. The fuel consumption data is used in the calculation to determine the efficiency of the engine. The data can also be monitored and may warn the operator of an engine failure, indicated by a deviation in the fuel consumption trend. A vessel is mounted on blade springs and the fuel mass is measured by means of a capacitive bridge supplied with a 500Hz square wave signal. The capacity of the bridge branches are measured and then returned via an amplifier resulting in a linear relationship between differential capacity and output voltage. Blade springs are used in the fuel balance as they have no hysteresis. When the vessel is empty it is filled automatically by opening a fuel valve and is often gravity fed. As there is no header tank, this design replaces gravity feed by a Bosch fuel pump to fill the vessel. While the vessel is being filled the mass is changing and no measurement is possible. The AVL returns a zero reading for the duration of the filling. The return fuel from the engine is returned back to the AVL without influencing the flow reading. A photograph of the AVL with the covers removed in Figure 3-18.

Figure 3-18: AVL internal view of the vessel and electronics

The AVL is connected to a controller in the 19” cabinet and includes the following features: a fuel level display; settings for the time measurement increments; calibration instructions; type of reading (kg/h or g) and a 0-10V output for external readings. Since the fuel level is changing and the vessel is mounted on blade springs oscillations may occur causing incorrect readings. To prevent this there is a damping pot, but on taking delivery of the unit this was not filled to the correct level as oil had been spilled during transportation. To correct this, the remainder of the oil was drained and the damper was refilled with a single grade 10 weight oil (Castrol Fork Oil SAE 10W). This eliminated the oscillations and stable readings were obtained.

3.5.3 Calibration of AVL and D360

The AVL calibration of the controller is a simple step that can be done from the control room. The controller must be switched on in the following sequence, module 7030-F02 and then 7030-F01 to ensure that the processor starts correctly. When this is done the “CAL. WEIGHT” button on the controller must be held down for 10 seconds until a calibrated concentric weight has been lowered. The button can then be released removing the weight from the vessel. It is also important to verify that the gain and linearity are correct as the vessel operates between a full and empty state. The procedure and associated adjustments are clearly documented in the AVL user manual (AVL, 1984). The voltage output of the AVL is calibrated using a laboratory scale and a stop watch. Fuel is allowed to flow into the calibration container at various flow rates over the AVL’s operating range while the time is recorded. The mass of fuel is then weighed and the flow rate is determined by dividing the mass by the time. Table 3-1 shows the data recorded from which the AVL is calibrated.

Table 3-1: Recorded data for AVL calibration

	Low flow	Medium flow	High flow
Fuel (g)	287.00	316.20	517.20
Time (s)	97.00	49.00	36.60
Calculated flow rate (g/s)	2.96	6.45	14.13

The load cell of the dynamometer must also be calibrated with weights placed on a calibration arm. The calibration arms were manufactured in the workshop with the calibration setup is shown in Appendix C. When the controller is switched on a zero reading must be obtained or it must be adjusted to 0 Nm on the torque unit. The calibrations arms can then be bolted to the dynamometer, the weight tray added, and a counter weight used to adjust the torque reading to 0 Nm. 10 kg weights are then packed on the weight tray one at a time and the reading noted. Each kilogram corresponds to 10 Nm for the 1021 mm arm, so the reading can be adjusted accordingly. Once all the weights are present, they are removed one at a time and the readings rechecked to ensure that there is no hysteresis in the system.

The calibration certificates are stored in the “Test” file in the control room, along with the other calibration certificates and test results.

3.6 Ventilation

Ventilation in the test cell and control room is important because air is the medium through which excess heat, fumes and gasses are removed. An overview of the existing ventilation system is given in this section.

The inlet air comes in half way up the wall on the opposite side of the extraction duct. This flow arrangement is suitable as the air in the test cell is moved past the engine. A cross section schematic as viewed towards the control room is shown in Figure 3-19 to illustrate the flow of air in the test cell. As can be seen, the inlet is slightly above the engine so two floor fans (Figure 3-20) are added on either side of the engine to help move air over it and out the extraction duct.

In control rooms with emissions testing equipment, the power into the room must be calculated to check heat loading. If this is the case, ventilation or an air conditioning unit must be installed. For the BTF control room there are no large heat generators, so open windows or doors suffice.

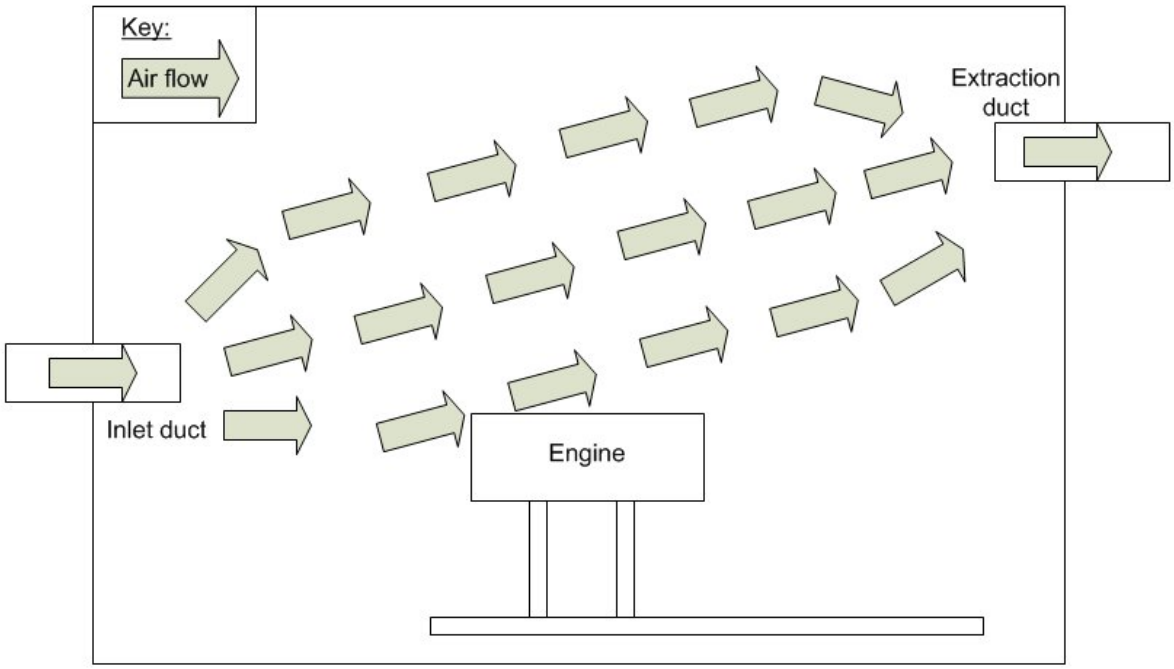

Figure 3-19: Test cell air flow showing air flow past the engine

Figure 3-20: 18" Spot fan for additional air movement

3.7 Wiring, sensors and electronics

The electronics and wiring for the test cell will be described in sections to simplify the explanation and understanding of the wiring diagrams. The pin labelling is consistent throughout so, for example if the label "*IN1+*" appears in separate diagrams, it refers to the same physical pin.
The labels should be interpreted as follows:

- Vps : Separate power supply connected to the mains
- Vdc : Power supplied by the PLC
- Vbat : Power from the battery in the test cell
- *Italics* : Pins on the PLC

The PLC (Allen Bradley Micrologix 1200) is used to sample all analogue and digital channels as well as providing the various voltage and current outputs. The PLC consists of the main 1200 module, a 4 channel analogue input module, a two input, two output analogue module and 3 thermocouple modules. Figure 3-21 shows the main 1200 module on the left with the 5 expansion modules on the right. The serial port on the PC is used to communicate with the PLC using the RsLinx® software. RsLogix® is Rockwell Automation® ladder logic software in which the PLC is programmed to perform the desired functions.

In this facility the majority of the programming and channel setup will be done via the PC and the software package called ETA® (see section 3.8.1).

The upper rows of connections of the 1200 module (Figure 3-21) are the inputs, in this case the only input used is allocated as the emergency stop. The bottom rows are the output relays used for the starter, glow plugs, 3-way valve actuator and the ignition. The first module's (2A2D in Figure 3-21) consists of two analogue inputs and one analogue output connected to the D360 controller and the other output controls the rack. The four analogue inputs (4A) are ambient pressure, relative humidity, oil pressure and fuel consumption. The three remaining cards (T1, T2 and T3) are coupled to the thermocouples. The pin connections for the PLC are shown in Appendix E and the wiring diagrams in Appendix K.

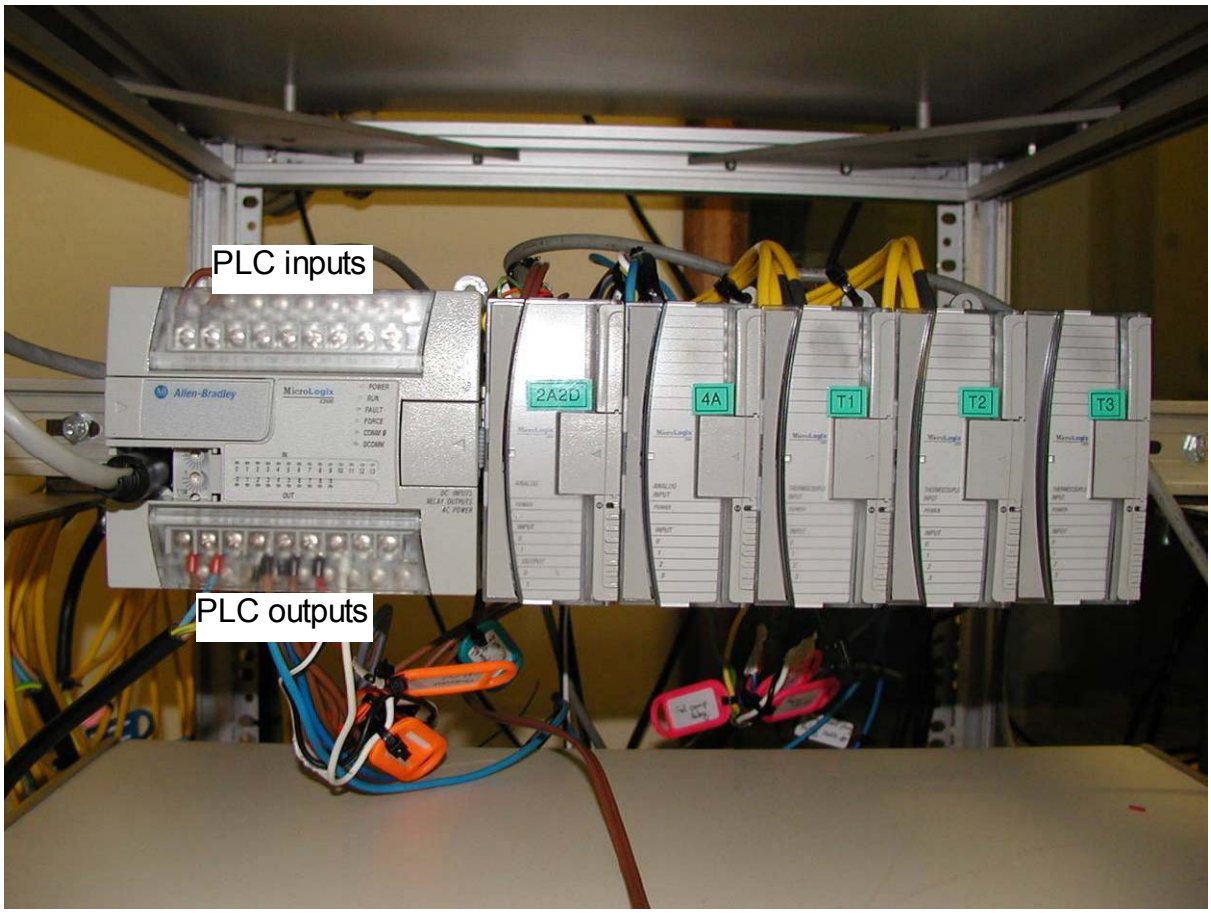

Figure 3-21: Allen-Bradley Micrologix PLC on the left with the 5 expansion modules on the right

3.7.1 Emergency stop and fuel relay

There is an emergency stop mounted in the middle of the desk within easy reach of the operator should a catastrophic failure occur. The emergency stop or e-stop consists of two contactors, one normally open (NO) and the other normally closed (NC) (see Figure 3-22). The NO contactor is connected to pin *IN0* and is a software interrupt. When the interrupt occurs the software will take the rack position to 0 and set the dynamometer to full load, stopping the test in the shortest possible time. This can damage the engine due to the shock loading of the dyno. The NC contactor is hard wired to the injection pump in the event of a software failure or if the PC hangs. The emergency stop wiring diagram is shown in Figure 3-23.

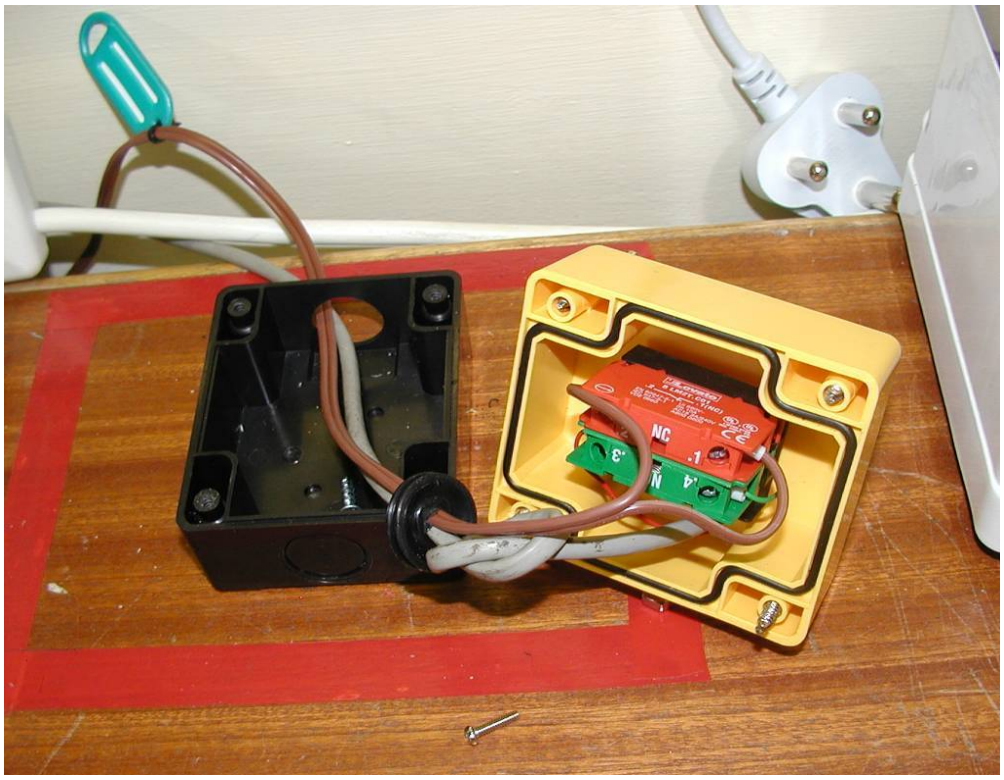

Figure 3-22: Emergency stop opened displaying contactors

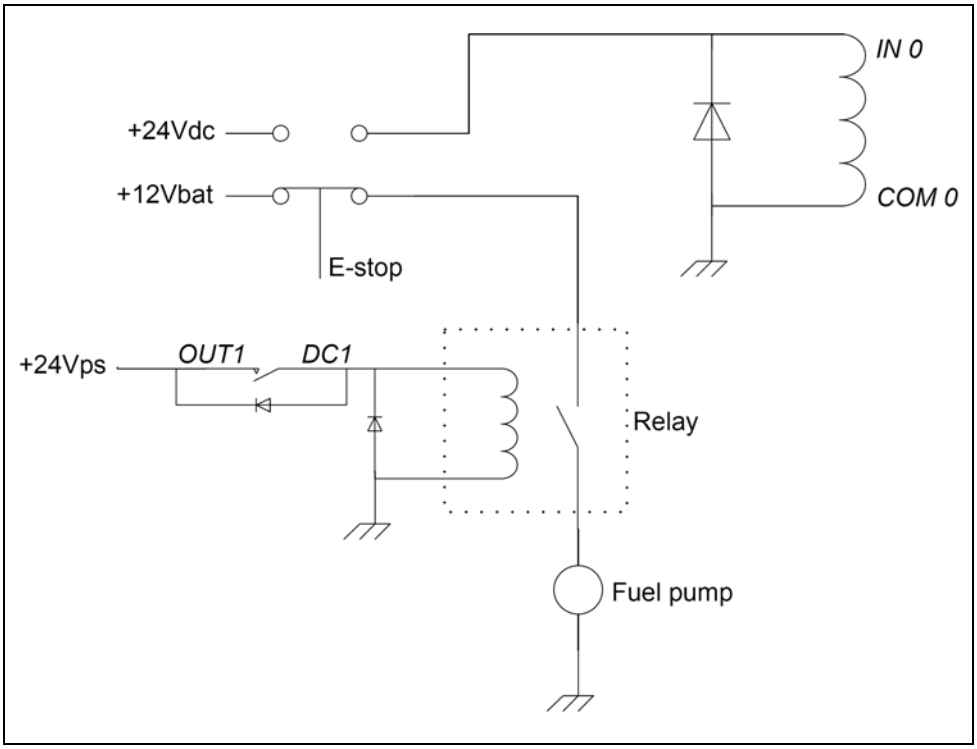

Figure 3-23: Emergency stop wiring diagram

The injection pump relay is energised from a 24V switch mode power supply (labelled: 24Vps). Pin *OUT1* is used to close the relay via a radio button in ETA to

activate the injection pump. This control is also used to switch the engine off. Flywheel diodes are placed over all the internal and external DC relay coils to prevent voltage spikes. The relay circuit is interlocked with the emergency stop and is shown in Figure 3-23.

3.7.2 Glow plug and starter relays

The glow plug and starter relays operate in a similar fashion to the fuel pump relay using pins *OUT2* and *OUT3* and “bounce back” radio buttons. When the engine has been started these buttons are deactivated to prevent them from being “pushed”. If the engine stops, the injection pump will have to be switched off and back on again to reset the buttons. The glow plug relay drives a larger relay located on the engine as the glow plugs can draw up to 70A (Figure 3-24). The diagrams for the starter and glow plugs are given in Figure 3-25 and Figure 3-26, respectively.

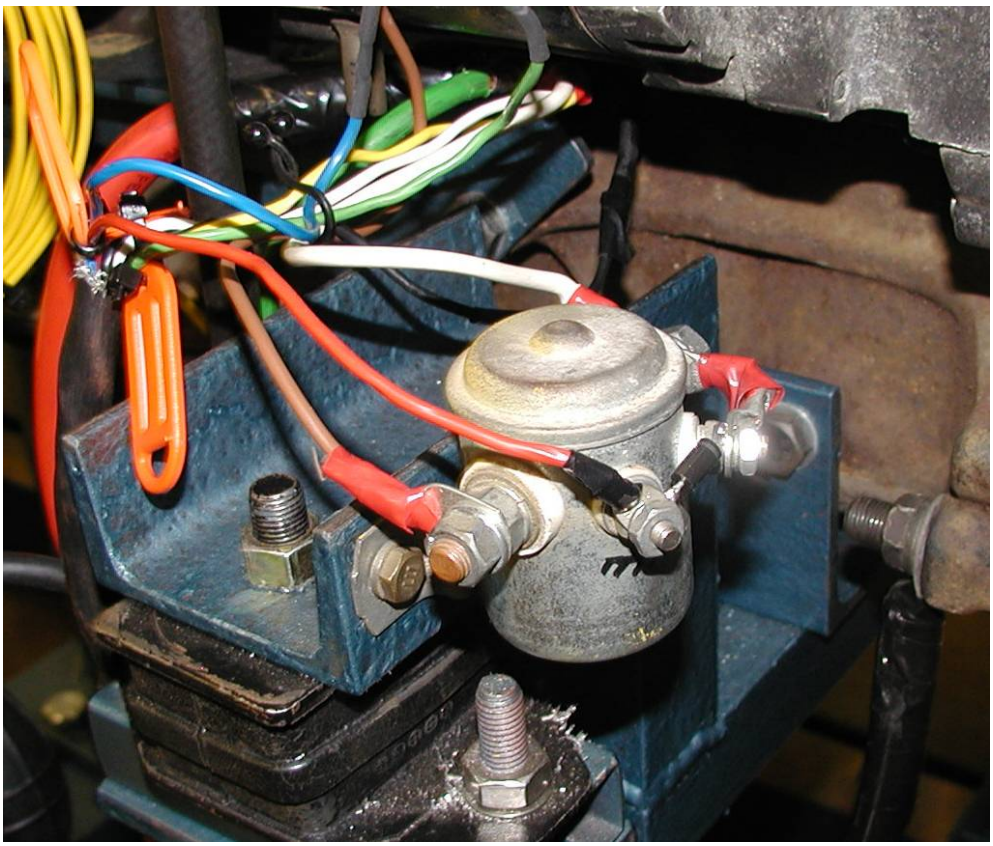

Figure 3-24: Glow plug relay

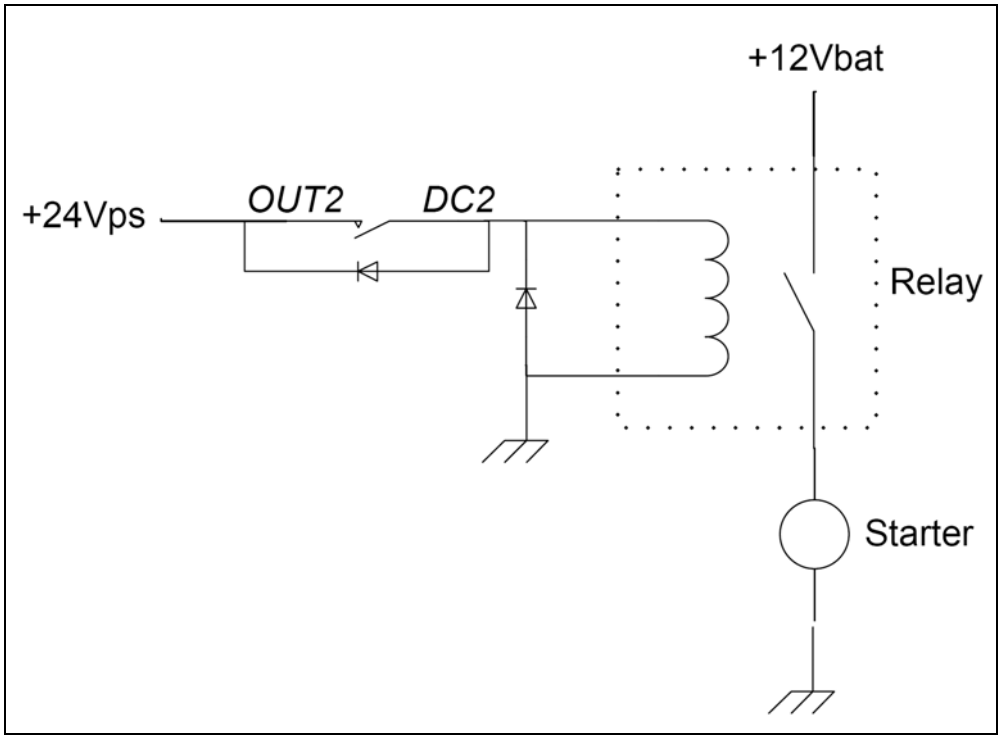

Figure 3-25: Starter wiring diagram

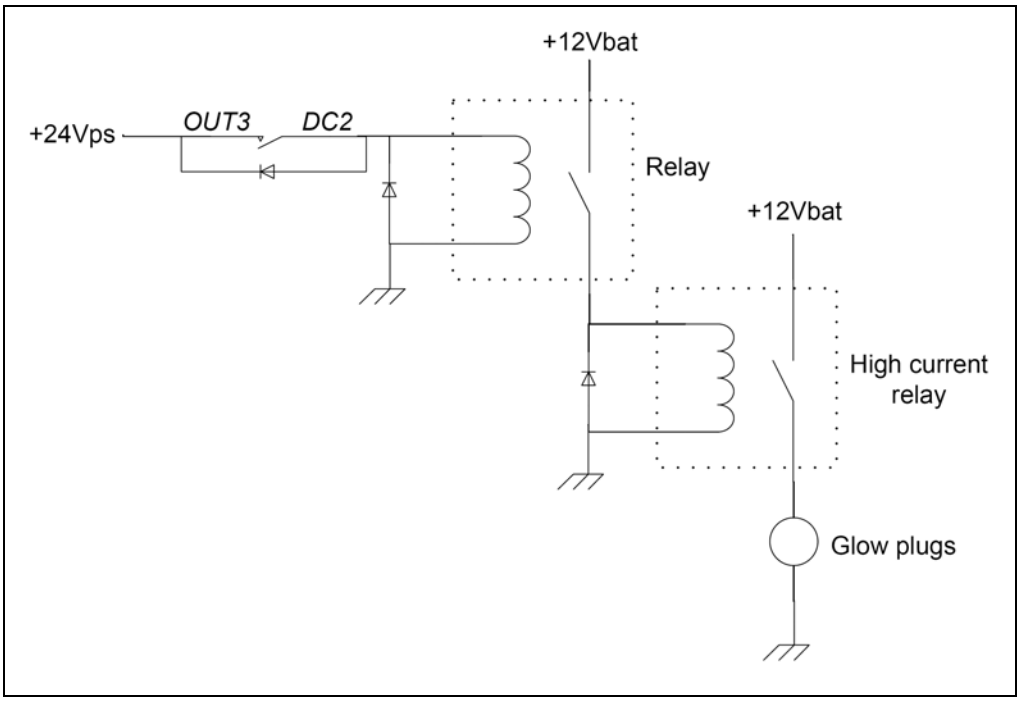

Figure 3-26: Glow plug wiring diagram

3.7.3 Rack controller

The rack controller allows the rack to be adjusted from the control room, essential for the automated test. Off-the-shelf rack actuators are expensive so an in-house design was implemented. This particular rack linkage on the Toyota engine allows a coupling directly on its shaft, eliminating the need for cables. A JR 8511 digital servo from a model shop was used to actuate the rack. The specifications are shown in Appendix D and the mounted servo is shown in Figure 3-27.

The servo operates on 5V DC and can draw up to 700mA depending on the load. A small switch mode power supply (labelled: 5Vps) was purchased to power the servo. Three wires have to be connected to the servo for it to operate: +5V (red), ground (brown) and a pulse width modulation (PWM) signal (orange). These colours are specific to JR servos and other manufactures will have different colour codes (see Figure 3-28).

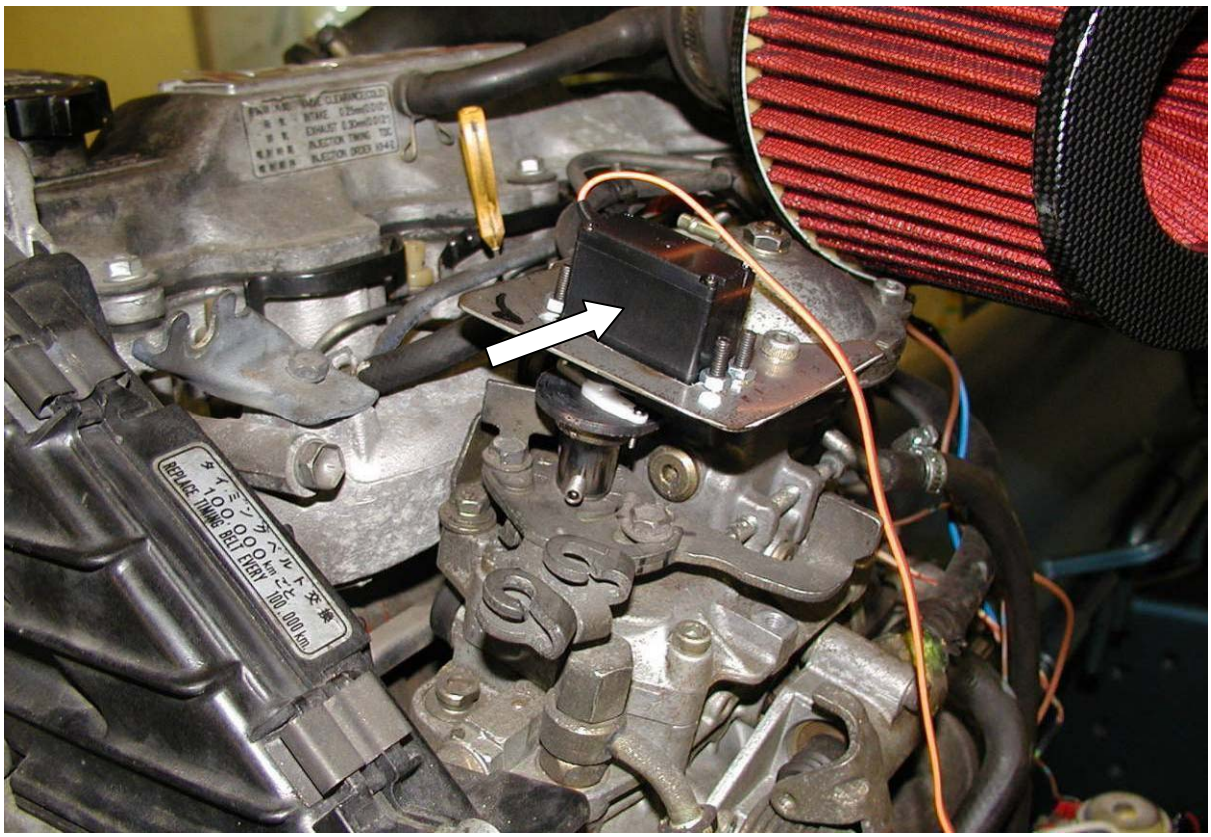

Figure 3-27: Rack servo

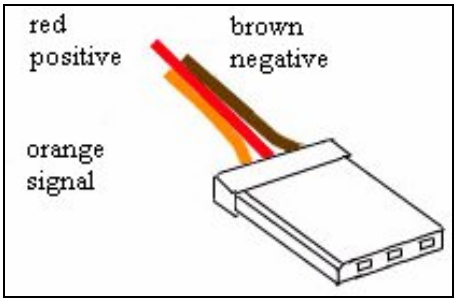

Figure 3-28: JR servo wiring (Venter, 2005)

The duty cycle of the 50 Hz PWM signal will determine the position of the servo. The servo operates as follows: with a 600µs pulse width the servo will be at -45^0 and with a 2.4 ms pulse width at $+45^0$. The servo is able to rotate at a speed of 0.19 s/60^0, which is faster than the reaction time of the engine. As the PLC is not able to generate a PWM output, a custom built modulator was obtained to convert the 0-10V analogue voltage to a PWM signal (see Figure 3-29). The converter has a voltage divider circuit to limit the input to 5V and a PIC microprocessor to generate the PWM signal. The power supply and servo grounds are connected in the analogue to PWM converter box. Figure 3-30 shows the servo and converter wiring diagram.

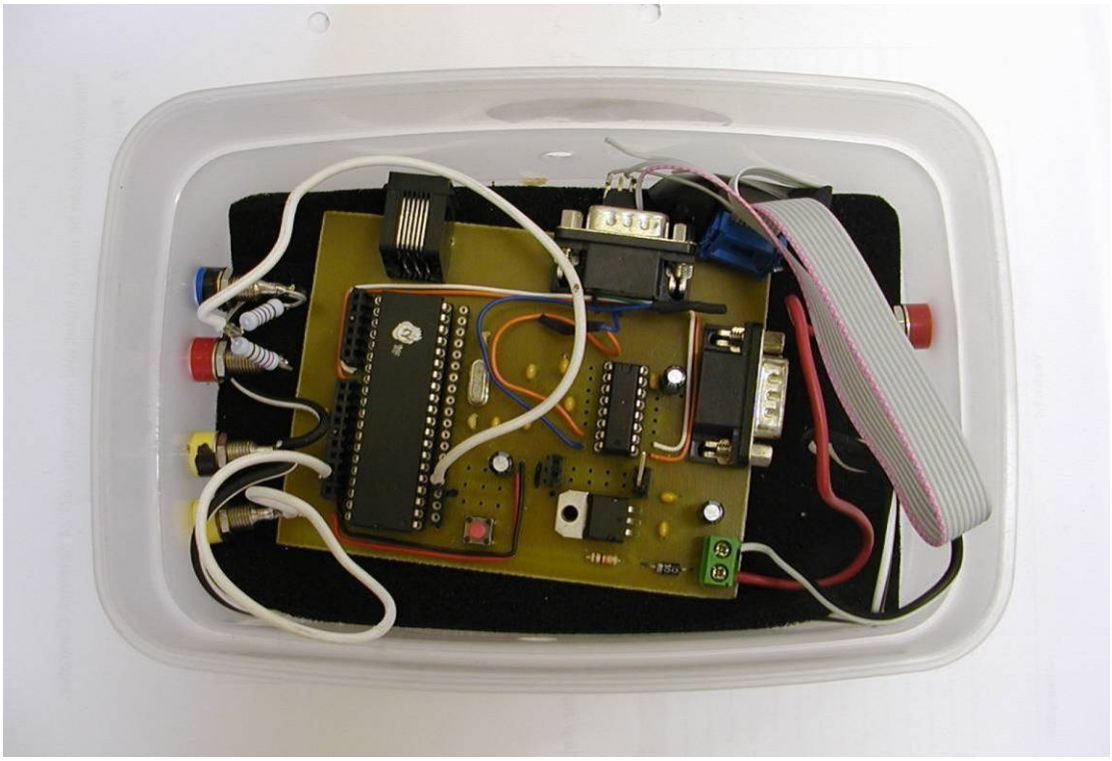

Figure 3-29: PWM module to modulate a 0-10 V output voltage

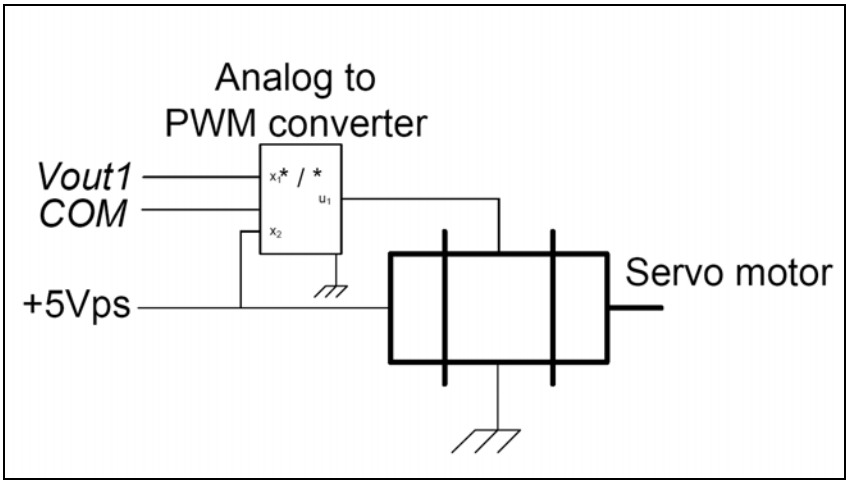

Figure 3-30: Rack servo wiring diagram

3.7.4 Water temperature controller

The function of the water controller has been discussed in section 3.4.2 which shows that the mixing of cold and recycled hot engine coolant is set by the position of the mixing valve. The mixing valve actuator is driven by a bi-directional 24Vac motor without feedback or settable limits, but the actuator has internal protection to protect the motor should the mixing valve limits be reached. The available 3-way valve was originally part of a stand-alone Honeywell temperature controller but has been modified to allow PLC control. The Honeywell controller is still used to power the actuator and allow communication between the PLC and actuator.

There is only one supply wire to the actuator, but two return wires that connect to a common point. Depending on which of the two return wires is connected to the common point; the actuator will open or close. The PLC connection with the two inputs and one common was chosen for this purpose. The internal wiring of the actuator is shown in Figure 3-31 and the wiring to the PLC in Figure 3-32.

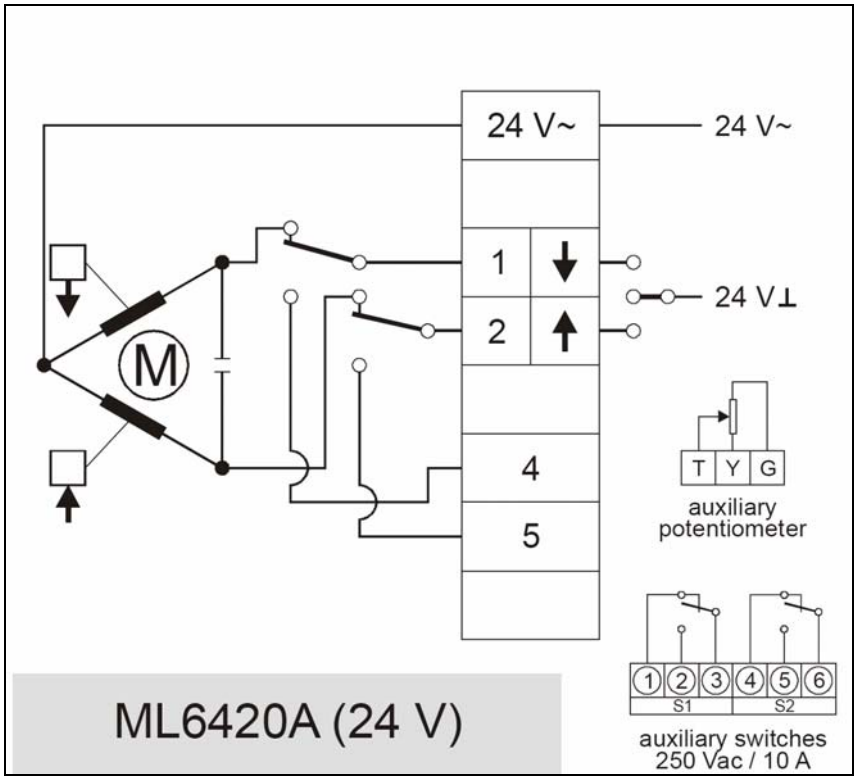

Figure 3-31: Actuator internal wiring (Honeywell, 2006)

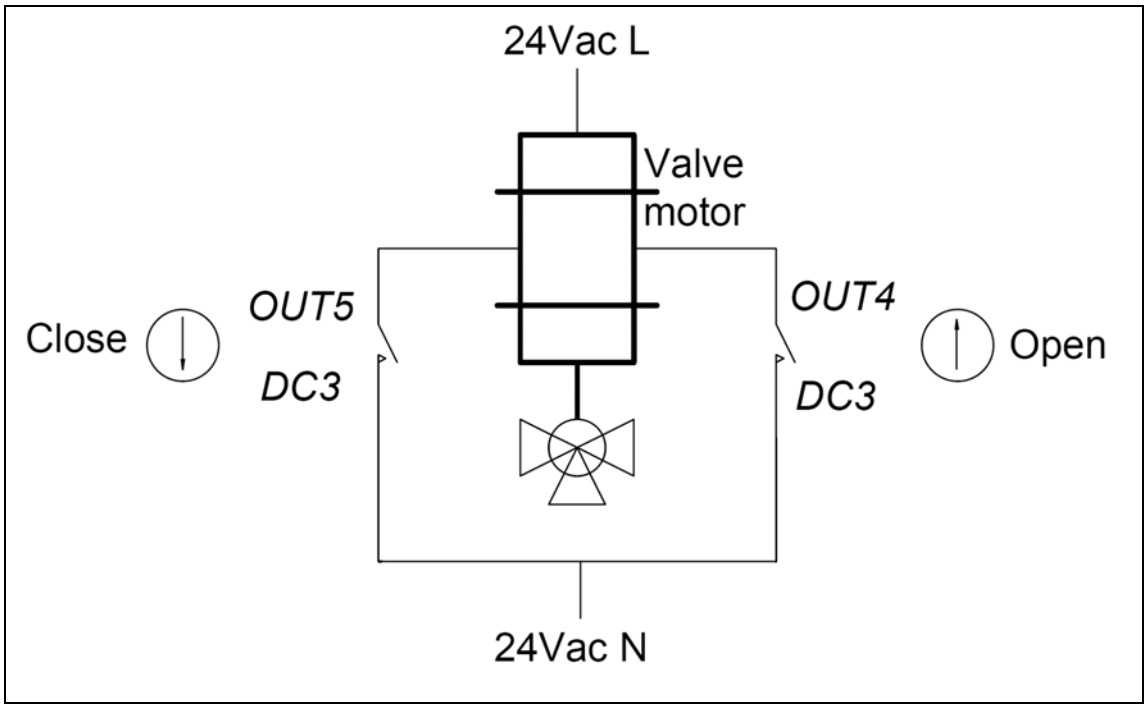

Figure 3-32: 3-way valve actuator wiring diagram

3.7.5 Ambient Measurements and AVL

The barometric pressure, relative humidity and temperature are recorded and used in a correction factor to compensate for day to day changes in ambient test cell conditions. An in depth explanation of the compensation is given in section 3.8.1. The sensors were mounted on the wall in the test cell and a protective plate was made to prevent physical damage and limit the effect of direct heat radiation. Figure 3-33 shows the sensors and Figure 3-34 shows the protective covering.

Figure 3-33: Ambient pressure sensors; barometric pressure on the left, humidity probe above right and the thermocouple

Figure 3-34: Ambient sensor's enclosure

The Vaisala PTB 110 barometric pressure transducer has a 0-5V output and is connected to *IN2+*. The input channels on the PLC are normally set for current input, so this channel had to be reconfigured. The configuration switch is located on the top of the module and switches the input from the 4-20 mA to a high impedance sensing one. The Vaisala HMD60 relative humidity sensor is a 4-20mA sensor and the thermocouple to record temperature is wired onto the thermocouple card.

The connections to the 4 channel input card are shown in Figure 3-35.

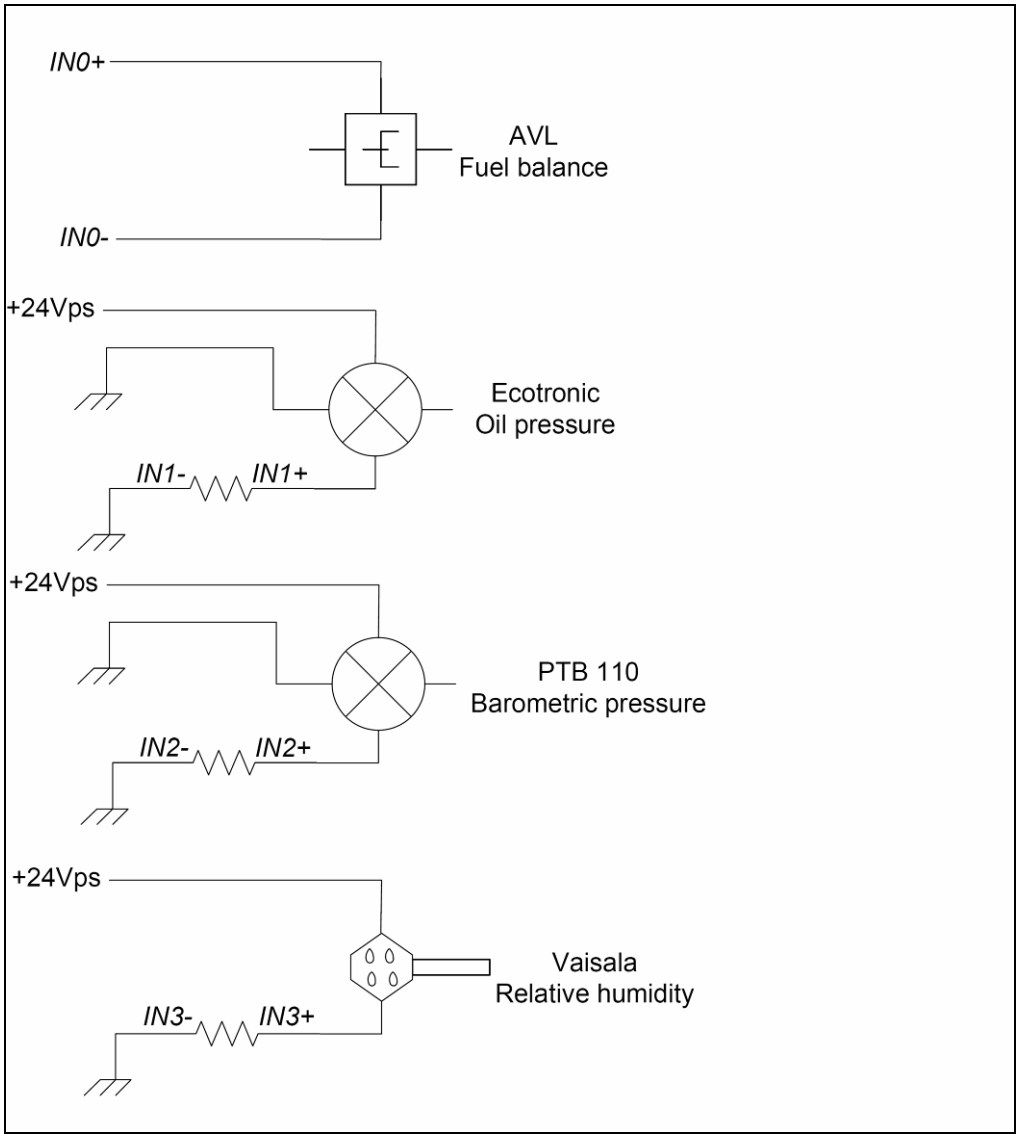

Figure 3-35: 4 Channel analogue inputs

3.7.6 Schenck D360 controller

Similar to the AVL the D360 controller has 0-10V torque and speed outputs. The D360 also requires a voltage input to control the stepper motor which sets the torque. The D360 input voltage is written out from the PLC pin *Vout2* and its output voltages sensed on *IN0+* and *IN1+* (see Figure 3-36).

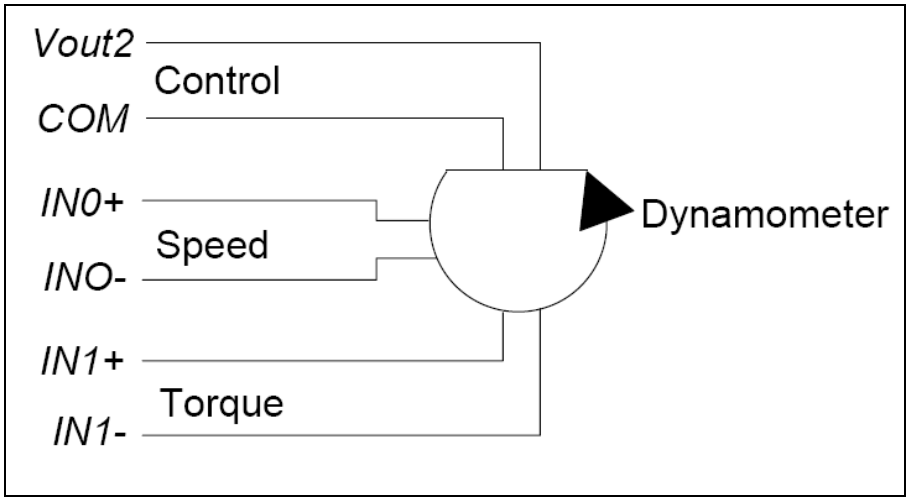

Figure 3-36: Dynamometer wiring diagram

3.7.7 Wall mounted junction box

A junction box was installed on the wall between the control room and the test cell to facilitate engine changes. The box is permanently wired with screened cable to the PLC. When the engine is changed the sensors can simply be plugged into or out of the junction box as needed. The engine has been instrumented with thermocouples to record various temperatures: Inlet and outlet water, oil, exhaust, inlet air and dynamometer temperatures. The junction box also provides for the rack servo and oil pressure transducer to be readily unplugged. The junction box is shown in Figure 3-37 and the wiring for the thermocouples in Figure 3-38.

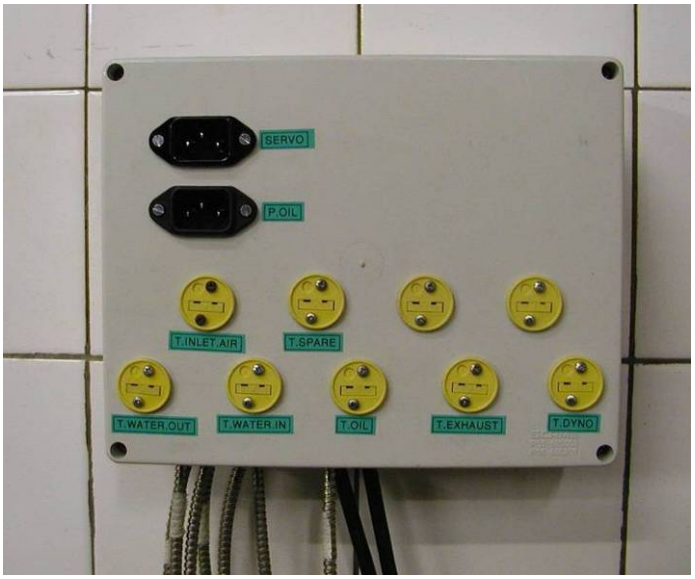

Figure 3-37: Junction box

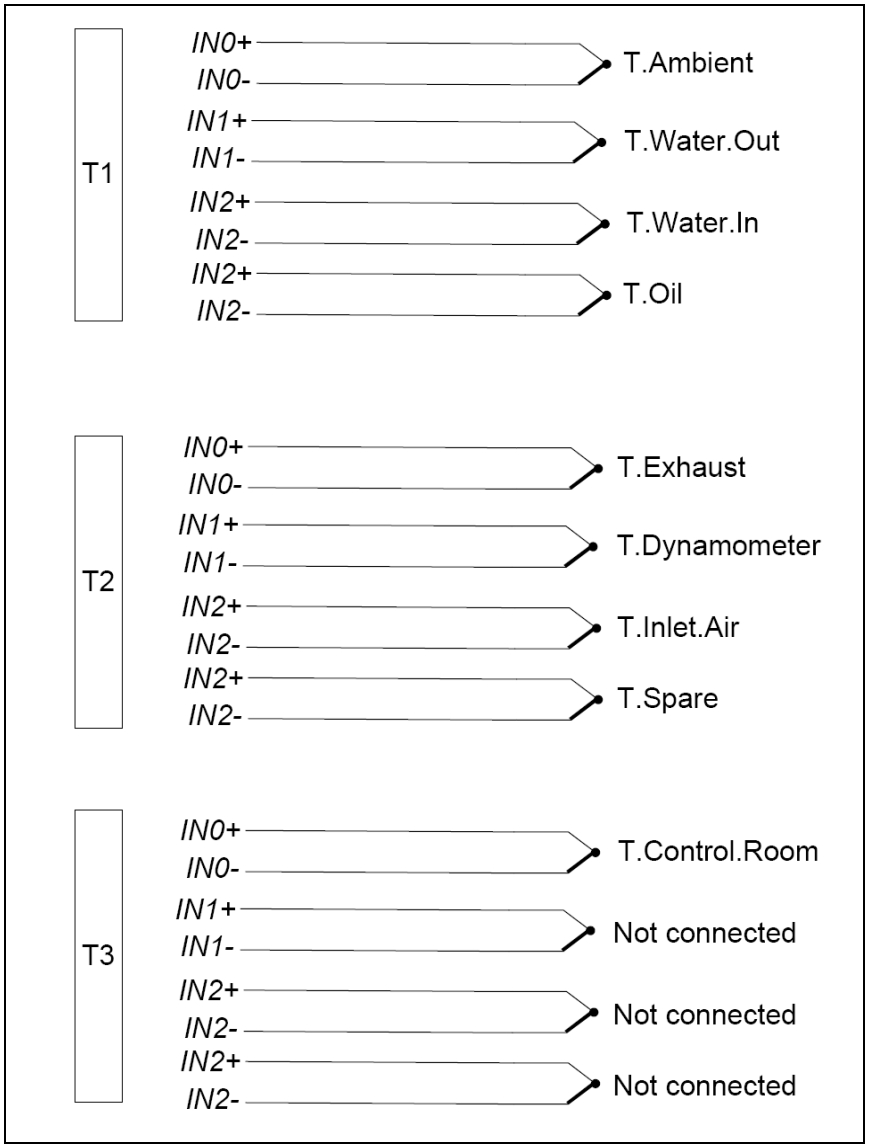

Figure 3-38: Thermocouple wiring

3.7.8 19” Cabinet

The PLC, controllers, power supplies and wiring are located in a 19” cabinet in the control room. Each wire in the cabinet has been labelled for future reference and each connection to the PLC has been documented. The cabinet contains the following from top to bottom: PLC, Honeywell controller, AVL controller, Schenck torque unit and the Schenck controller. The equipment in the cabinet has been labelled in Figure 3-39.

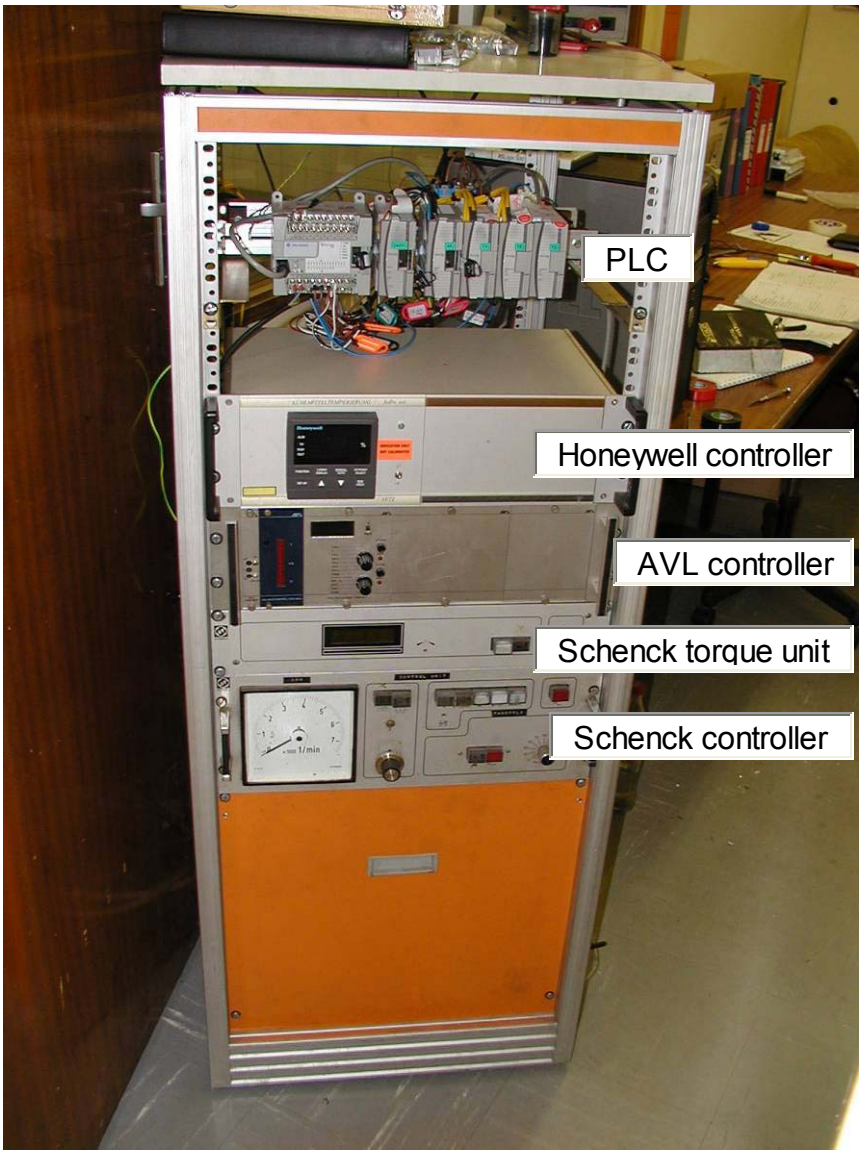

Figure 3-39: 19" Cabinet

3.8 Software and automation

Two software packages were installed and commissioned; ETA and the RSLogix 500. They are programmed to sample and store the data and to automate the test cell.

3.8.1 ETA

ETA or 'Engine Test Automation' was written in Delphi to integrate different manufacturer's hardware into a single environment. ETA communicates with the hardware by using various PC's communication protocols. The data written to the

hardware is typically used for controlling the test while the data received from the hardware is used to determine the state of the test or for test analysis. The data obtained is stored for future access in ETA's database. Listed below are some of ETA's features (CAE, 2005):

- Alarms
- Automated test control
- Sensor calibration
- Equation editor
- Signal conditioning tools
- Data logging, analysis and reporting

ETA was purchased from and installed by CAE (Cape Advanced Engineering). ETA controls the engine test, monitors conditions and records the data. After installation ETA was set up for the type of test that is going to be performed, namely an autonomously run performance curve.

The PLC is linked to ETA using the RSLinx software. Initially there was a problem interfacing the two components as the freeware version of RSlinx does not support DDE communication. The full version of RSLinx was purchased which solved this problem. Data are passed on the DDE client between ETA and the PLC by setting up input (labelled: N10) and output channels (labelled: N14). Dedicated digitals channels must be created by using an analogue base channel and addressing the individual bits. When the channel has been created the desired output is specified on the PLC. All data are passed as raw values from zero to 32767 (equivalent to 15 bits). For example a 10 V output from ETA is passed as 32767 to the PLC which then converts it back to 10 V.

It is not always possible to have a test cell at reference conditions; therefore a correction factor can be implemented if ambient temperature, barometric pressure and relative humidity are known. The EEC correction factor is implemented in ETA. The formula for this calculated factor is obtained from the 80/1269/EEC European Union agreement for adoption of uniform conditions for vehicle and parts testing. Equation 3 is the implemented equation for a turbo-charged engine.

$$\alpha = \left(\frac{990}{P_s - P_d} \right)^{0.7} \times \left(\frac{T}{298} \right)^{1.5} \qquad \textbf{(Eq. 3)}$$

Where:

P_s = Pressure at the engine air inlet (mbar).

P_d = Vapour partial pressure determined by multiplying the relative humidity with the saturation vapour pressure with is a function of temperature (mbar).

T = Ambient temperature in Kelvin.

ETA's user interface was optimised for the Biofuel Test Facility. The interface is shown in Figure 3-40 and each channel is labelled followed by an explanation.

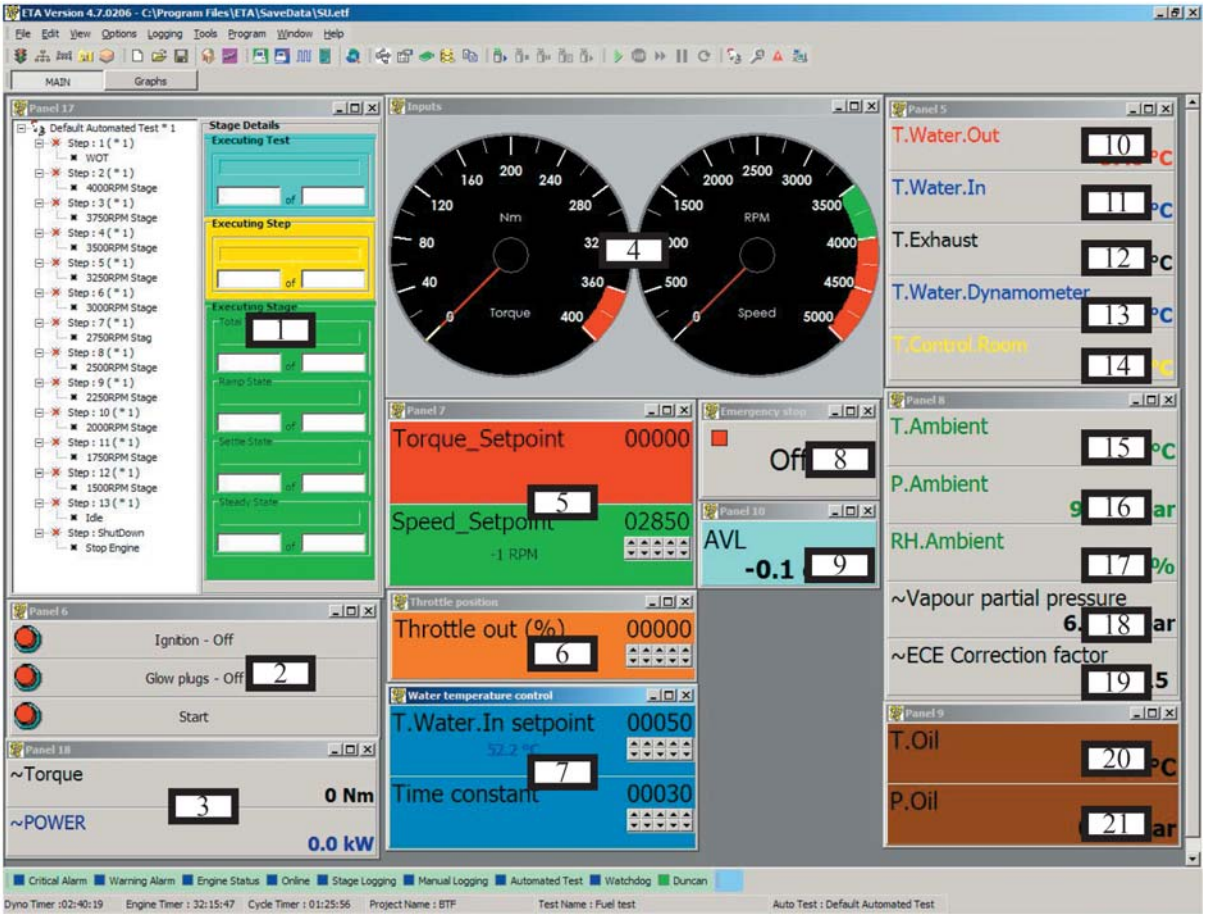

Figure 3-40: ETA's user interface, labelled for explanations

1. Automated test sequence

2. Radio buttons for starting and stopping the engine.
3. ~Torque: The measured torque multiplied by the correction factor is the value recorded and used for calculation (Nm). ~Power: ~Torque x Speed x 104.72 x 10^{-6} (kW)
4. Dials for graphical indication of torque and speed
5. Speed/Torque control and their set points
6. Rack control: 0% is closed and 100% is fully open
7. Set point for the water temperature controller (°C) and time constant for the water temperature controller.
8. Emergency stop button indicator to notify user if the emergency button is depressed.
9. AVL: Fuel consumption in g/s obtained from the AVL dynamic fuel balance.
10. T.Water.Out: Engine coolant temperature on the outlet side of the engine (°C).
11. T.Water.In: Engine coolant temperature on the inlet side of the engine. This value is also fed back into the water temperature controller and is used to determine one of the controllers time constants (°C).
12. T.Exhaust: Exhaust gas temperature. As there is no shielding over the thermocouple it is only an indication of the exhaust gas temperature. The exact temperature is not required as comparative testing is being done (°C).
13. T.Dynamometer: Water temperature on the outlet side of the dynamometer (should never exceed 50°C).
14. T.Control.Room. Temperature measured behind the 19” cabinet in the control room (°C).
15. T.Ambient: Ambient temperature in the test cell (°C).
16. P.Ambient: Ambient pressure (bar).
17. RH.Ambient: Ambient relative humidity (%).
18. ~Partial vapour pressure: Calculation of the partial saturation vapour pressure used in the EEC correction factor (mbar).
19. ~Correction factor: Correction factor calculated to compensate for the change in ambient conditions according to the EEC specification.
20. T.Oil: Oil temperature in the sump (°C).
21. P.Oil: Oil pressure in the crankcase (bar).

When the graphical user interface (GUI) has been created, each channel can be calibrated in ETA by creating a trend line from two or more points. The thermocouples were calibrated with a Unomat Druk calibration unit. The thermocouple is replaced with the Druk that simulates a temperature so the channel can be adjusted accordingly. Pressures are also calibrated with the Druk calibration unit. The speed pickup on the dynamometer has 60 teeth so 1 Hz is equal to 1 RPM. A signal generator can therefore be substituted for the speed pickup and the speed input calibrated. Torque and speed outputs where calibrated while the engine was running and the signal should be the inverse of their respective input channels, which can be used as a validation check. The Schenck dynamometer calibration procedure was followed as explained in section 3.5.3 and the trend line recorded. Screen shots of channel calibration are shown in Appendix G for each type of channel.

ETA's "User Administrator Manual" was printed, bound and stored in the test cell. It gives in-depth explanations on creating channels, automated tests and using ETA.

3.8.2 PLC ladder program

The PLC firmware was programmed in RSLogix 500 and is subdivided into three sections. The MAIN program runs continuously and calls the two subroutines; IN and OUT.

The IN ladder samples the channels on the PLC (temperature and analogue inputs) and then passes them to ETA as a N10:x value. The N99 buffer is reserved for the digital inputs while the other channels are from N10:0 to N10:13. The ladder code is shown in Appendix H and Appendix I and is coded according to the specific expansion modules.

Similar to the IN ladder, the OUT ladder places the values from ETA onto the PLC. The N14:99 buffer is reserved for the digital outputs (injection pump; starter and glow plugs) while N14:1 and N14:2 are for the voltage outputs. In order to switch the Schenck controller between torque and speed mode the relevant pin must be

grounded and the torque or speed output channel selected. This was implemented with a timer to prevent both pins being grounded at the same time. The ladder logic is shown in Appendix H.

The program code for the water temperature controller had to be programmed in the PLC as ETA does not facilitate on/off control. As it is an output, it is coded in the OUT ladder, but shown in Appendix I separately for clarity. A partial controller was implemented, with adjustable set points and system time constants, through ETA. The set point is the desired engine coolant inlet temperature and the feedback is from T.Water.In. The difference between the set point and the actual value is scaled and used to determine the time that the valve must be open or closed. The system is then allowed settling time according to a system time constant.

3.8.3 Test program

Torque or speed mode can be selected by clicking on the “bumpless control” in ETA (see number 5 in Figure 3-40). In torque mode the user defines the torque set point and rack position. This is used mostly for emissions testing and will only be used when such equipment is available. When speed mode is selected the speed set point is set and the control system varies the torque until the set point is reached. A performance curve utilises speed mode control and generates a curve as follows: the rack is set to fully open and then measurements are taken at 250 RPM intervals. 250 RPM intervals were chosen as enough data points are generated to obtain a performance curve while keeping the time and cost of the test to a minimum. The test sequence steps are executed automatically in ETA:

- Full rack
- 4000 RPM to 1500 RPM
- Idle
- Engine off

The ramp time and settle time for each of the 4000 RPM to 1500 RPM steps was set to 5 and 10 seconds respectively, after which the data were recorded for 10 seconds to allow averaging. In the idle state the engine runs at 1000 RPM for one minute to

maintain oil pressure while the turbo spools down and for uniform cooling of the blades. The ignition is then switched off.

The data are stored in ETA's data base and can be exported to a .csv file to allow the user to manipulate the data post acquisition.

3.8.4 Backups and storing data

An image of the hard drive is stored on a removable USB storage disk. Should a failure occur, all data and programs can be reinstalled.

Data from tests and calibration certificates are printed and stored in a labelled file in the control room and organised according to the date of the test. Electronic copies are available in the C:\BTF\Test directory.
The "User manuals" file in the control room contains all the manuals for the equipment in the test cell and in the control room. Items are filed alphabetically.

3.9 Summary

As with any design there are teething problems and limitations. The basic hardware for the test cell was installed along with the various sensors and software. During the first test an overheating problem was solved and a perceived anomaly in a power curve was examined and resolved (section 4.2). The implemented test cell can measure performance and fuel consumption but not having emissions testing equipment is a limitation. Emissions testing is important for industry but less so for student research. The data obtained from testing were within boundaries, test work on the biodiesel commenced.

4. Fuel testing and results

The following section presents results from fuel and performance testing. These results are used to evaluate the performance of the test cell and draw conclusions with regards to the performance of biodiesel compared to that of mineral diesel. Tables with the data can be found in Appendix N.

4.1 Test fuel properties

The biodiesel used for testing was donated by The Biodiesel Centre in Durbanville and was manufactured from waste vegetable cooking oil sourced in the Western Cape. A sample of the biodiesel was sent away for chemical analysis at Bioservices CC and yielded the following results (Table 4-1).

Table 4-1: Biodiesel properties from chemical analysis

Analysis	**Specification: SANS 1935:2004**	**Result**
Appearance		Clear
Density @ 15°C (kg/l)	0.860-0.900	0.893
Viscosity @ 40°C (mm^2/s)	3.5-5.0	7.91
Flash point (°C)	120 min	Fail
Calculated cetane index	51 min	49
Sulphated ash (%)	0.02 max	0.025
Water content (%)	0.05 max	0.08
Acid value (mg KOH/g)	0.5 max	0.78
Iodine value (mg I/g)	140 max	69.5
Free glycerol (%)	0.02 max	0.041
Total glycerol (%)	0.25 max	3.44

As can be seen from Table 4-1 it is not a high quality biodiesel because only the iodine and density properties are within specification. This fuel should not be used for prolonged periods in the engine as it could cause corrosion damage due to the high water and acid content and the high viscosity may damage the injector pump.

However, normally these shortcomings are negated when the biodiesel is blended with mineral diesel in low ratios.

Ultra low sulphur diesel (ULSD) was used as the comparative base line to which the biodiesel would be compared. The biodiesel was also mixed with ULSD in the following biodiesel:ULSD diesel ratios: 5%; 10%; 15%; 50%, also known as B5, B10, B15 and B50. The blending was done on a volumetric basis in 20 litre fuel containers which can easily be interchanged during testing. Pure biodiesel was run directly from the 20 litre shipping containers after which the fuel system was flushed with mineral diesel.

4.2 Problem solving and commissioning

There were two problems discovered during the first autonomous test; the engine was over heating and there was a power curve dip anomaly near the top of the power curve. After these problems were solved (see section 4.2.1 and 4.2.2) the test cell was commissioned.

4.2.1 Engine over heating

During the first tests, the engine was over heating with the water temperature approaching boiling point, resulting in the test having to be terminated. The exact cause of this problem was not known as the engine was within its temperature limit at high revolutions but would heat up at lower RPM's. It was suspected that the water pump was functional but the frictional losses in the system were too high. The water system was therefore disassembled and inspected internally for restrictions and the coolant outlet hose tail was found to be damaged causing a restriction in the flow. A replacement part was designed and manufactured. The old hose tail with the restriction is shown in Figure 4-1 and the redesigned item in Figure 4-2. The thermostat was another possible cause of restriction in the flow, so it was removed. The engine was then run at full power and reached 63 ^{0}C, which is too cold for normal operating conditions. Various size orifice plates were inserted instead of the thermostat until the engine ran at the correct temperature.

Figure 4-1: Damaged coolant outlet pipe limiting flow

Figure 4-2: Redesigned coolant outlet pipe

4.2.2 Perceived anomaly in the power curve

It was discovered at the top end of the power curve that there was a slight decrease in power at 3750 RPM (Figure 4-3). The decrease in power could be a characteristic of the particular Toyota engine, but there is also the possibility that it was a test cell error.

To investigate this anomaly it was decided to introduce a constant offset in the cell torque measurement. If after mathematically compensating for this offset the resulting power curve was unchanged the source of the anomaly is considered part of the motor and is not introduced by the test cell. The dynamometer was therefore loaded with a fixed weight to give an offset of 174 Nm and then 274 Nm and the test repeated. This introduces a shift in the operating point.

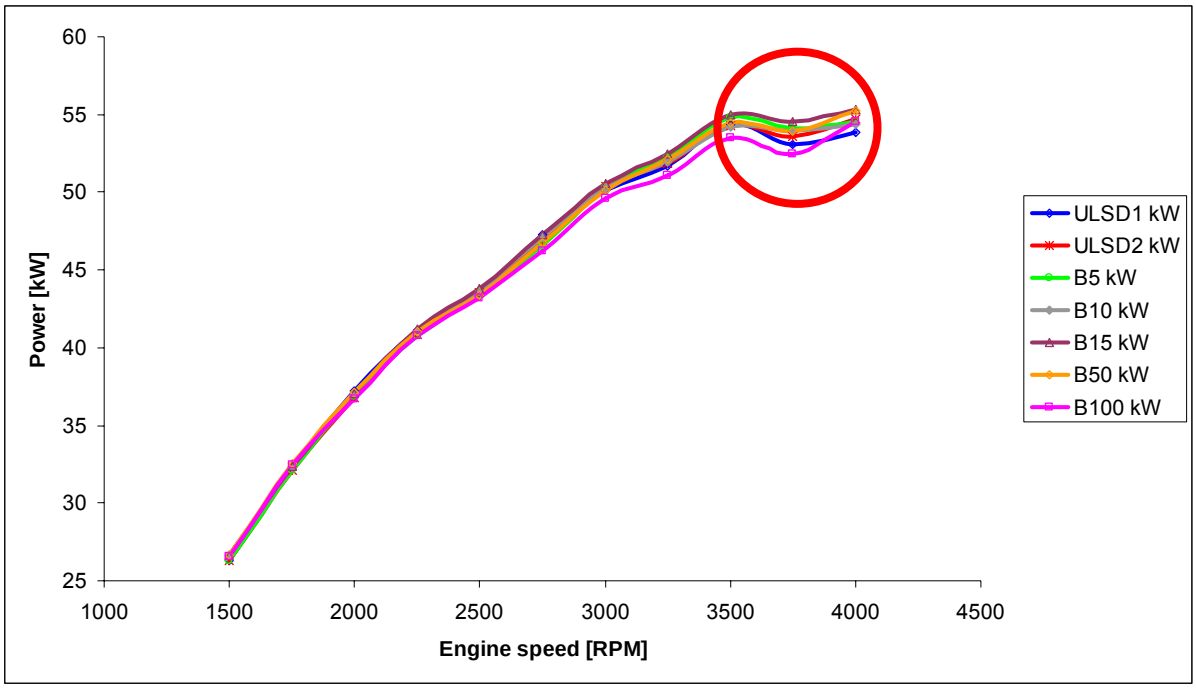

Figure 4-3: Anomaly in power curve

The test was repeated and yielded the same results with the anomaly in power curve at 3750 RPM. The torque preload was subtracted from the readings before the graph was plotted so the results could be compared (Figure 4-4). The axes were also kept the same so the results can be compared with Figure 4-3. Since a preload was added it required the control system to adapt and move away from the previous

operating point. The results show that the dip in power is a characteristic of the engine at 3750 RPM and not of the test cell.

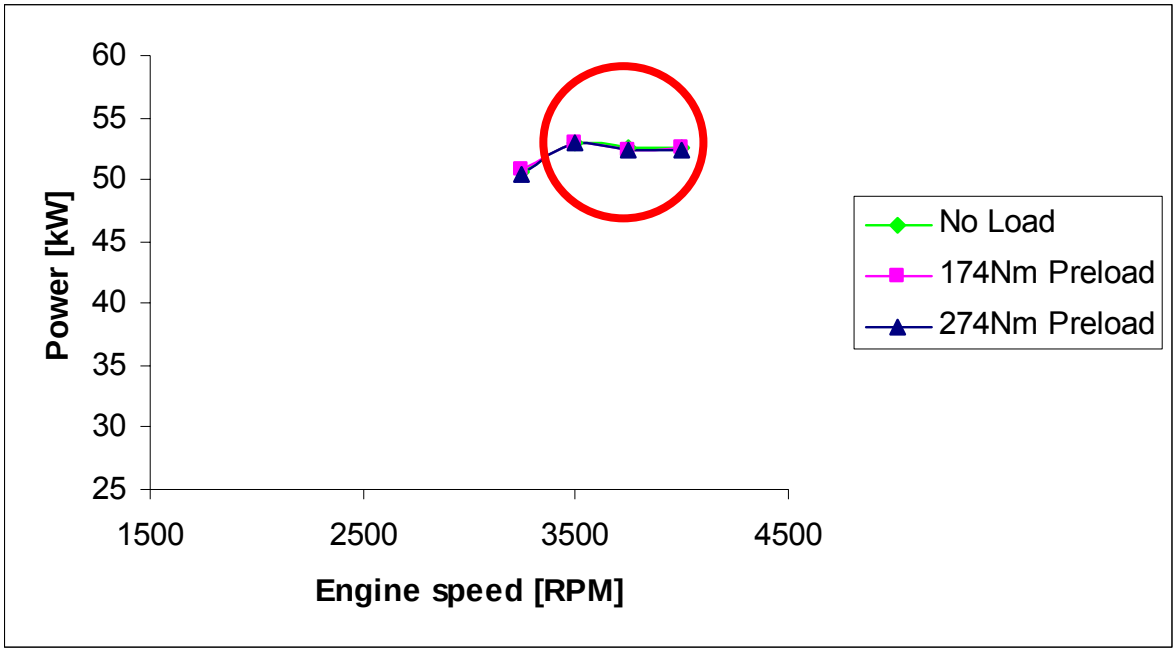

Figure 4-4: Test with preloads showing the anomaly in the power curve is not introduced by the test cell but rather an engine characteristic

4.2.3 Commissioning

After the problems discussed in the previous section had been solved and the perceived anomaly proved to be an engine characteristic, the test cell was commissioned for the testing of biofuels.

4.3 Automated test and repeatability

The automated test is started by the operator and executes the programmed test sequence, allows the engine to cool and then switches off the engine. The automated test in Figure 4-5 was implemented and executed successfully in the test cell and has been set as the default test to ensure repeatability.

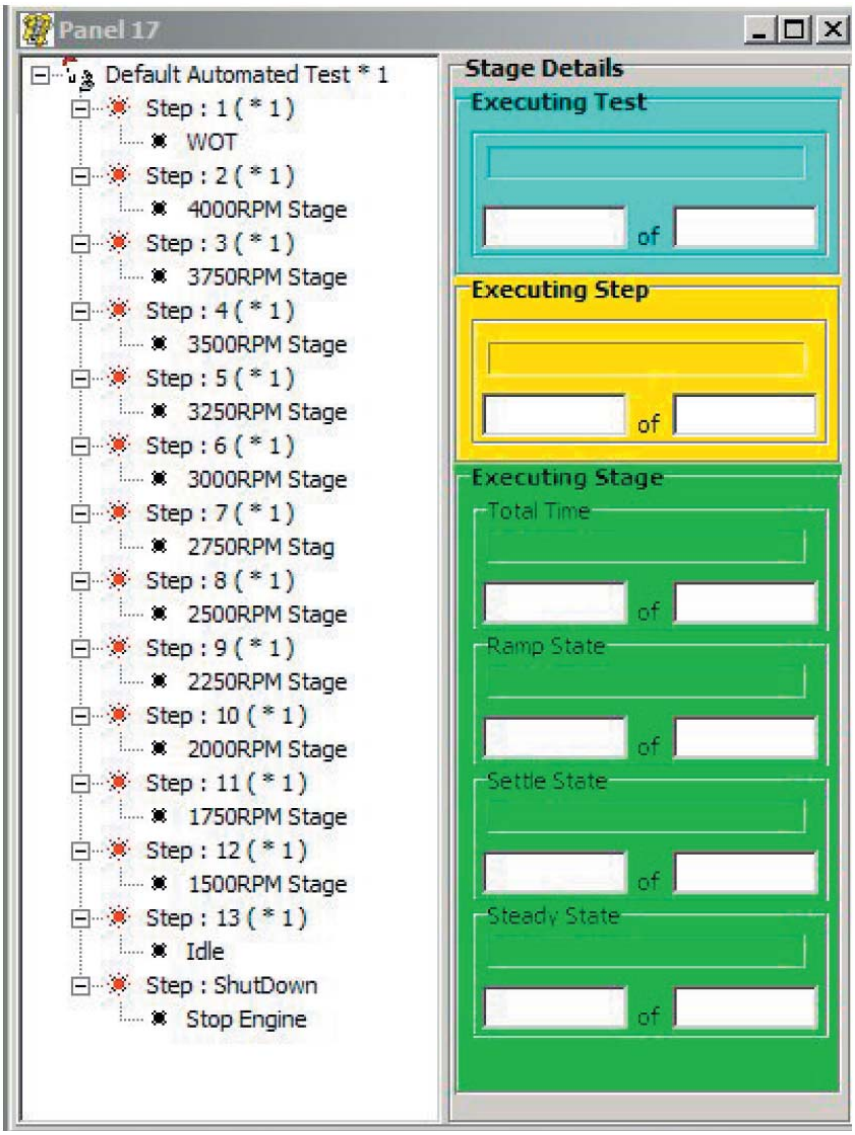

Figure 4-5: Automated test successfully executed

After the dynamometer had been calibrated, a fixed weight was applied and the value recorded as a reference test. This reference weight is applied immediately before and after each test to ensure consistency and to verify that the system maintains calibration. A reading of 473 Nm was recorded before and after testing, indicating that no change in setup conditions occurred. The reference weights are labelled and stored in the test cell for easy access.

Ultra low sulphur diesel (ULSD) was tested before and after the biofuel mixtures tests to ensure repeatability and to be used as a reference. The maximum deviation in power was 1.5% between the two tests. The dynamometer was run without water and it was recorded that there was a 25 Nm frictional force in the bearings of the

dynamometer at full rack which can account for the small deviation between tests. The performance curve illustrating the repeatability is shown in Figure 4-6, where ULSD1 was the initial run and ULSD2 the final run.

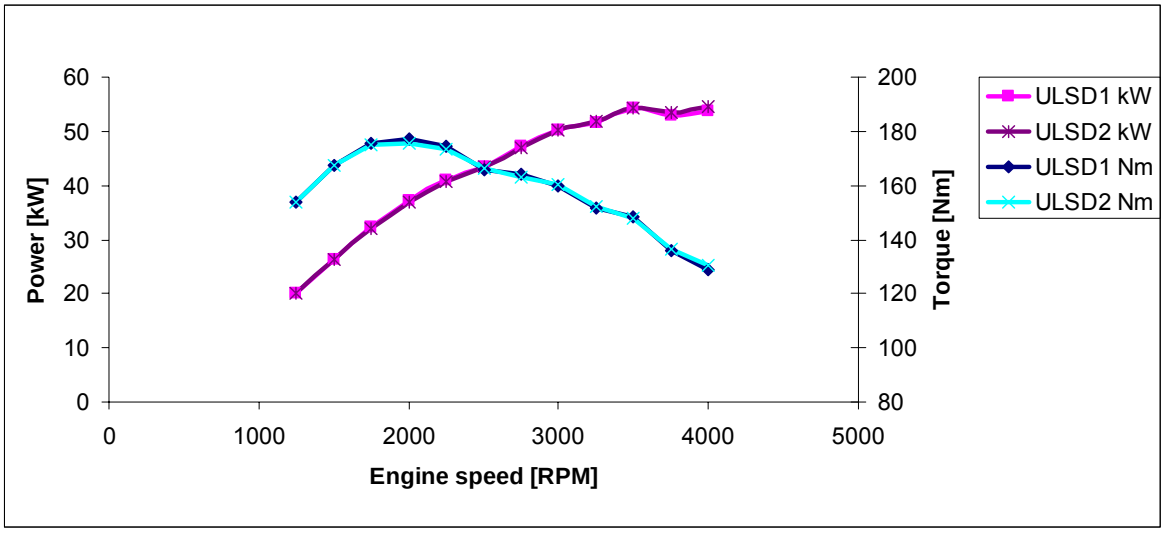

Figure 4-6: ULSD Performance curves showing repeatability

Similar to the power curves, the fuel consumption measurement from the AVL fuel balance must also be checked for repeatability. The measurements from the before and after ULSD tests are plotted in Figure 4-7. The two curves are almost identical with maximum deviation of 0.324 g/s (or 2.74%) occurring at 4000 RPM, concluding that the consumption readings are repeatable.

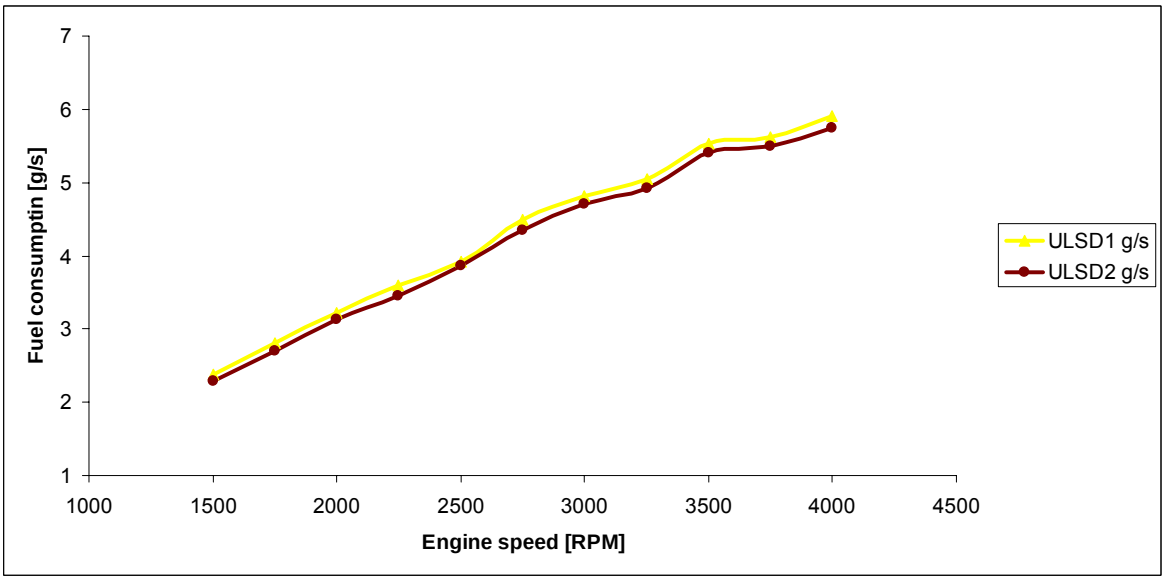

Figure 4-7: AVL results showing ULSD fuel consumption

4.4 Performance curves

The ULSD, biodiesel and its blends were tested and the power curve results plotted to graphically illustrate the performance differences of each fuel (Figure 4-8). It can be seen that the fuels are similar in performance, though the engine produces slightly less power when operating on B100. The maximum difference between biodiesel and ULSD is 1.58% at 3750 RPM and on average there is a 0.42% decrease in power. Under normal driving conditions this would barely be noticeable as it is a 0.85 kW power decrease, while ambient conditions such as temperature and altitude can be expected to have a bigger effect. Diesel engines generally produce maximum torque between 1800 and 2100 RPM and for this particular engine it is around 1900 RPM. Figure 4-9 shows the test torque curves.

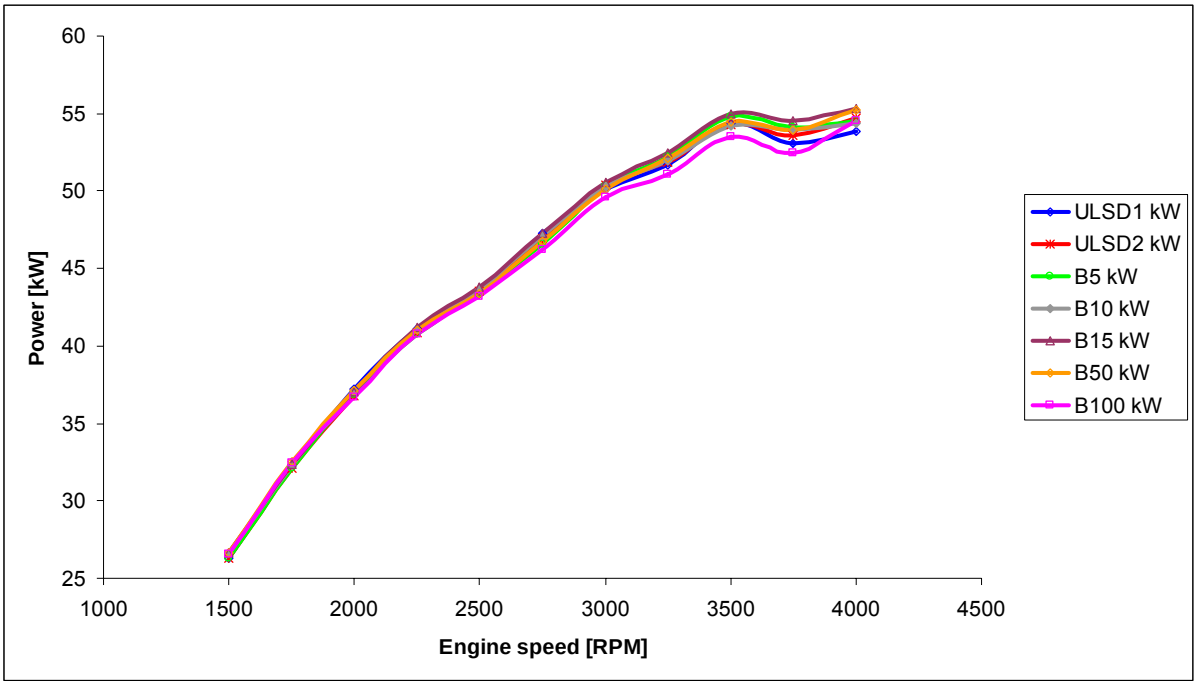

Figure 4-8: Power curves of ULSD, biodiesel and its blends

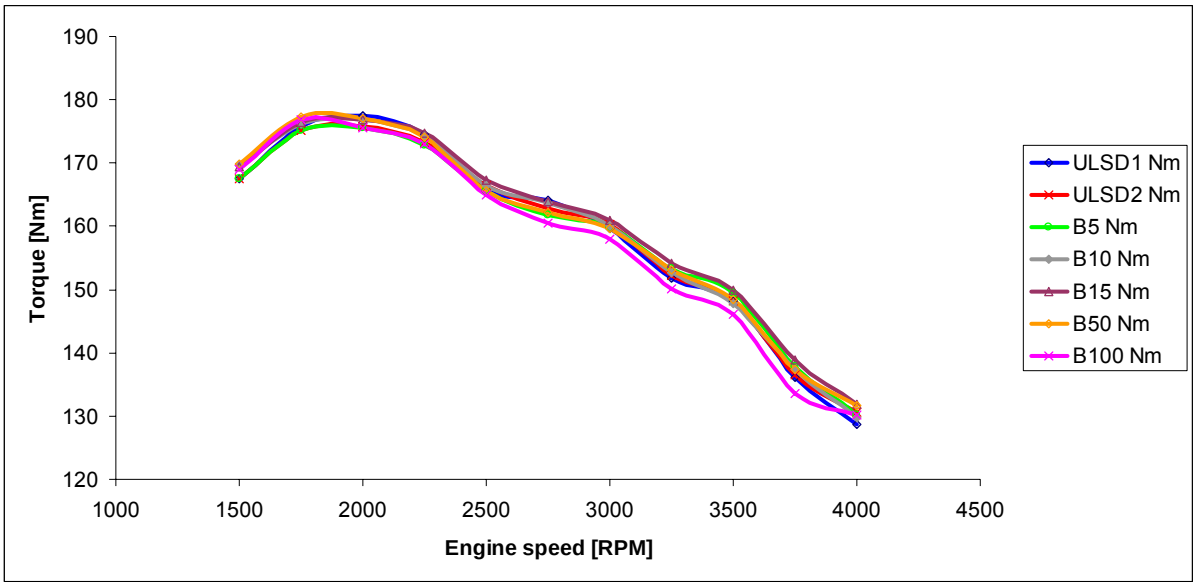

Figure 4-9: Torque curve for ULSD, biodiesel and its blends

The individual performance curve for B100 (pure biodiesel) is plotted in Figure 4-10. The performance curves for the blends are shown in Appendix J as they are almost identical to the B100 plot. Differences between performance curves can only be observed when plotted together, as in Figure 4-8 and Figure 4-9. In Figure 4-10 the power (kW) is displayed in pink and plotted against the left hand side y-axis while the torque (Nm) is plotted in blue against the right hand side y-axis.

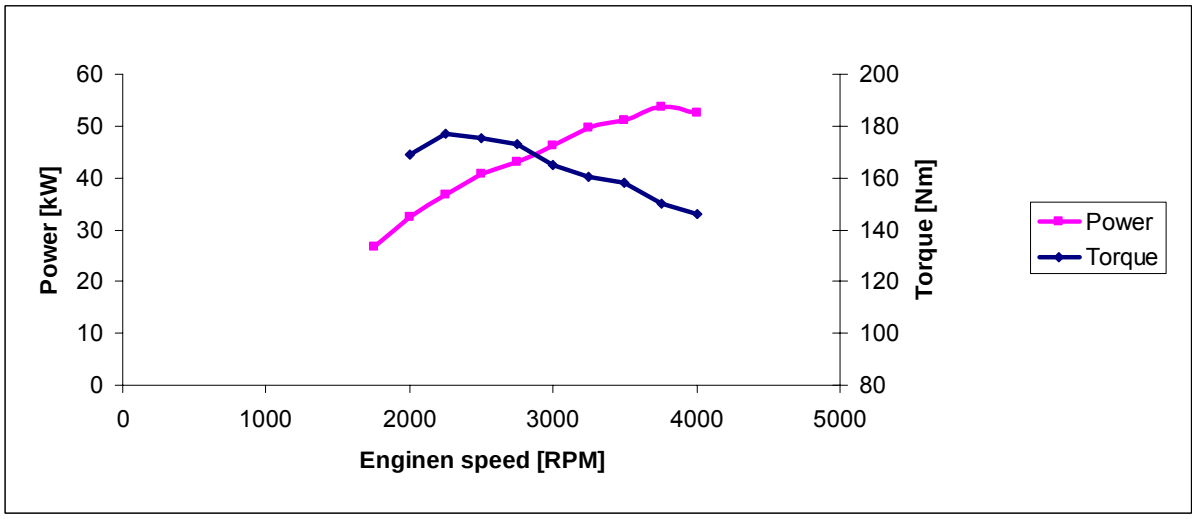

Figure 4-10: B100 performance curve

Diesel engines are often preferred for normal driving conditions because the maximum torque is available from lower revolutions when compared to petrol

engines. The torque curve for this Toyota engine running on biodiesel (Figure 4-10) tapers off almost linearly from 1900 RPM as reflected in the linear power increase because power = torque x speed ($P=T\omega$). The performance curve not only shows the engine power characteristics but can also be used to check engine condition as the power will decrease if there is a non-critical fault.

All engine parameters, such as exhaust and oil temperatures, are approximately the same whether running on biodiesel or ULSD. For example at 2750 RPM (halfway through a test) the exhaust temperature for diesel and biodiesel are 757.8°C and 753.2°C, respectively. The 4.5°C or 0.59% decrease is negliable. Similarly, the difference in coolant temperature is 0.1°C, oil temperature is 0.2°C and oil pressure is 0.1 bar. For practical purposes the results can be seen as the same because they are within the tolerance of the sensors. Engine operating parameters thus stay the same when biodiesel or mineral diesel is used.

4.5 Fuel consumption

The fuel consumption results from the tests are plotted in Figure 4-11. From the figure it can be seen that pure Biodiesel has the worst fuel consumption which improves as the mineral diesel:biodiesel ratio increases. This was expected since the energy content of biodiesel is lower than that of mineral diesel (section 4.6). The lower blends, B5 to B15 have a minimal effect on the fuel consumption. Government legislation (as stipulated in the 2013 White Paper) requires 10,000 GWh of renewable energy to be contributed to the final energy consumption by 2013 (Department of Minerals and Energy, 2003). The use of low biodiesel blends could help meet this target.

Even though the biodiesel used for testing was of poor quality (section 4.1) it has little effect on the performance relative to diesel, though the long term effects are not known as endurance tests were not performed. From the performance and fuel consumption results it can be suggested that biodiesel quality has little effect on fuel combustion.

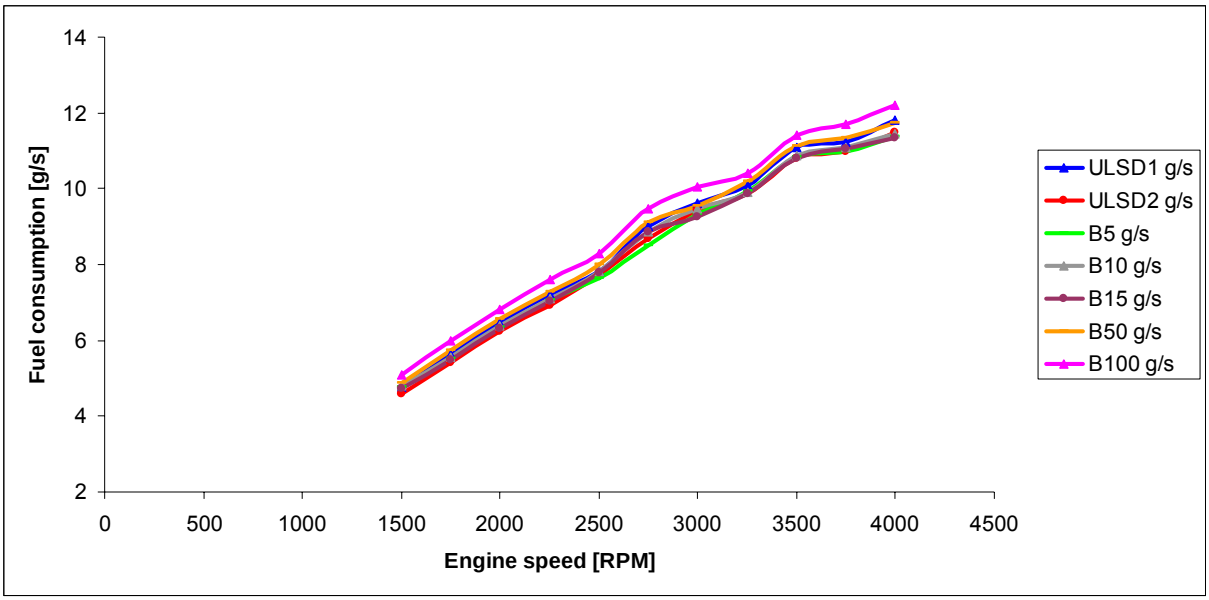

Figure 4-11: Fuel consumption curves for ULSD, biodiesel and its blends

Specific fuel consumption is a measure of engine efficiency (Ferguson and Kirkpatrick, 2001). It can be assumed that the engine efficiency remains constant throughout testing, thus the specific fuel consumption should also remain constant. This is indeed the case as illustrated in Figure 4-12.

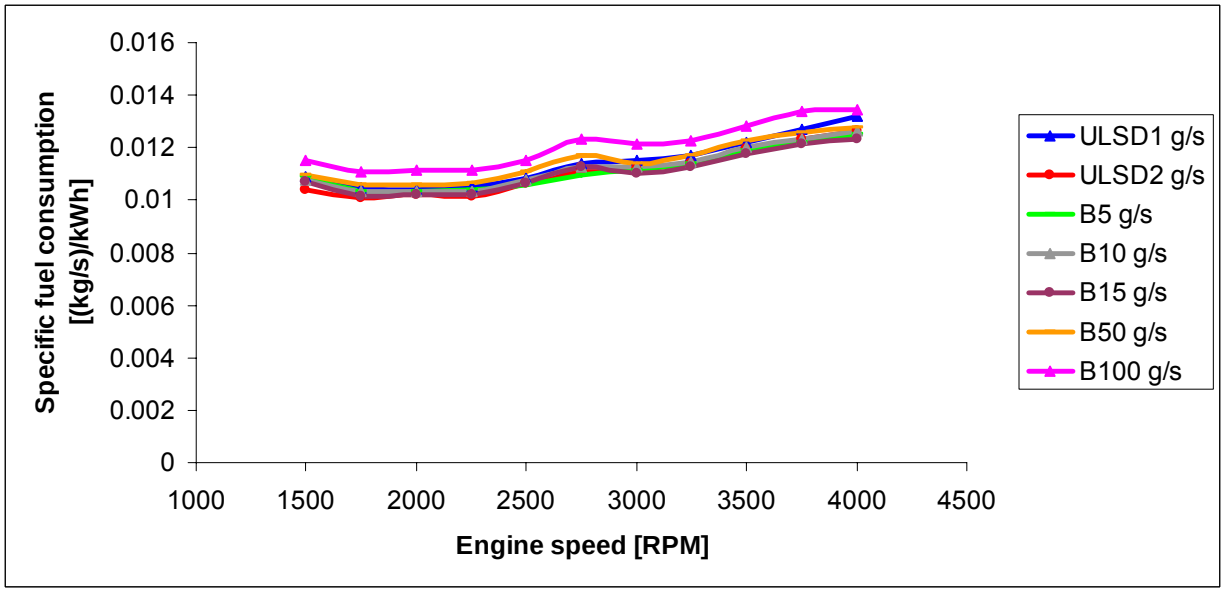

Figure 4-12: Energy consumption in kg/kWh

4.6 Energy balance

To determine the efficiency of the engine an energy balance test was designed and executed. An energy balance was performed by subtracting the energy flow out of a system from the energy into the system. The difference is the loss due to convection and radiation, which would otherwise be nearly impossible to measure. The energy balance is also used as a final validation for the test cell as the equation will not balance if all energies cannot be accounted for.

The results from the test are shown in Table 4-2. The energy balance for diesel was calculated first, from which the calorific value of biodiesel could be determined. This calculated calorific value was then compared to the value from a calorie bomb test. The calorific value for diesel was obtained from Ferguson and Kirkpatrick (2001).

Table 4-2: Energy balance data (table adapted from Martyr and Plint, 2007)

		Results	
Parameter	**Symbol**	**Mineral diesel**	**Biodiesel**
Engine speed (RPM)	ω	3000	3000
Power output (kW)	P_s	49.12	47.45
Fuel consumption rate (kg/s)	$\sim m_f$	0.0043	0.00459
Air consumption rate (kg/s)	$\sim m_a$	0.0657	0.0657
Lower calorific value of the fuel (MJ/kg)	C_L	42.5	?
Exhaust temperature (°C)	T_c	767.937	746.687
Coolant flow rate (kg/s)	$\sim m_w$	0.564	0.564
Coolant inlet temperature	T_{1w}	47.57	47.94
Coolant outlet temperature	T_{2w}	68.82	68.35
Inlet air temperature	T_a	21.81	21.81

The calorific value for biodiesel was calculated in Appendix M using the convection and radiation energy losses calculated from the mineral diesel tests. The losses are assumed to be the same, as the test setup did not change between the two fuel tests. The calculated calorific value for biodiesel (38.462 MJ/kg) is within 2.1% of the calorie bomb test (39.336 MJ/kg). The thermal efficiency of the engine can then be calculated:

$$\eta_{Diesel} = \frac{P_{Ds}}{H_{D1}}$$

$$\eta_{Diesel} = 26.87\,\%$$

$$\eta_{Biodiesel} = \frac{P_{Bs}}{H_{B1}}$$

$$\eta_{Biodiesel} = 26.61\,\%$$

As can be seem from the thermal efficiencies there is no noticeable difference whether the engine is running on mineral diesel or biodiesel. This is to be expected as the thermal efficiency is an engine characteristic, and thus independent of what fuel is used. From the above discussion it can be concluded that a diesel engine can be run on biodiesel without any modifications. Fuel consumption is the only parameter that is immediately affected while long term effects require further investigation.

The energy balance calculations are the final check that the test cell has been correctly calibrated. The engine is operating at a 26.87% thermal efficiency which corresponds to the literature (25-30%) for an engine of similar size (Martyr and Plint, 2007). The losses to convection and radiation are 13.56%, which is also similar to the literature (Martyr and Plint, 2007).

4.8 Summary

Tests were conducted to ensure that the test cell operates autonomously and the results are repeatable and accurate.

The results from the biodiesel analysis showed that most chemical properties were not within specification, indicating a low quality biodiesel. After testing it can be suggested that this does not have a major influence on the performance of biodiesel in a compression ignition engine.

Biodiesel and its blends were tested against ultra low sulphur diesel to determine the differences in performance and fuel consumption. The data shows that the two fuels

are similar in performance but the fuel consumption for biodiesel is higher as it is has a lower calorific value. The calorific value of biodiesel was determined from an energy balance and compared with the laboratory calorie bomb experiment. Similar calorific values were obtained indicating that the test cell is correctly calibrated and that the measurements are accurate. The successful testing and analysis of biodiesel concluded that the project goals were met.

5. Conclusions and recommendations

The following conclusions are based on the work performed and the results obtained during the development of a biofuels engine testing facility at Stellenbosch University.

- A literature review on biodiesel has shown it to be a potentially viable automotive engine fuel replacement despite its possible influence on the food industry (see sections 2.1-2.3)
- A further in depth literature study on engine test cells showed that most of the information needed to design a test cell is available in the literature (see sections 2.4-2.7). There are however some aspects that can only be gained from experience, for example how to best set the water flow to the dynamometer using a gate valve coupled directly to the supply (see section 3.5.1) .
- An engine test cell has been designed, built and commissioned in less than 2 man-years (see chapter 3). Of note is that:
    - The cell was designed from the ground up and conforms to the traditional test cell layout;
    - A test cell can be designed on a stringent budget, but at the expense of time and effort to source used equipment and information.
- The test results are repeatable and accurate (see section 4.3). An anomaly in the power curve was found during a validation test but was proven, by shifting the work point of the control system, to be an engine characteristic (see section 4.2.2).
- Final validation of the test cell was performed by means of an energy balance. The calorific value for biodiesel was determined to be 38.5 MJ/kg and was within the assumed accuracy of the system (see section 4.6).
- The engine successfully ran on biodiesel for the duration of testing where:
    - No engine modifications were needed;
    - The combustion energy released and the yield properties showed no dependence on the quality of the biodiesel (see section 4.1);

- The fuel consumption using pure biodiesel was, as expected, higher than when using mineral diesel because of the lower energy content. Biodiesel blends show little or no consumption difference (see section 4.5).

- The test cells software and graphical user interface were designed in such a way to make it an adaptable research tool that can be used by a technically competent person. Careful attention has been paid to detailed and extensive documentation to ensure this is possible.

The following test cell upgrades are recommended to improve the functionality and scope of the test cell when the appropriate budget is available:

- Develop customised in-house test cell control software
- Implement a permanent air and water flow meter to calculate energy balance;
- Control the temperature and humidity in the test cell;
- Add emissions testing equipment, in-cylinder pressure transducer, fuel conditioning unit, carbon monoxide detector and a ‘Druk’ test cell calibration unit;
- Design a palette system for mounting and aligning engines with a quick connector box.

References

AVL, *Dynamic fuel consumption operation equipment 7030*, Australia, 1984.

CAE, *ETA power user manual*, SSI002, Version 2.0, December 2005.

Craig, R.R. Jr., *Mechanics of materials*, USA, Wiley and Sons, 2000.

Crowe, C.T., Elger, D.F., Roberson, J.A., *Engineering fluid mechanics*, USA, John Wiley and Sons, 2001.

Demirbas, A., *Biodiesel fuels from vegetable oils via catalytic and non-catalytic supercritical alcohol transesterfication and other methods: a survey*, Turkey, Karadeniz Technical University, December 2002.]

Demirbas, *A, Biodiesel production via non-catalytic SCF method and biodiesel fuel characteristics*, Turkey, Karadeniz Technical University, 2006.

Department of minerals and energy, *White paper on the renewable energy policy of the republic of South Africa*, Notice 513 of 2004, November 2003.

Desantes, J.M., Arregle, J. Ruiz, S., Delange, A., C*haracterization of the injection-combustion process in a D.I. diesel engine running with rape oil methyl ester*, SAE, 1999.

Felizardo, P., Correia, M., Raposo, I., Mendes, J., Berkemeier, R., Bordado, J., *Production of biodiesel from waste frying oils*, Elsevier, 17 June 2005.

Ferguson, C.R. and Kirkpatrick, A.T., I*nternal combustion engines*, John Wiley and Sons Inc, 2001.

Honeywell, *ML6420A/ML7420A Electric linear valve actuators*, USA, 2006.

http://www.biodiesel.org/markets/pre/, 11 September 2007.

http://www.biodieselsa.co.za/what.htm, 6 Spetember 2007.

http://www.britannica.com/eb/article-9075513/viscosity20 February 2008.

http://www.planetark.org/dailynewsstory.cfm/newsid/41147/story.htm, 30 July 2008

http://www.salvadori.org/aobc/handouts/handout_inertia.pdf, 10 October 2007.

http://www.sapia.co.za/stats/demand.htm, 30 July 2008

http://www.shaval.co.za/index.jsp?page=warranties, 10 September 2007.

http://www.smartveg.com/shop/pre.php, 30 July 2008

Kiong, E,. NZ firm makes bio-diesel from sewage in world first, New Zealand, NZ Herald, 12 May 2006.

Klok, R. and Verveer, H.H., *Process for producing fatty-aid lower-alkyl mono esters European*, patent EP 0391 485 A1, 1990.

Knothe, G. and Steidley, K.R, *Kinematic viscosity of biodiesel components (fatty acid alkyl esters) and related compounds at low temperatures*, USA, Elsevier, 27 September 2006.

Li, Z., Zhang, X., Wu, Z., Deng, J.,Huang., *Experimental study of biodiesel spray and combustion parameters*, Shanghai, Tongi & Shanghai Jiao Tong Universities, 2006.

Martyr, A.J. and Plint, M.A., Engine testing, United Kingdom, Elsevier, 2007 Third edition.

McCormick, R.L., Tennant, C., Hayes, R.R., Black, S., Irelan, J., McDaniel, T., Williams, A.,Frailey, M., Sharp, C., *Regulated emissions from biodiesel tested in heavy duty engines meeting 2004 emission standards*, USA, Department of Energy & Southwest Research institute, 2005.

Mittlebach, M. and Remschmidt, C., *Biodiesel, the comprehensive handbook*, Vienna, Boersedruck Ges.m.b.H, 2005.

Schenck Pegasus GmbH, *Test- and Automation Systems: MTU_D2-7600_GD03en.doc*, Schenck, 23 July 2001.

Shigley, J.E. and Mischke, C.R., *Mechanical engineering design*, Singapore, Mcgraw-hill, 2001.

Sonntag, R.E. and Borgnakke, C., Introduction to engineering thermodynamics, USA, John Wiley and Sons, 2001.

Standards South Africa, *Automotive diesel fuel, South Africa*, South African National Fuel Standards, 8 November 2002.

Tsolakis, A., Megaritis, A., Wyszynski, M.L., Theninnoi, K., *Engine performance and emissions of a diesel engine operating on diesel-RME blend with EGR*, United Kingdom, Elsevier, 2007.

Van Gerpen, J., *Biodiesel production and fuel quality*, University of Idaho, 2005.

Venter, J., *The A to Z of Servos*, Stellenbsoch, 5 May 2005.

Waina, K.S., Pereza, J.M., Chapmanb, E., Boehman, A.L, *Alternative and low sulfur fuel options: boundary lubrication performance and potential problems*, USA, Tribology International, 2005.

Appendix A: Research methodology mind map

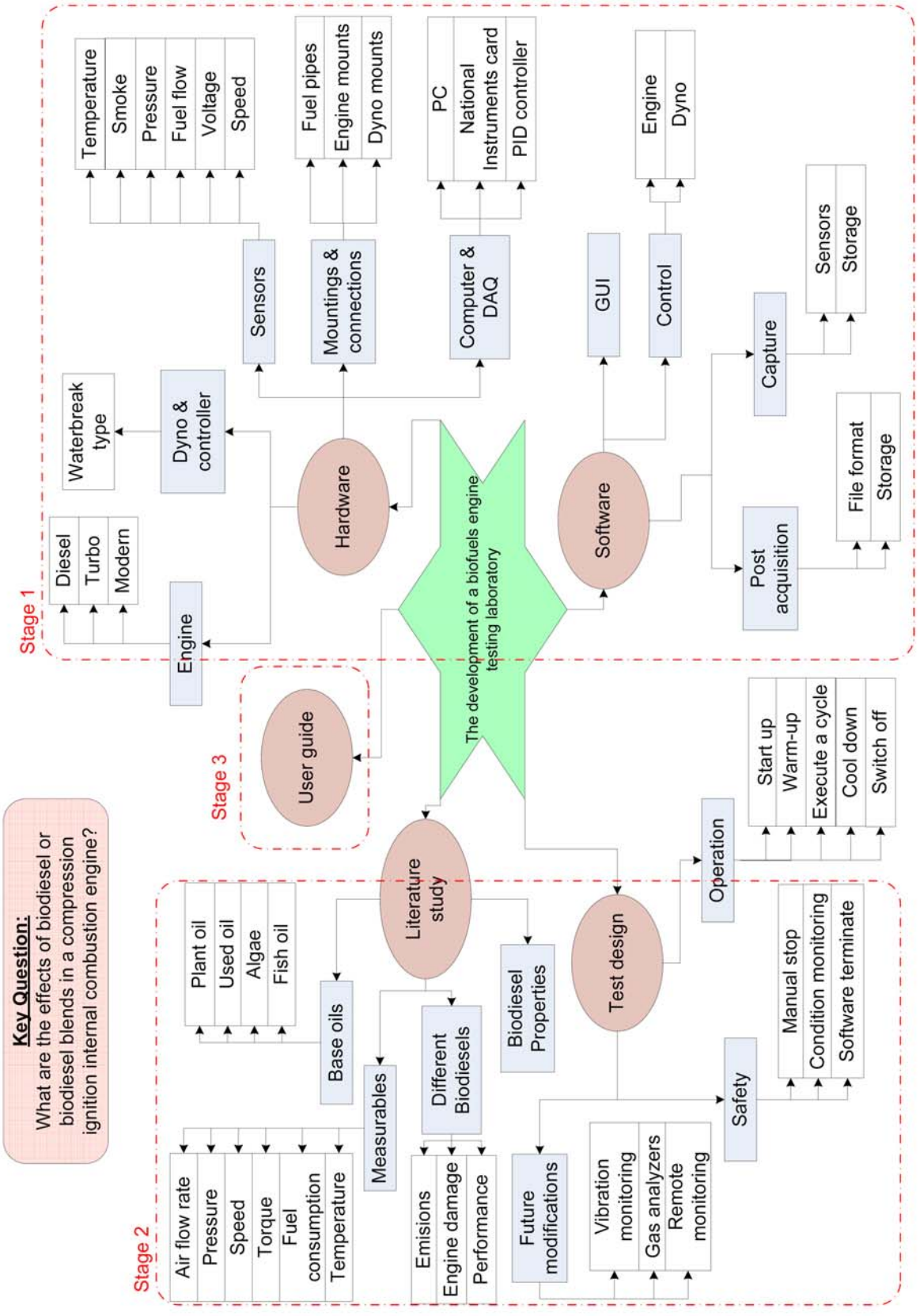

Appendix B: Gantry crane calculations

A crane was required to get the equipment on and off the test bench. It was thought to mount a beam on the roof of the test cell parallel with the test bed. This was however discarded as it is not used on a regular basis and cannot be used elsewhere in the test cell. A portable gantry on castor wheels (see Figure B-1) was design and manufactured.

Figure B-1: Picture of the gantry crane with a hoist and beam trolley

The initial Toyota engine setup weighed around 300kg, which would only require a half ton gantry. The test cell, however, may be used for commercial engines such as the 300kW John Deere tractor engines, which would weigh more. It was decided to construct a 1 ton gantry that could be disassembled to get it in and out of the test cell doors. Since a beam trolley is being used, the weight of the load could be carried by

a single support when the trolley is moved to the side. All equations and material properties were obtained from Craig (2000).

A fixed-free column is assumed as the horizontal beam is bolted to the supports while the wheels are free to rotate on the ground, thus K = 2 (effective length factor). The Euler buckling load (compressive force) is given in Equation B-1. The column however is most stressed under the elastic buckling load, given in Equation B-2.

$$Pcr = \frac{\pi^2 EI}{L} \quad \textbf{(Eq. B-1)}$$

$$Pcr = \frac{\pi^2 EI}{(KL)^2} \quad \textbf{(Eq. B-2)}$$

Where:

E = 200 GPa for structural steel

I = Moment of inertia for an I-beam

L = Effective length

K = Effective length factor

The moment of inertia for an I-beam illustrated in Figure B-2 (www.salvadori.org, 2007) is calculated using Equation B-3.

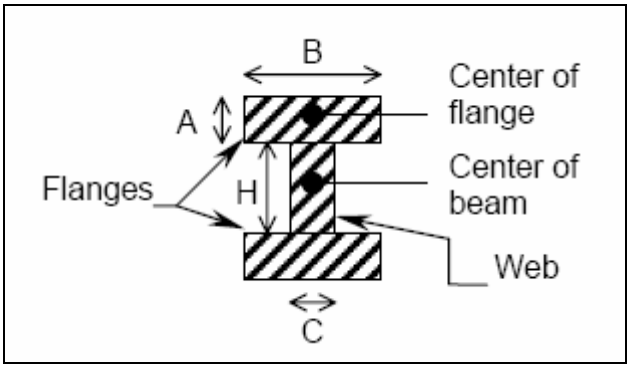

Figure B-2: I-beam moment of inertia

$$I = 2(\mathrm{AB})\left(\frac{\mathrm{H}}{2} + \frac{\mathrm{A}}{2}\right)^2 + \left(\frac{\mathrm{CH}}{12}\right)^3 \quad \textbf{(Eq. B-3)}$$

Two ∅77*x*2300*x*3 mm pipe sections were in stock, already with flat plates welded on either end. The above equations were put into an Excel document (see Table B-1).

Table B-1: Gantry calculations

Material properties			
E	=	2.00E+11	GPa
Effective Length factor – K	=	2	
Ro	=	38.5	mm
Wall thickness	=	3	mm
Ri	=	35.5	mm
I	=	4.78E-07	m^4
L	=	2.3	
Governing Equation		Pcr = (pi^2*EI)/((KL)^2)	
Calculations			
Tubing: compression only			
Pcr	=	1.78E+02	kN
	=	18.19	tons
Tubing: Elastic Buckling Load			
Pcr	=	4.46E+01	kN
	=	4.55	tons

From the above table it can be seen that the tube maximum Euler buckling load is 18 tons and the maximum Elastic buckling load is 4.5 tons. The tube section is therefore more than sufficient for the given 1 ton load.

The stress in the 150mm plate which was welded to the I-beam and bolted to the uprights was calculated to be 4.62 MPa under maximum load, far less than the 300MPa yield strength for a steel weld (Shigley and Mischke, 2001). Removable gussets were later added to reduce the flex in the uprights when the gantry is moved

by applying force to one side (i.e. when moved by one person). The addition of the gussets further reduced the stress in the weld, making it neglible.

The maximum load of 500kg/castor would occur when the trolley is moved to one side (1000kg divided between the two castors). After some research it was found that the maximum rating of most common castors was 450 - 480kg. These may be acceptable although not too spec, therefore it was decided to source and use larger 680kg rated castors.

Appendix C: Dynamometer calibration arms

The dynamometer calibration arms were manufactured as they are no longer available from the supplier. The arms were manufactured from 100 x 12mm flat bar (drawing shown in Figure C-1). The amount of material cut away from arm 1 was calculated and then the same volume removed from arm 2 to keep them in equilibrium. This is only a rough guide as during calibration a separate counter weight still needs to be added to arm 2 to counter the weight of the sling and weight tray. Calibration setup is shown in Figure C-2 (Schenck Pegasus GmbH, 2001).

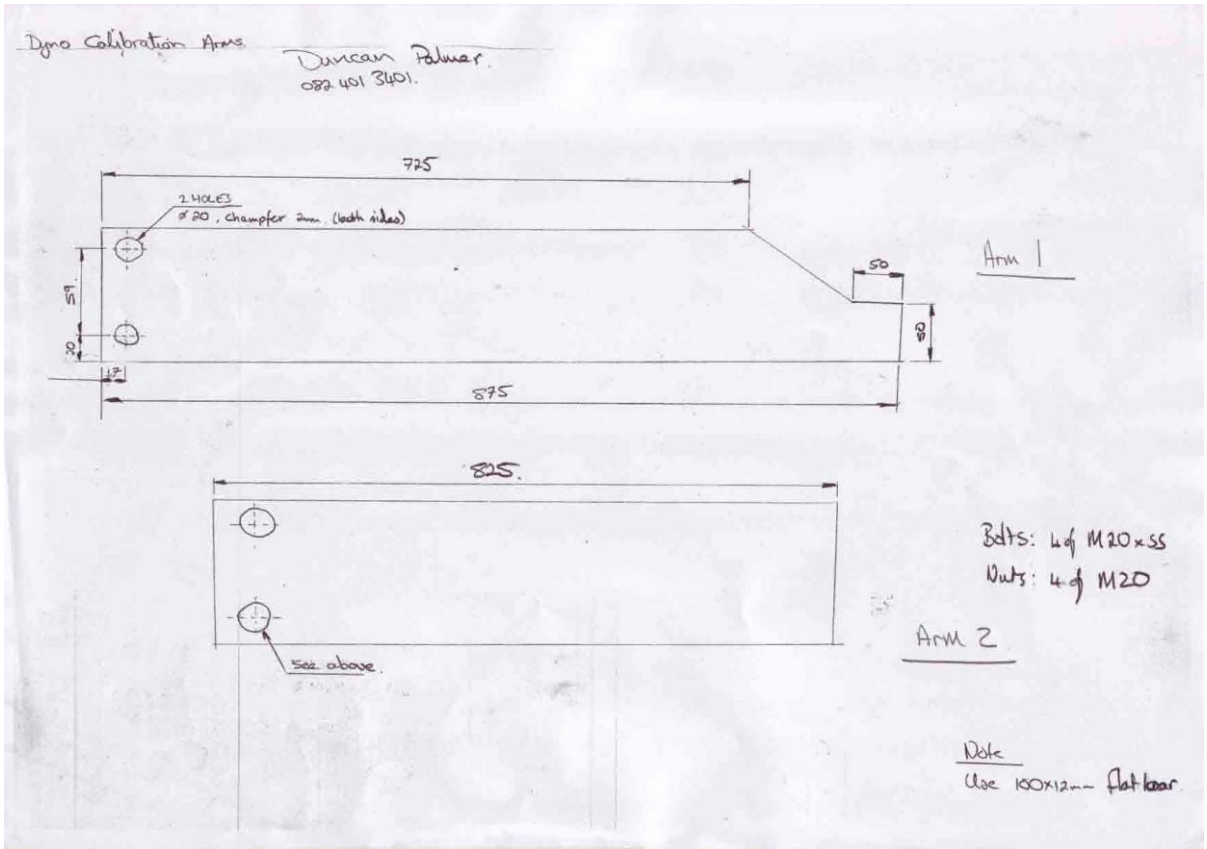

Figure C-1: Calibration arm drawing

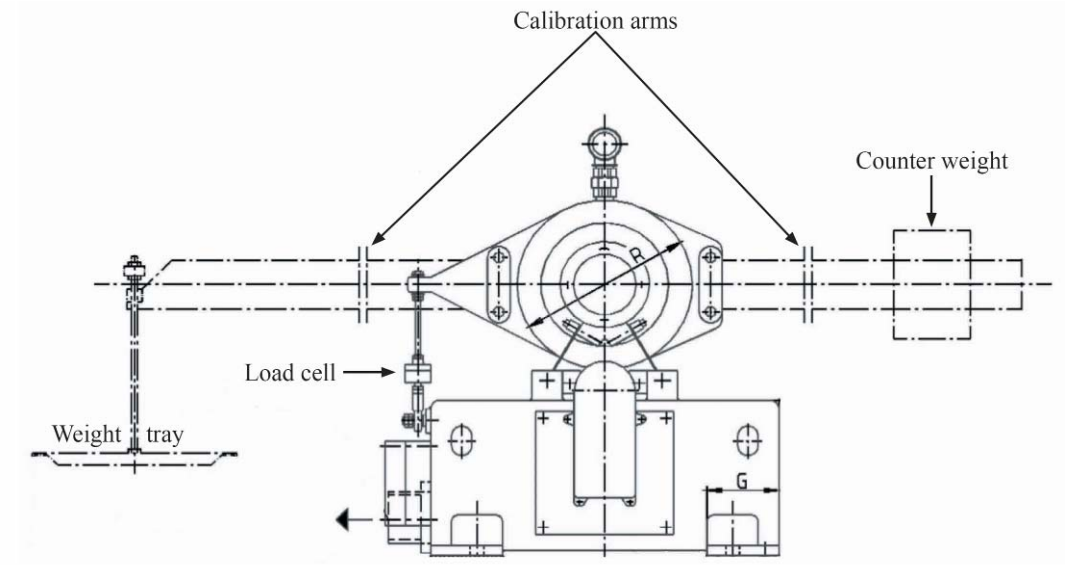

Figure C-2: Dynamometer calibration setup

The manufacturer recommended a distance of 1019mm from the centre of the dynamometer to the weight tray with a g = 9.81 $m^3.kg^{-1}.s^{-2}$ to give a reading of 1Nm per kilogram added. In Stellenbosch g =9.79325 $m^3.kg^{-1}.s^{-2}$, thus the length of the arm was recalculated to 1021mm. The manufactured arms were then attached, levelled, and 1021mm was measured and marked on arm 1. The arm was returned to the workshop to machine a V shape slot into which the sling will rest. It was decided not to make the arm adjustable as this will prevent any tampering or incorrect readings in the future.

Appendix D: Servo Specifications

JR DS-8511

NEW DS-8511 Standard Size Digital Servo

Standard Super Hi-Torque Digital Servo for Aerobatic Airplanes / Gliders - Car & Boat

DS-8511

DS-8511 Specifications	
Type	Digital FET
Size	Hi-Torque Standard Servo
Torque	15.0 kg/cm
Speed	0.19 S/60°
Length	40.0 mm
Width	21.0 mm
Height	35.0 mm
Weight	66 g
Bearings	Double Ball Bearing
Gears	Metal (Alloy)
Remarks	Aerobatic Airplanes / Gliders / C & B

Appendix E: PLC pin connections

Module	Pin	Connection
1200		
	+24Vdc	Emergency stop +
	IN 0	Emergency stop -
	IN 2	
	C0M 1	
	IN 5	
	IN 7	
	IN 9	
	IN 11	
	IN 13	
	24 COM	COM 0
	COM 0	24 COM
	IN 1	
	IN 3	
	IN 4	
	IN 6	
	IN 8	
	IN 10	
	IN 12	
	VAC L1	220 Vac Live
	VAC NEUT	220 Vac Neutral
	OUT 0	
	OUT 1	Fuel relay +24Vps
	OUT 2	Starter relay +24Vps
	VAC DC 3	
	OUT 5	3-way valve actuator UP
	OUT 6	
	OUT8	
	EARTH	220 Vac Protective earth
	VAC DC 0	
	VAC DC 1	Fuel relay Earth
	VAC DC 2	Starter/Glow plug relay Common earth
	OUT 3	Glow plug relay +24Vps
	OUT 4	3-way valve actuator DOWN
	VAC DC 4	
	OUT 7	
	OUT 9	
2A + 2D		
	IN 0	D360 Speed
	IN 1	D360 Torque
	OUT 0	D360 Control
	OUT 1	PWM Throttle controller
4A		
	IN 0	AVL Fuel consumption
	IN 1	P.oil 4-20mA
	IN 2	P.ambient 0-5V
	IN 3	Relative humidity 4-20mA
T1		
	IN 0	T.ambient
	IN 1	T.water.out
	IN 2	T.water.in
	IN 3	T.oil
T2		
	IN 0	T.exhaust
	IN 1	T.dyno
	IN 2	T.inlet.air
	IN 3	T.spare
T3		
	IN 0	T.control.room
	IN 1	
	IN 2	
	IN 3	

Appendix F: Löbro shaft catalogue pages

Constant velocity drive shafts and joints
with length variation

Type **104**

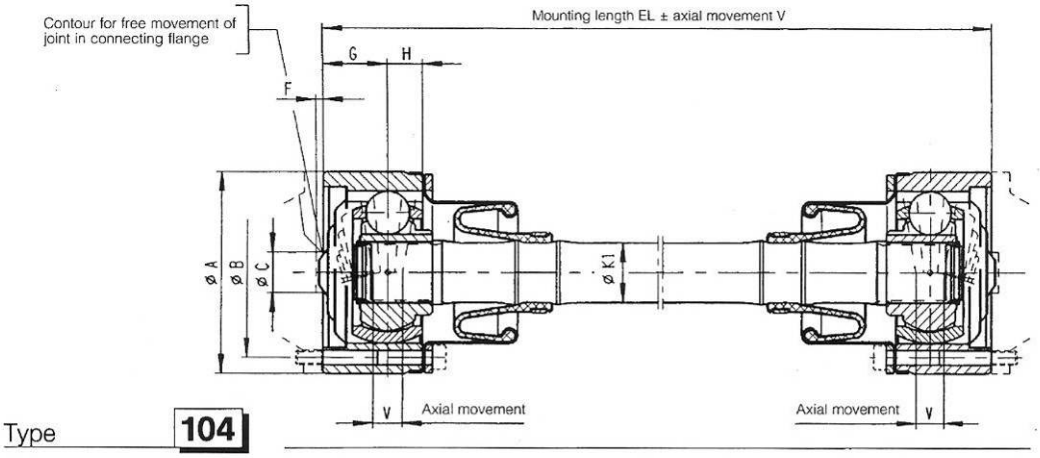

Type **110**

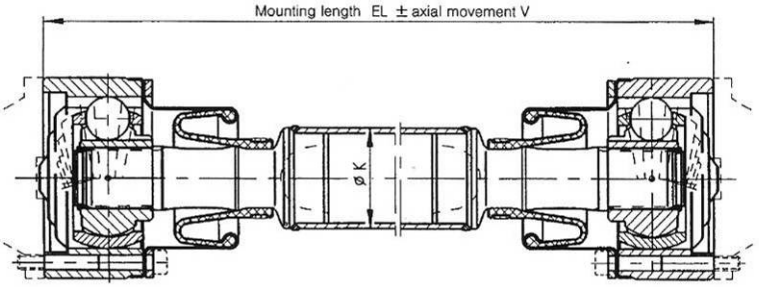

Type **164**

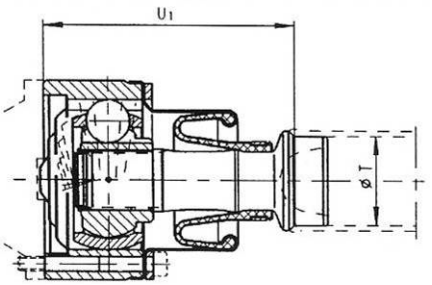

Type **174**

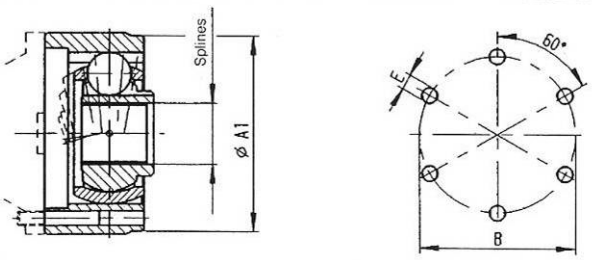

Joints have a permanent lubrication
(except for type 174)

9

Type 104 – 110 – 164 – 174

Joint size	Speed max. [rpm]	Shaft angle max. for plunging joint	ØA -0,2	ØB ±0,1	ØC	ØE	F	G	H	Plunge V per joint
10	8000	10°	100,2	84	20	8,2	3	26,5	13	12

Type 104

Joint size	max. static Torque [Nm]	Weight m [kg]	Inertia moment I [kgm²]	Tors. stiffness Ct [kNm/rad]	Weight + m [kg]	Inertia moment + I [kgm²]	Tors. stiffness + Ct [kNm/rad]	ØK1	min. mounting length EL	Code number
		for min. mounting length EL			supplement per 100 mm length					
10	2300	4,5	0,0055	38,3	0,36	0,00003	26,2	24	173	06 104 10 00

Example of an order:
required: Type 104
Joint size 10
EL = 425 (±12 mm)

Order details

0	6	1	0	4	1	0	0	0	4	2	5
Code number								EL			

Type 110

Joint size	max. static Torque [Nm]	Weight m [kg]	Inertia moment I [kgm²]	Tors. stiffness Ct [kNm/rad]	Weight + m [kg]	Inertia moment + I [kgm²]	Tors. stiffness + Ct [kNm/rad]	ØK	min. mounting length EL	Code number
		for min. mounting length EL			supplement per 100 mm length					
10	1300	5,1	0,0057	31,4	0,35	0,00019	197,9	50 x 3	263	06 110 10 00

Example of an order:
required: Type 110
Joint size 10
EL = 425 (±12 mm)

Order details

0	6	1	1	0	1	0	0	0	4	2	5
Code number								EL			

Type 164

Joint size	ØT -0,1	U1	Weight m [kg]	Code number
10	44,3	104,5	2,4	06 164 10 00

Example of an order:
required: Type 164
Joint size 10

Order details

0	6	1	6	4	1	0	0	0	0	0	0
Code number											

Type 174

Joint size	Splines DP	Z	⊲	ØA1	Weight m [kg]	Code number
10	24/48	24	45°	98,1	1,6	06 174 10 **01**

Example of an order:
required: Type 174
Joint size 10

Order details

0	6	1	7	4	1	0	**0**	**1**	0	0	0	0
Code number												

Appendix G: Calibrated channels in ETA

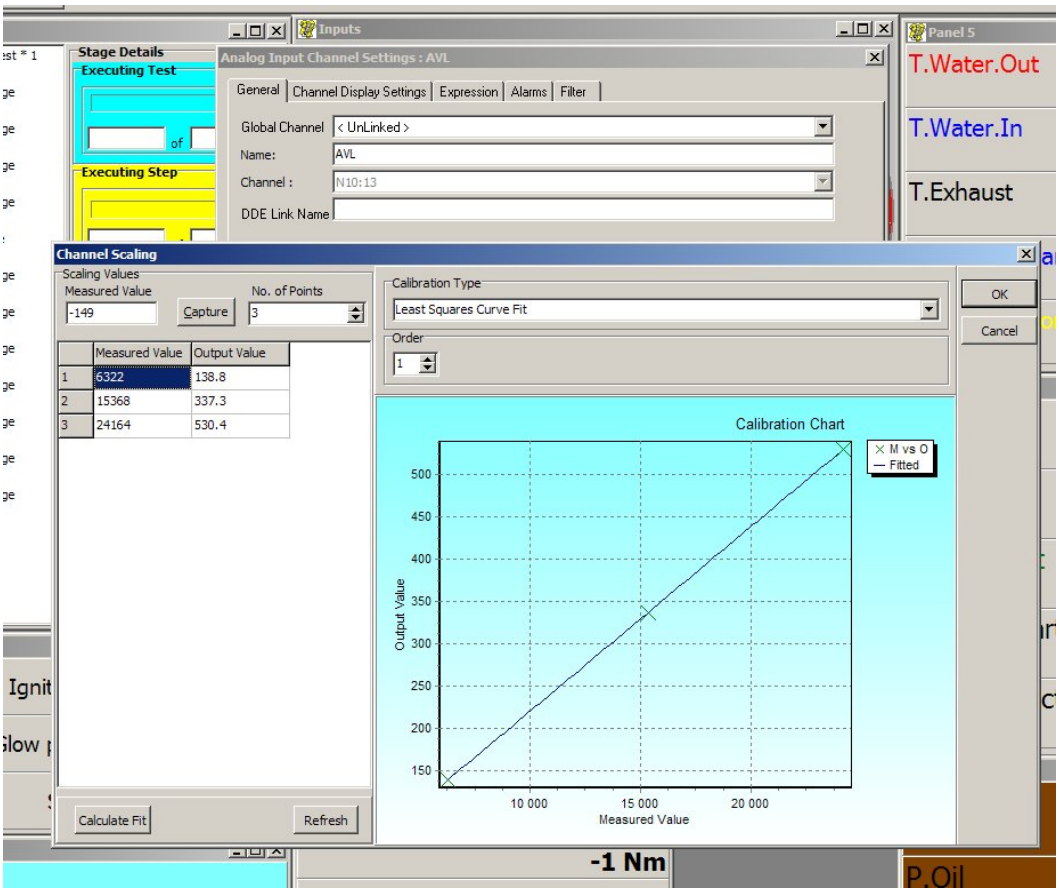

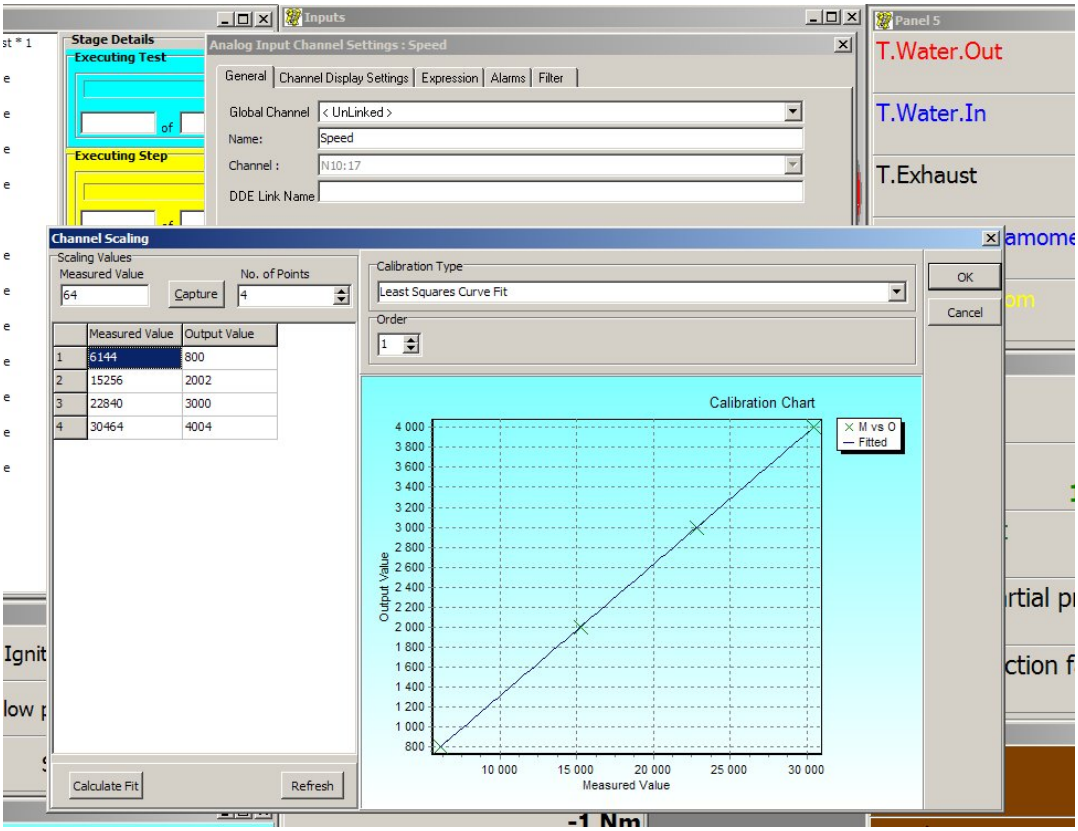

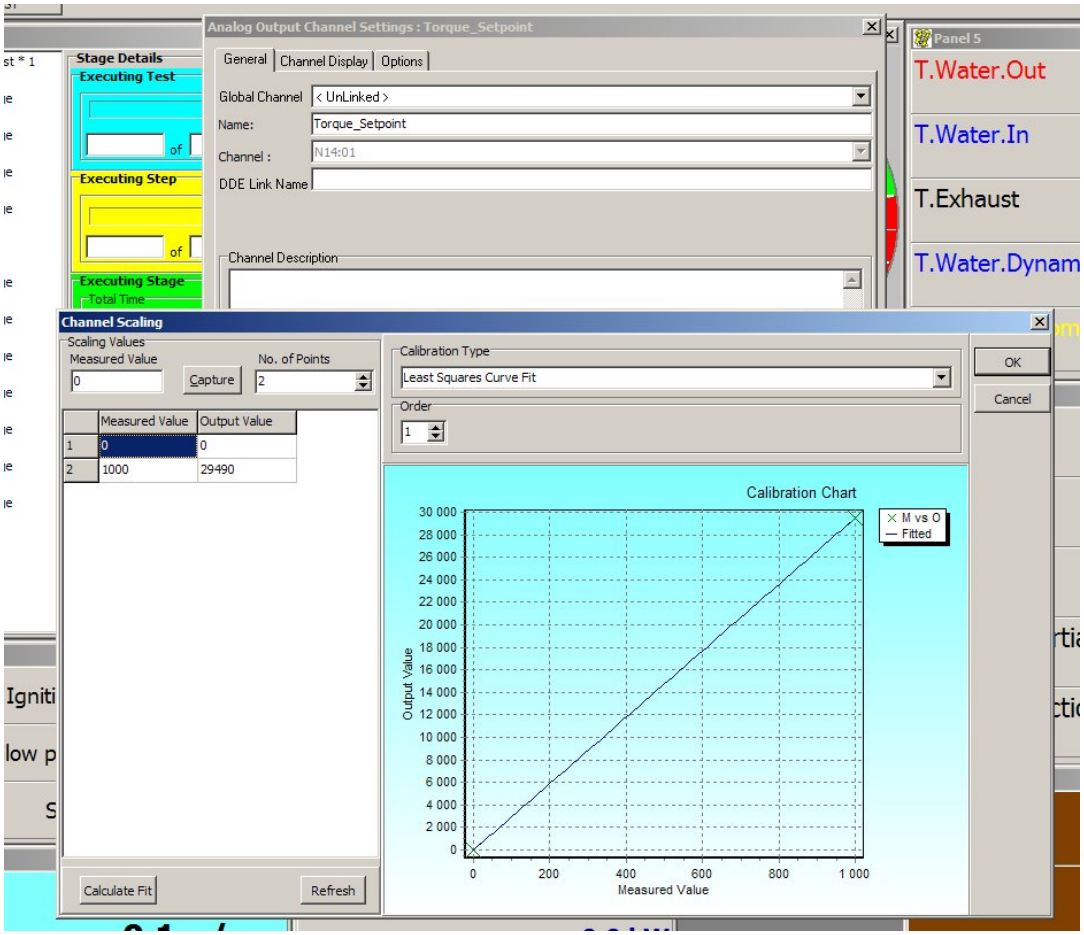
Analog Output Channel Settings : Torque_Setpoint
General
Channel Display
Options
Global Channel
< UnLinked >
Name:
Torque_Setpoint
Channel :
N14:01
DDE Link Name
Channel Description
Stage Details
Executing Test
Executing Step
Executing Stage
Total Time
Panel 5
T.Water.Out
T.Water.In
T.Exhaust
T.Water.Dynam
Channel Scaling
Scaling Values
Measured Value
Capture
No. of Points
Calibration Type
Least Squares Curve Fit
Order
OK
Cancel
Measured Value
Output Value
1 0 0
2 1000 29490
Calculate Fit
Refresh
Calibration Chart
M vs O
Fitted
Output Value
Measured Value

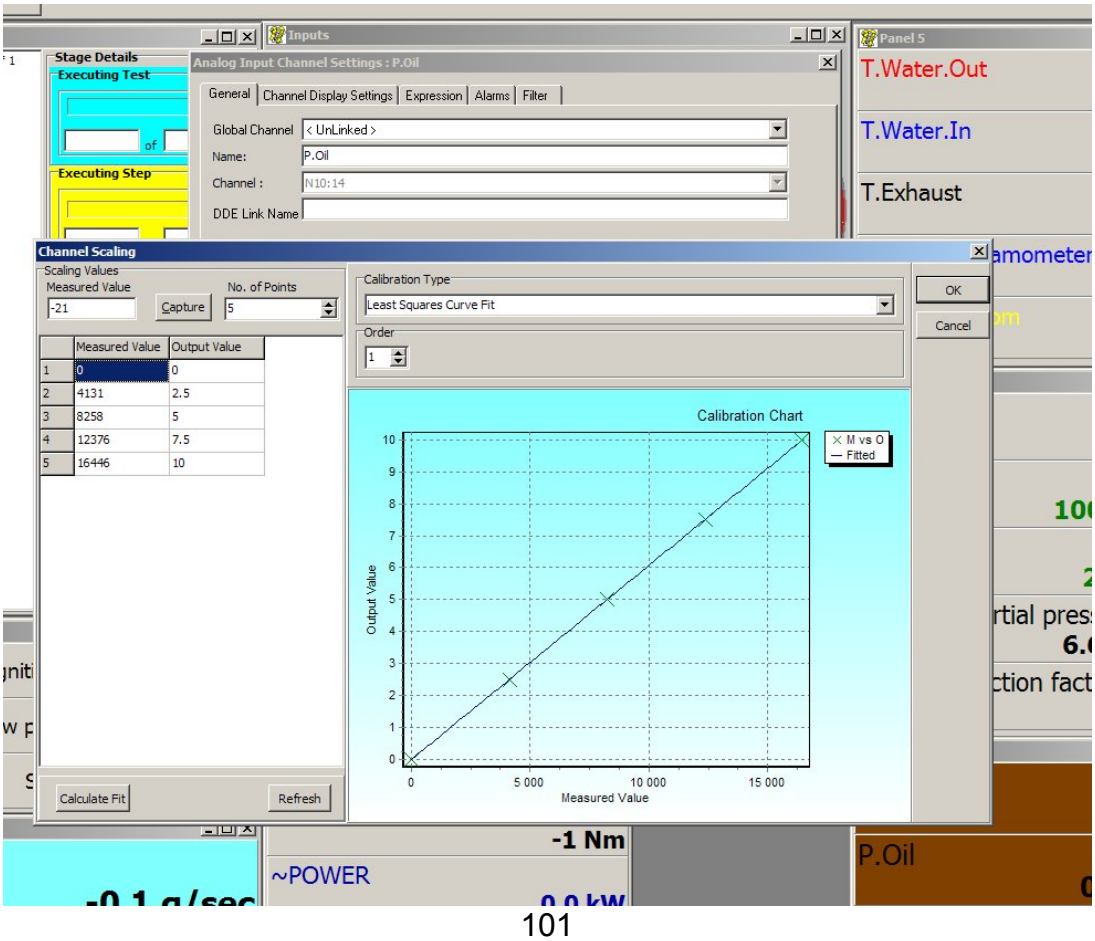
Inputs
Analog Input Channel Settings : P.Oil
General
Channel Display Settings
Expression
Alarms
Filter
Global Channel
< UnLinked >
Name:
P.Oil
Channel :
N10:14
DDE Link Name
Stage Details
Executing Test
Executing Step
Panel 5
T.Water.Out
T.Water.In
T.Exhaust
Channel Scaling
Scaling Values
Measured Value
Capture
No. of Points
Calibration Type
Least Squares Curve Fit
Order
OK
Cancel
Measured Value
Output Value
1 0 0
2 4131 2.5
3 8258 5
4 12376 7.5
5 16446 10
Calculate Fit
Refresh
Calibration Chart
M vs O
Fitted
Output Value
Measured Value
-1 Nm
~POWER
P.Oil

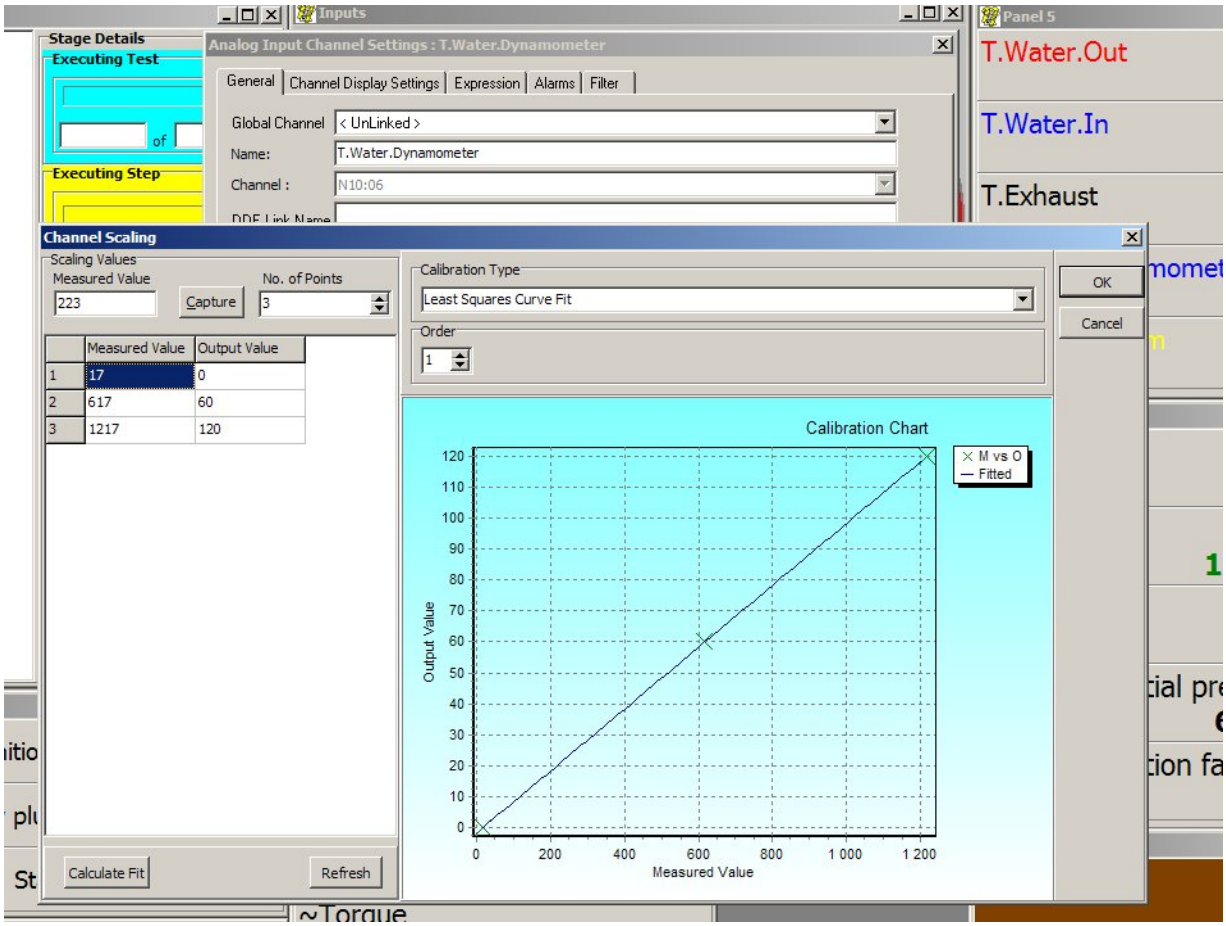
Inputs
Stage Details
Executing Test
of
Executing Step
Analog Input Channel Settings : T.Water.Dynamometer
General
Channel Display Settings
Expression
Alarms
Filter
Global Channel
< UnLinked >
Name:
T.Water.Dynamometer
Channel :
N10:06
Panel 5
T.Water.Out
T.Water.In
T.Exhaust
Channel Scaling
Scaling Values
Measured Value
223
Capture
No. of Points
3
Measured Value
Output Value
1
17
0
2
617
60
3
1217
120
Calculate Fit
Refresh
Calibration Type
Least Squares Curve Fit
Order
1
OK
Cancel
Calibration Chart
M vs O
Fitted
Output Value
Measured Value
0
10
20
30
40
50
60
70
80
90
100
110
120
200
400
600
800
1 000
1 200

Appendix H: IN and OUT ladder logic for the PLC

LAD 3 - OUT --- Total Rungs in File = 11
Injection pump
N14:99
0
O:0
1
Bul.1762
0000
Starter
N14:99
1
O:0
3
Bul.1762
0001
Glow plug
N14:99
2
O:0
2
Bul.1762
0002
Throttle
COP
Copy File
Source #N14:6
Dest #O:1.1
Length 1
0003
Time delay before change to speed mode
SPEED_TIMER
N14:99
3
TON
Timer On Delay
Timer T4:0
Time Base 1.0
Preset 1<
Accum 1<
EN
DN
0004
Time delay before change to torque mode
TORQUE_TIMER
N14:99
3
TON
Timer On Delay
Timer T4:1
Time Base 1.0
Preset 1<
Accum 0<
EN
DN
0005
Change controller to speed mode
SPEED_TIMER/DN
T4:0
DN
O:0
6
Bul.1762
0006
Change controller to torque mode
TORQUE_TIMER/DN
T4:1
DN
O:0
7
Bul.1762
0007
Torque setpoint
N14:99
3
COP
Copy File
Source #N14:1
Dest #O:1.0
Length 1
0008

LAD 3 - OUT --- Total Rungs in File = 11

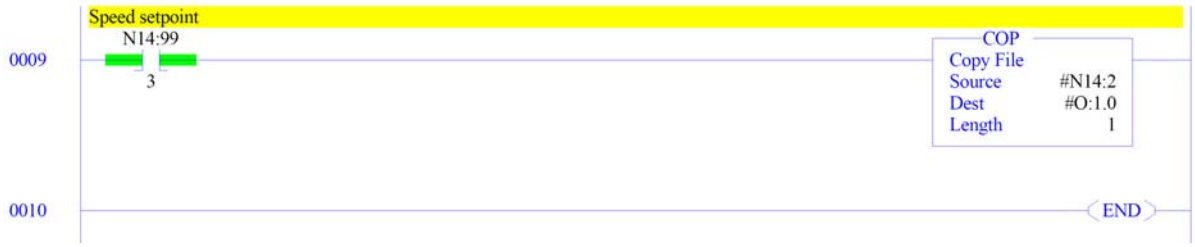

Appendix I: Water temperature controller flow diagram and ladder logic

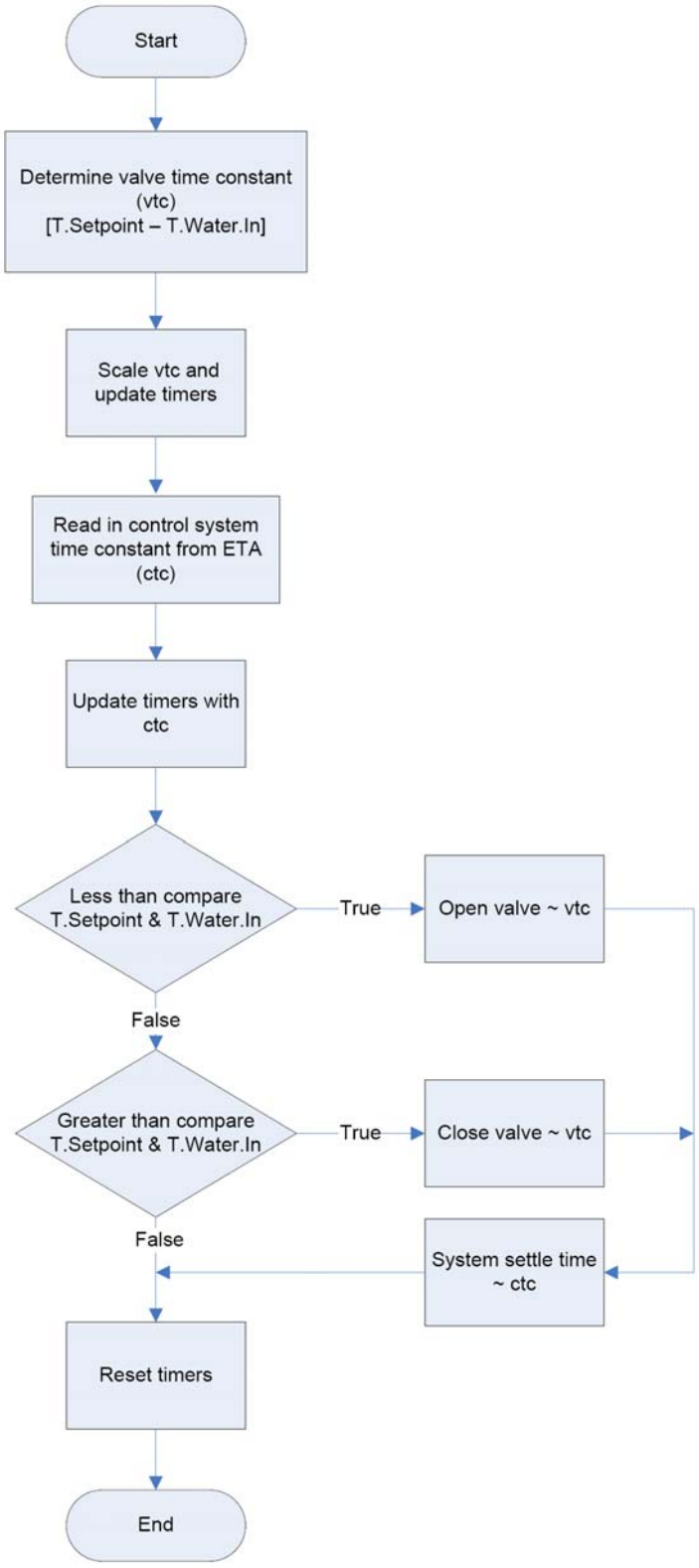

SU.RSS

LAD 3 - OUT --- Total Rungs in File = 22

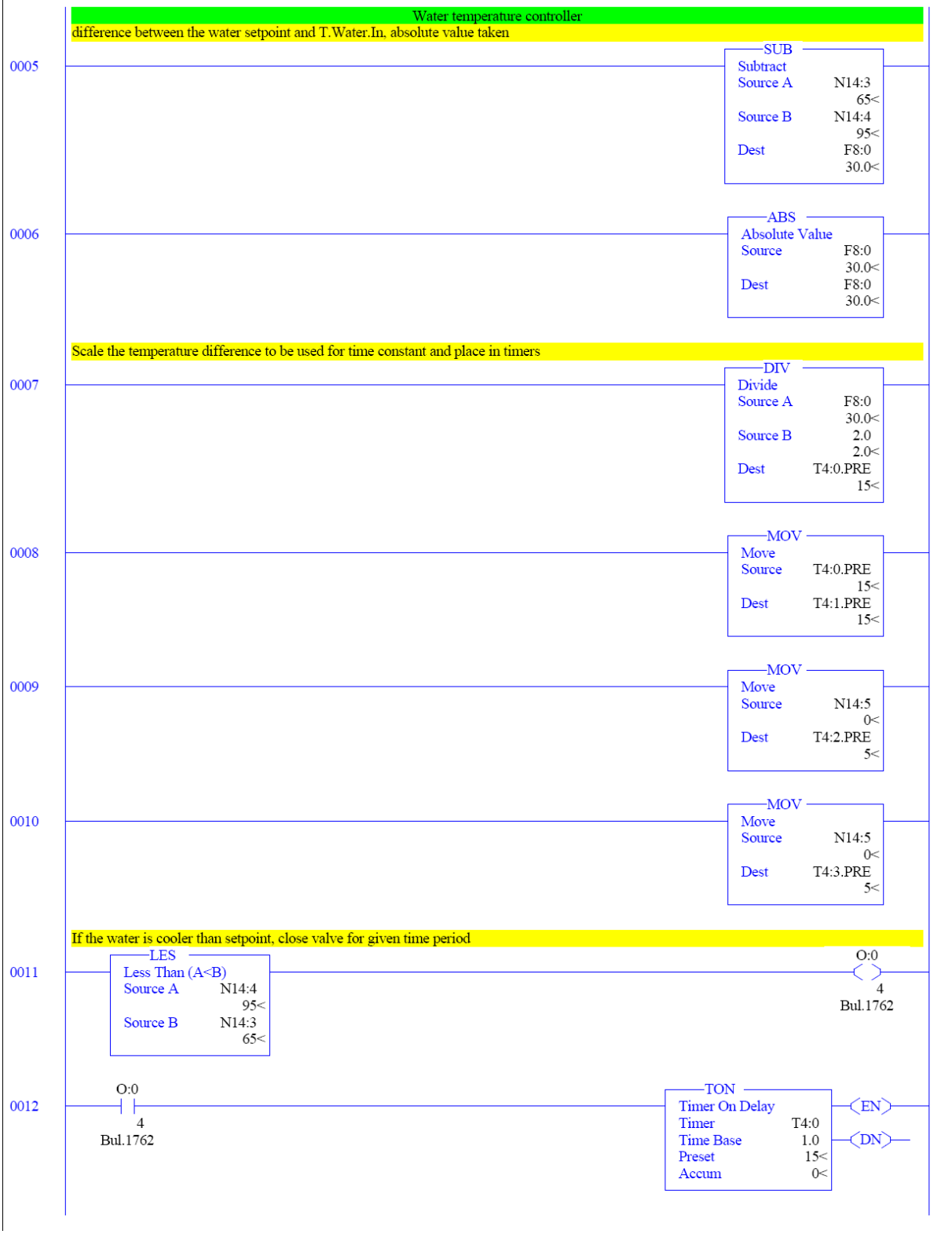

SU.RSS

LAD 3 - OUT --- Total Rungs in File = 22

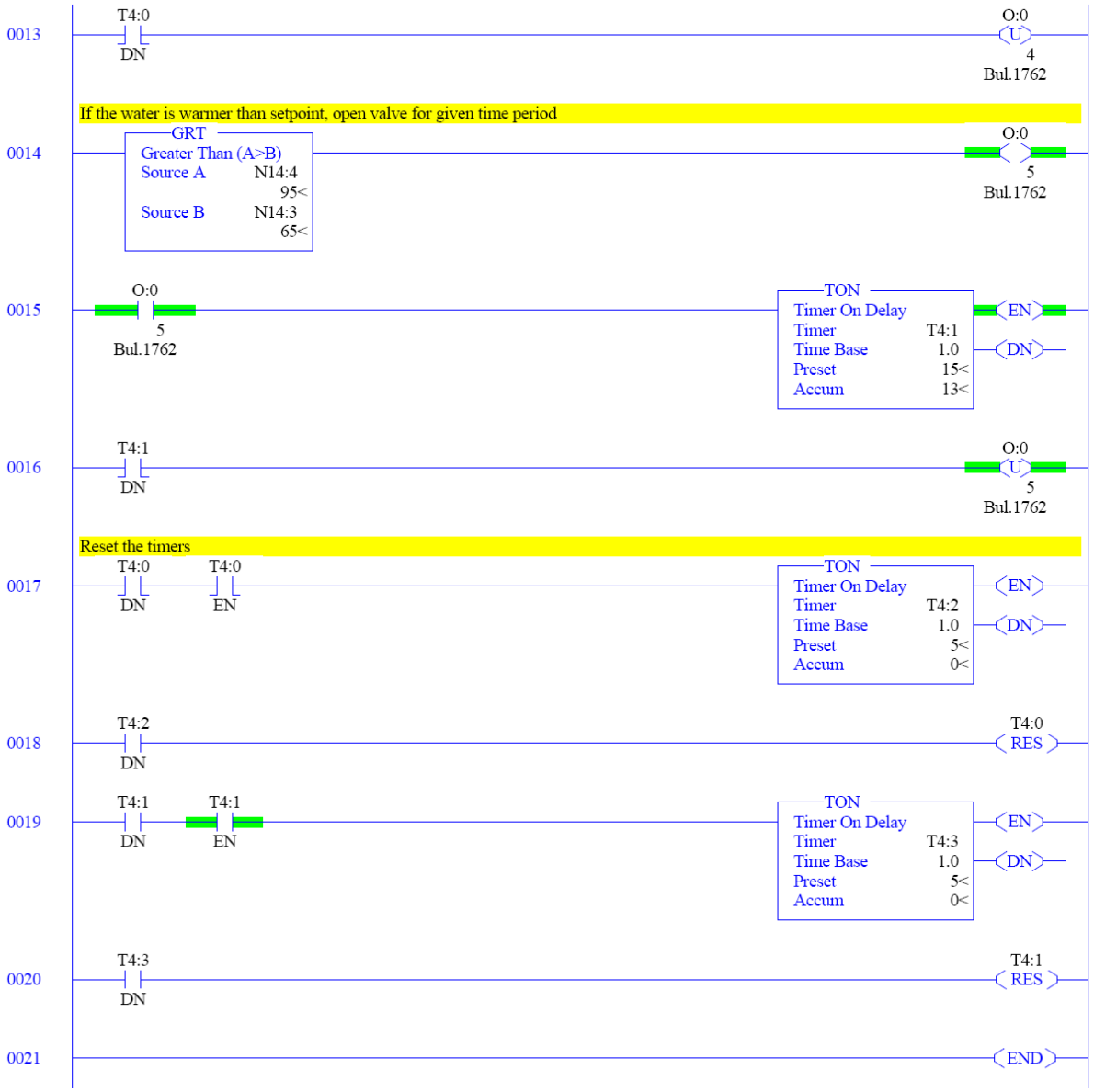

Appendix J: Performance curves; ULSD1, ULSD2, B5, B10, B15 and B50

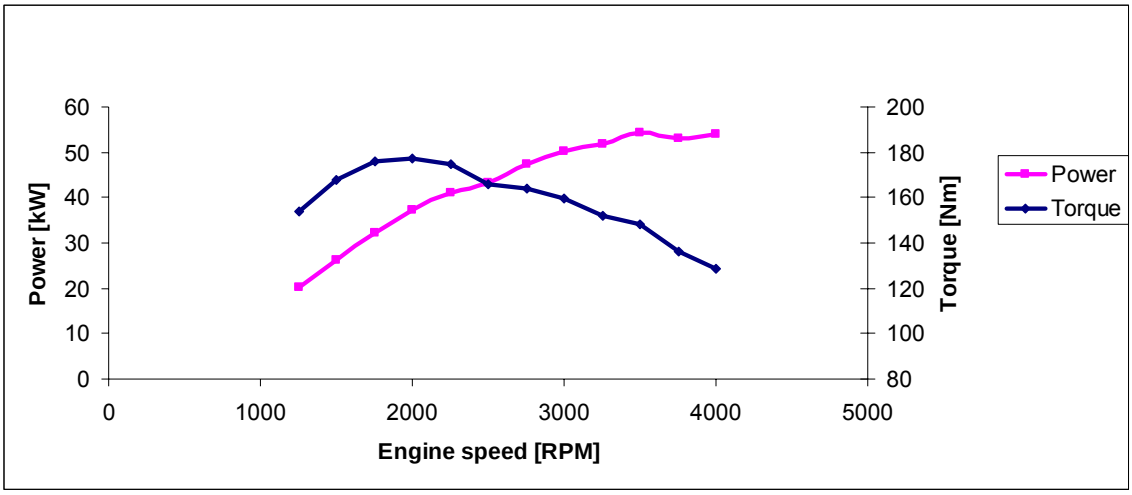

Figure J-1: ULSD1 Performance curve

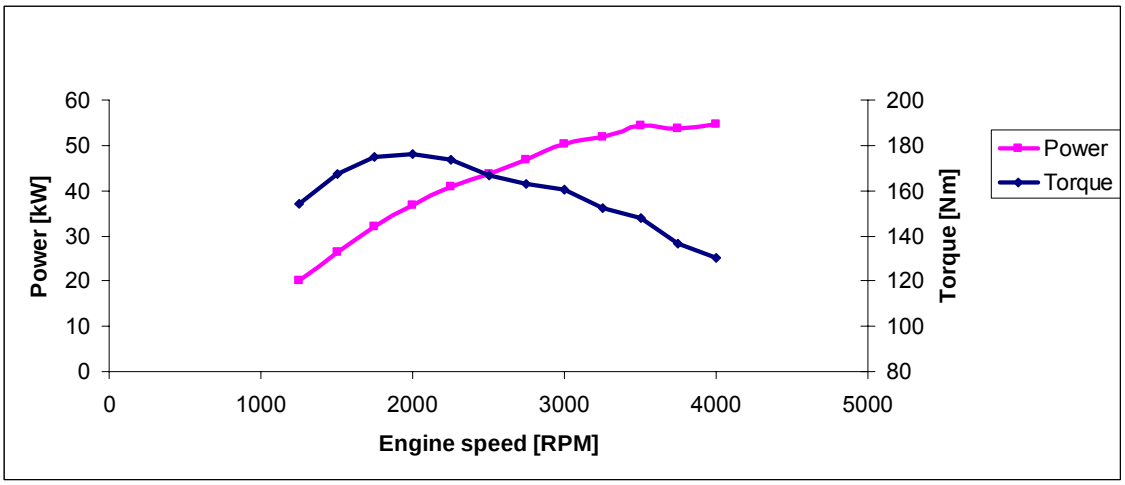

Figure J-2: ULSD2 Performance curve

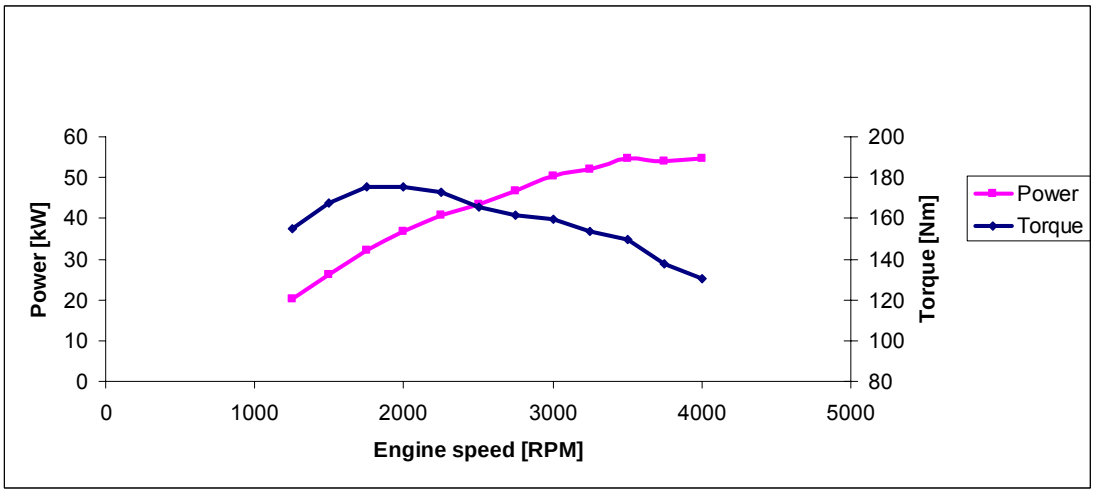

Figure J-3: B5 Performance curve

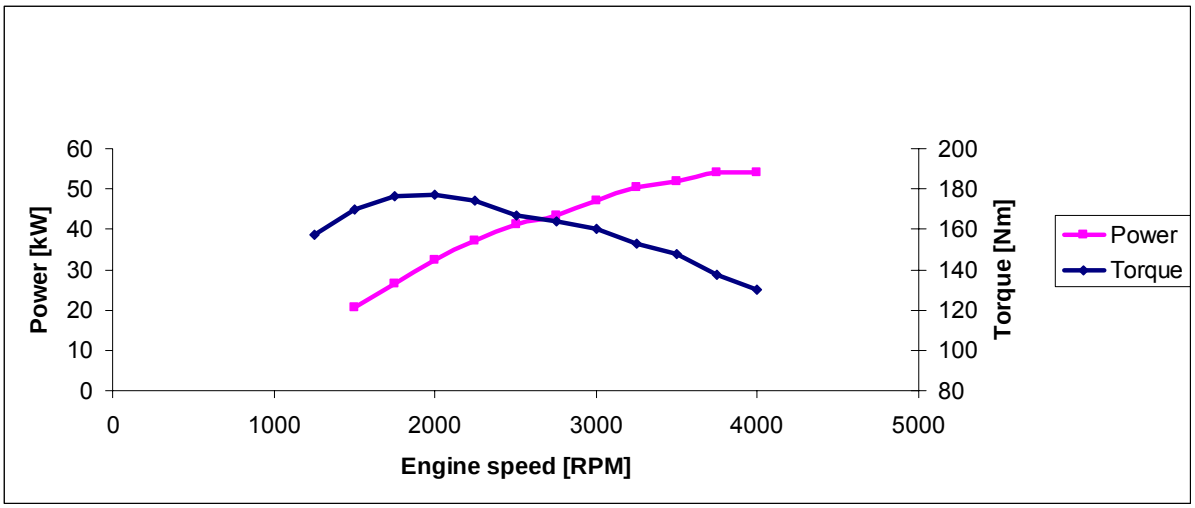

Figure J-4: B10 Performance curve

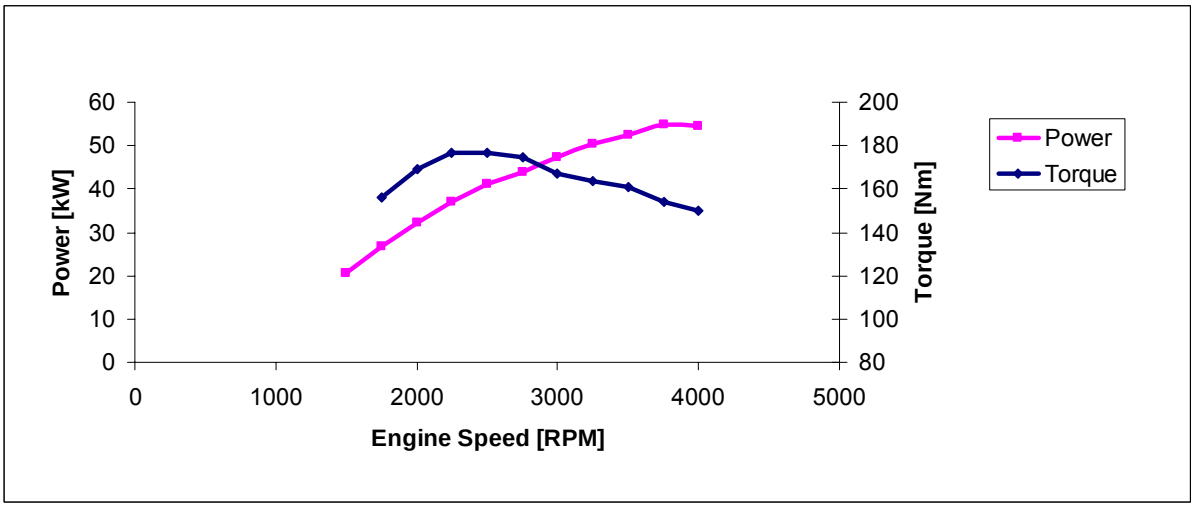

Figure J-5: B15 Performance curve

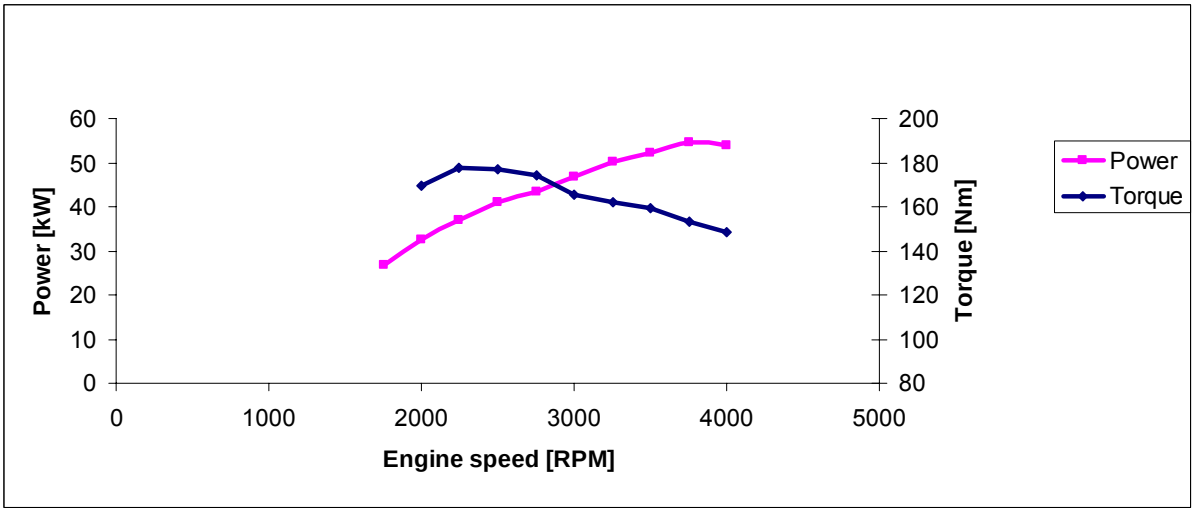

Figure J-6: B50 Performance curve

Appendix K: Wiring diagrams

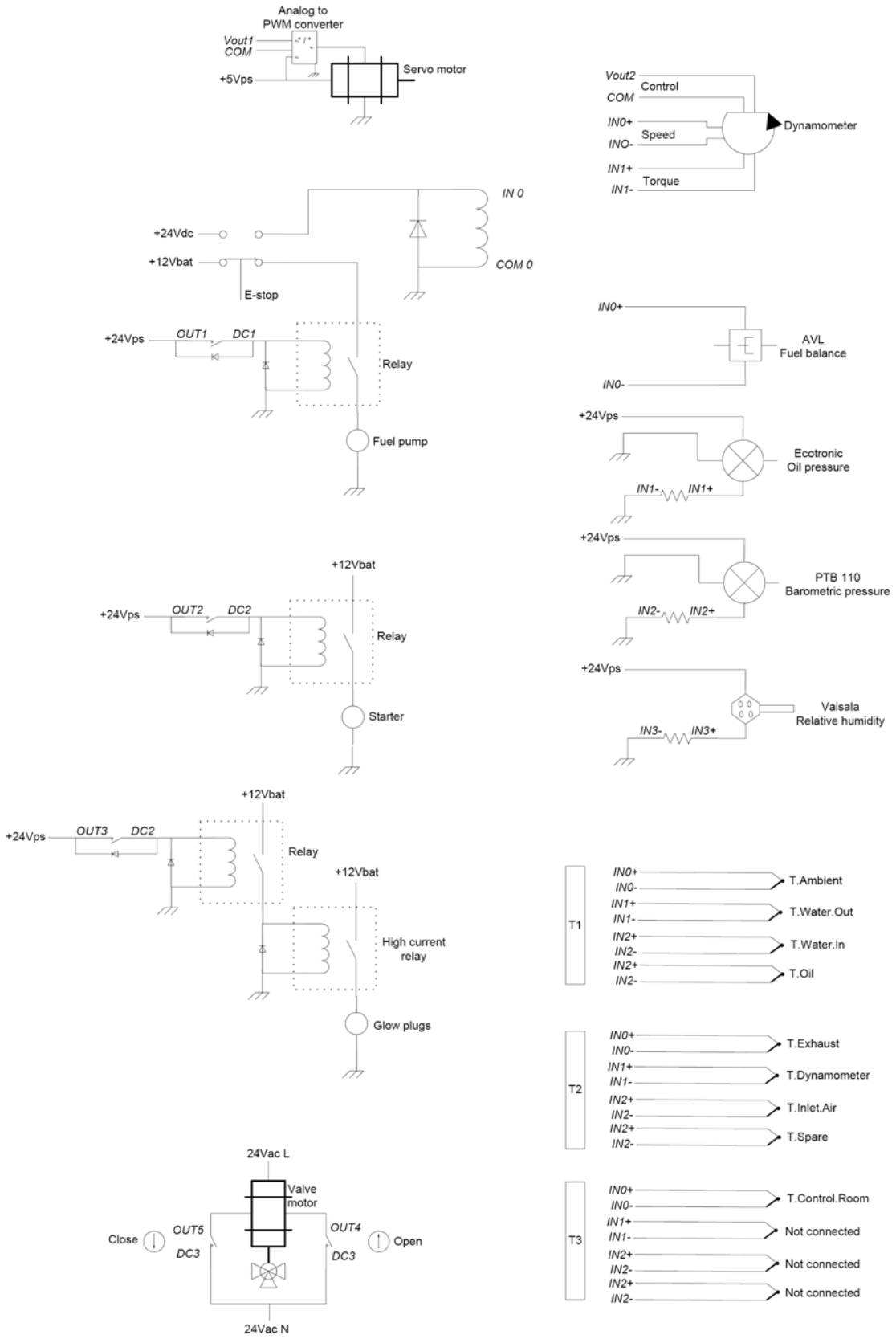

Appendix L: Fuel and water supply schematics with pictures

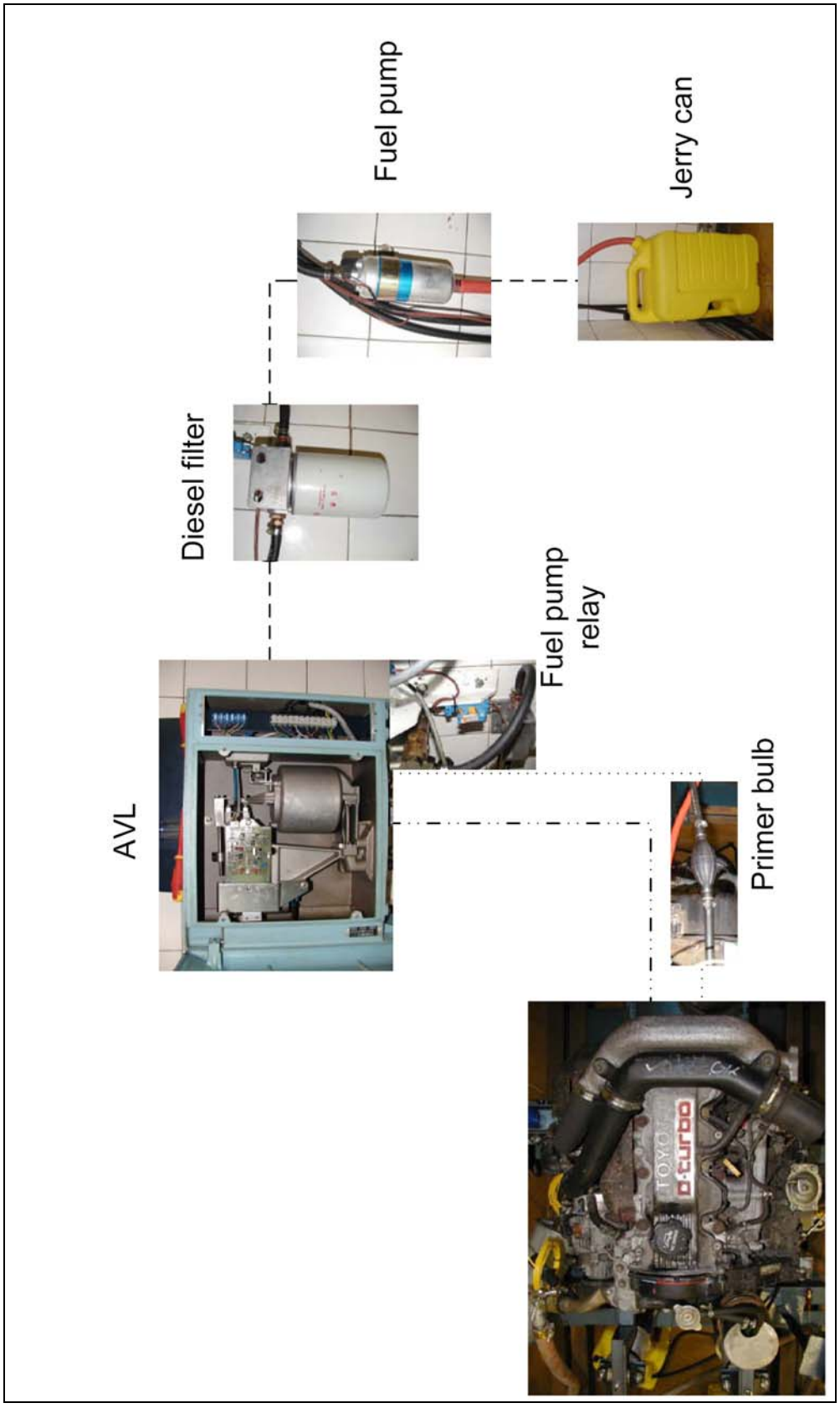

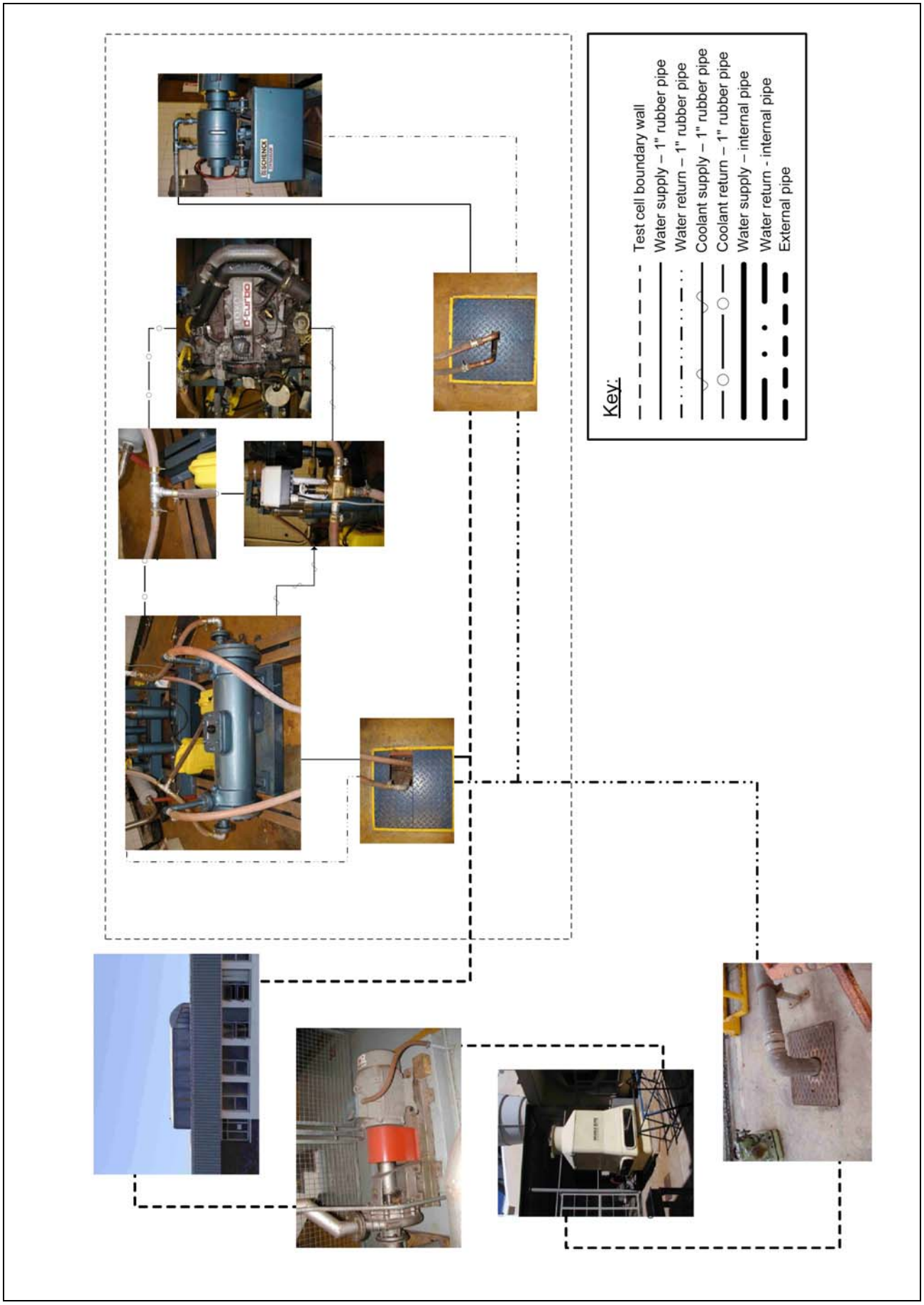
Key:
Test cell boundary wall
Water supply – 1" rubber pipe
Water return – 1" rubber pipe
Coolant supply – 1" rubber pipe
Coolant return – 1" rubber pipe
Water supply – internal pipe
Water return - internal pipe
External pipe

Appendix M: Energy balance calculations

A sharp edged orifice plate was used to determine the flow rate of engine coolant. The equations and methodology for the water flow calculations were obtained from Crowe et al (2001). The plate was installed as in Figure M-1, with D = 55 mm and d = 26 mm. A mercury-water manometer was used to measure the pressure difference of 10 mmHg. The water and air flow rates remained constant for both diesel and biodiesel.

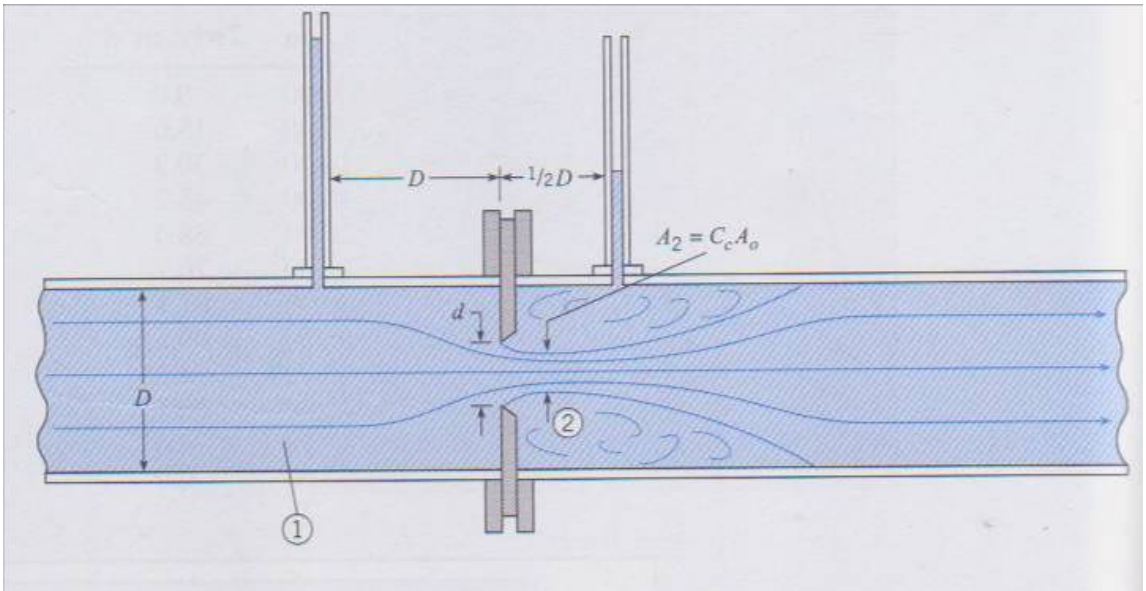

Figure M-1: Standard orifice plate setup as used in to determine the flow rate (Crowe et al., 2001)

Through interpolation of the water tables in Crowe et al (2001), the following water properties were obtained at 65°C to calculate the water flow rate:

- Kinematic viscosity: v = 4.435 X 10^{-6} m^2/s
- Density: ρ = 980 kg/m^3

Initially the piezometric head is calculated:

$$\Delta h = \Delta l(\frac{\rho_{Hg}}{\rho_w} - 1)$$

$$\Delta h = 128.776 \times 10^{-6}\ m\ of\ water$$

With the head the known the parameter (Re_d/K) can be calculated:

$$\frac{d\sqrt{2g\Delta h}}{v} = \frac{0.026\sqrt{2\times 9.81\times 128.778\times 10^{-6}}}{4.435\times 10^{-6}}$$

$$\frac{d\sqrt{2g\Delta h}}{v} = 9.318$$

From Figure M-2 with $\frac{d}{D} = 0.473$ and $\frac{d\sqrt{2g\Delta h}}{v} = 9.318$ the value for flow coefficient (*K*) can be read off:

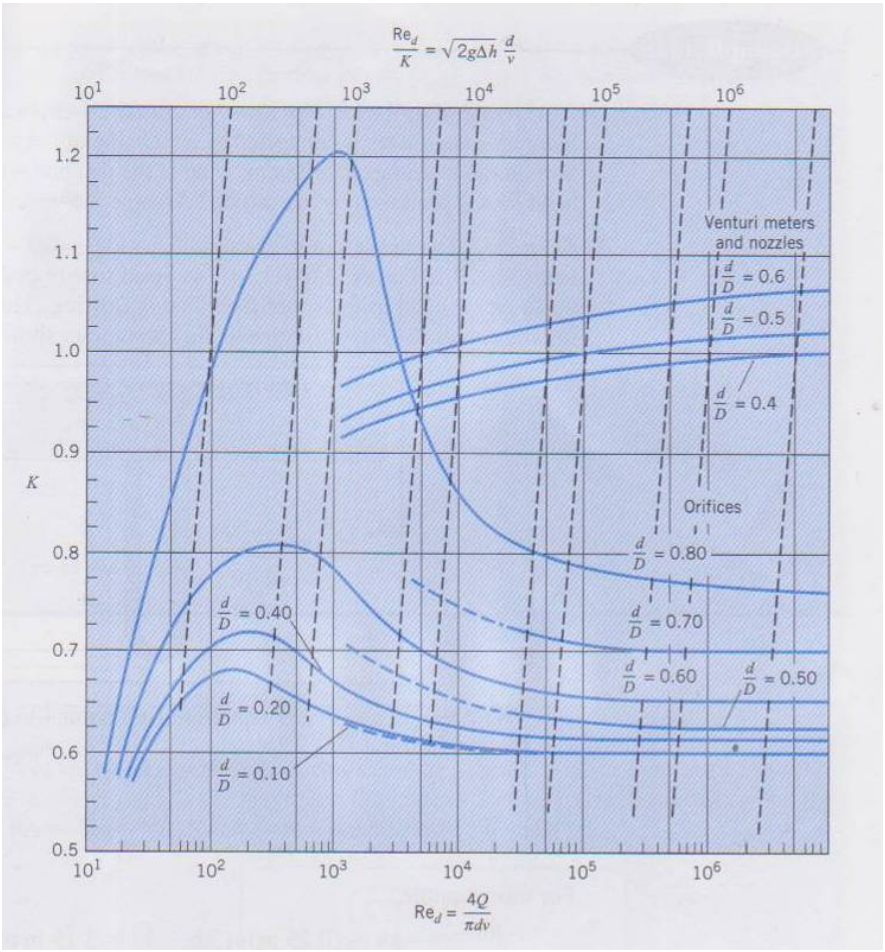

Figure M-2: Flow coefficient K and Re_d/K versus the Reynolds number (Crowe et al., 2001)

K=0.69. Substituting this into the flow equation:

$$Q_w = K\frac{\pi}{4}d^2\sqrt{2g\Delta h}$$

$$Q_w = 576.454\times 10^{-6}\ m^3/s$$

$$or\ Q_w = 564.925\times 10^{-3}\ kg/s$$

The following ambient air conditions and flow rates were recorded during the test using a handheld flow meter held at the engines air inlet and the test cell's ambient sensors:

- Temperature: T = 21.81°C
- Pressure: P = 100.07 kPa
- Air velocity: v = 16 m.s^{-1}
- Pipe diameter: d = 67 mm

The density of air at the given conditions was obtained from Sonntag and Borgnakke (2001).

- Density: ρ = 1.169 kg/m^3

The flow rate of the air into the engine can thus be determined:

$$Q_a = vA$$
$$Q_a = 56.41 \times 10^{-3}\ m^3/s$$
$$or\ Q_a = 65.662 \times 10^{-3}\ kg/s$$

From Martyr and Plint (2007) the following data were obtained:

- Specific heat of air at constant pressure: C_p = 1.004 kJ/kg.K
- Specific heat of water: C_w = 4.18 kJ/kg.K

The steady flow of energy (Martyr and Plint, 2007) was then calculated for diesel using the data in Table 4-2. All values are given in *kW*:

Combustion energy of fuel

$$H_{D1} = \sim m_f C_L \times 10^3$$
$$H_{D1} = 182.81$$

Enthalpy of exhaust gas

$$H_{D2} = (\sim m_f + \sim m_a) C_p T_e$$
$$H_{D2} = 78.166$$

Enthalpy of inlet air

$$H_{D3} = \sim m_a C_p T_a$$
$$H_{D3} = 19.37$$

Heat to cooling water

$$Q_{D1} = \sim m_w C_w (T_{2w} - T_{1w})$$
$$Q_{D1} = 50.05$$

The only remaining unknown is the loss due to convection and radiation. This is determined by drawing up an energy balance and subtracting the flow of energy out of the control volume (taken as the engine block) from the energy flowing into the control volume.

$$H_{D1} = P_s + (H_{D2} - H_{D3}) + Q_{D1} + Q_{D2}$$
$$\therefore Q_{D2} = H_{D1} + H_{D3} - P_s - H_{D2} - Q_{D1}$$
$$Q_{D2} = 24.843$$

The flow of energy out of the control volume was calculated for biodiesel with the data in Table 4-2.

Enthalpy of exhaust gas

$$H_{B2} = (\sim m_f + \sim m_a) C_p T_e$$
$$H_{B2} = 77.308$$

Enthalpy of inlet air

$$H_{B3} = \sim m_a C_p T_a$$
$$H_{B3} = 19.37$$

Heat to cooling water

$$Q_{B1} = \sim m_w C_w (T_{2w} - T_{1w})$$
$$Q_{B1} = 48.117$$

Since the engine and setup conditions were kept the same, it can assume that the convection and radiation losses remained the same. The remaining unknown is the

combustion energy which can now be calculated, and thus the calorific value of the biodiesel obtained.

$$Q_{B2} = Q_{D2}$$

$$H_{B1} = P_s + (H_{B2} - H_{B3}) + Q_{B1} + Q_{D2}$$

$$H_{B1} = 178.348\,kW$$

$$\therefore C_L = \frac{H_{B1}}{\sim m_f \times 10^3}$$

$$\therefore C_L = 38.462\,MJ/kg$$

Appendix N: Raw data tables of test results

	ULSD1			ULSD2			B5.1			B5.2		
RPM	Nm	kW	g/s	Nm	kW	g/s	Nm	kW	g/s	Nm	kW	g/s
4000	128.6423	53.87	11.823	130.5575	54.68991	11.49894	128.6543	53.89788	11.36178	131.6396	55.17144	
3750	136.0242	53.04016	11.25	136.467	53.60928	10.994	137.7991	54.10545	10.99836	137.6776	54.08695	10.96902
3500	148.2856	54.37616	11.0769	148.1427	54.31084	10.79641	148.9298	54.63114	10.84464	149.9668	54.99201	10.84892
3250	151.8043	51.6947	10.08405	152.3444	51.86249	9.853527	153.4045	52.25902	9.922543	153.1423	52.14728	9.922543
3000	159.5948	50.12155	9.6132	160.2548	50.35443	9.054498	160.39	50.40059	9.339612	159.3878	50.13282	9.339612
2750	164.0706	47.25404	8.988056	162.8436	46.90438	8.684957	162.4671	46.78884	8.492674	161.2857	46.43907	8.386301
2500	165.6063	43.33107	7.83	166.4031	43.54398	7.72904	165.6489	43.37251	7.858483	165.4814	43.31193	7.43299
2250	174.4446	41.08539	7.20045	173.3219	40.85058	6.92086	173.3829	40.88066	7.089057	172.3045	40.64045	7.07073
2000	177.3914	37.18119	6.455833	175.8338	36.81458	6.24907	175.6673	36.84026	6.343955	175.6955	36.82069	6.358823
1750	175.7985	32.24131	5.634347	175.136	32.12031	5.414006	175.2039	32.09538	5.522118	175.1631	32.15841	5.523757
1500	167.5355	26.3166	4.77	167.5355	26.3166	4.57	167.1973	26.25974	4.775085	167.8658	26.40135	4.771609

	B10.1			B10.2			B15.1			B15.2		
RPM	Nm	kW	g/s	Nm	kW	g/s	Nm	kW	g/s	Nm	kW	g/s
4000	129.4786	54.26973	11.41343	129.9558	54.43723	11.51498	131.7433	55.19548	11.38571	132.1359	55.40618	11.28802
3750	136.8821	53.78838	11.06119	137.7064	54.10452	11.09304	137.5261	53.98405	11.14248	140.2756	55.06825	10.97373
3500	148.0705	54.30596	10.85133	147.7046	54.15471	10.88918	149.7573	54.93326	10.82413	150.1497	55.05527	10.772
3250	152.9058	52.06228	9.901596	152.3832	51.89066	9.92076	154.0564	52.44078	9.873606	154.1477	52.49366	9.836538
3000	160.547	50.42783	9.36408	159.6487	50.17141	9.456699	160.7341	50.50227	9.365499	161.0129	50.57883	9.263163
2750	164.4895	47.38086	8.826563	162.7751	46.86085	8.888148	164.1091	47.27819	8.857392	163.6825	47.16976	8.498418
2500	167.1659	43.74513	7.787052	165.8918	43.43095	7.835414	167.6145	43.85811	7.831455	166.8037	43.68441	7.733672
2250	174.8867	41.18701	7.075157	173.6199	40.93664	7.098131	174.8524	41.19718	7.059038	174.6502	41.17942	6.971004
2000	177.0904	37.0911	6.347431	176.5763	36.98533	6.417512	176.7898	37.04997	6.351677	177.0804	37.11695	6.292903
1750	177.1429	32.48056	5.540938	175.1743	32.14806	5.557543	176.8343	32.38232	5.509086	175.8857	32.27822	5.45416
1500	170.4506	26.77813	4.785992	168.6252	26.48404	4.643759	170.1741	26.74237	4.761177	168.5057	26.47491	4.728365

	B50.1			B50.2			B100.1			B100.2		
RPM	Nm	kW	g/s	Nm	kW	g/s	Nm	kW	g/s	Nm	kW	g/s
4000	131.8161	55.24149	11.80035	131.6876	55.17992	11.6469	130.2124	54.56375	12.14538	130.2531	54.57881	12.29125
3750	137.5377	54.03638	11.36602	137.2141	53.86469	11.29836	133.7779	52.53115	11.6145	133.428	52.42811	11.75485
3500	148.5128	54.49333	11.13136	148.3793	54.4077	11.09431	147.2166	54.00554	11.30347	144.7602	53.07595	11.53771
3250	153.2509	52.16224	10.21532	152.854	52.02915	10.15401	151.7246	51.61608	10.32593	148.4389	50.53363	10.51677
3000	159.3996	50.10908	9.54985	159.7625	50.20442	9.546277	159.2761	50.01726	10.21168	156.4806	49.17354	9.86067
2750	162.1625	46.70459	9.121001	162.4315	46.81171	8.753251	162.0976	46.66562	9.47282	158.9337	45.79201	9.494443
2500	165.1843	43.25816	8.067757	166.1961	43.50199	7.960225	165.9006	43.45218	8.261636	164.1069	42.93068	8.3196
2250	173.3575	40.89501	7.307405	174.8578	41.21576	7.284045	173.6067	40.92013	7.564073	172.423	40.64555	7.623586
2000	176.0867	36.89014	6.549853	178.0807	37.2997	6.545799	175.6543	36.77072	6.762116	175.3421	36.70057	6.846579
1750	176.8036	32.40812	5.738145	177.8452	32.61193	5.700599	177.4547	32.51808	5.948481	176.3262	32.34879	6.034776
1500	169.2038	26.61259	4.888119	170.3221	26.76292	4.870167	169.7664	26.6905	5.062933	168.3658	26.45559	5.137161

Appendix O: Press articles

Die Burger: 10 September 2007

US kan navorsing oor biobrandstof versnel

VW skenk 2 enjins aan ingenieursfakulteit

Carin Smith, Kaapstad

Die pas van navorsing oor biobrandstof aan die Universiteit van Stellenbosch (US) se fakulteit van ingenieurswese kan nou versnel danksy 'n skenking deur Volkswagen Suid-Afrika.

Dié motorvervaardiger het onlangs twee VW 1.9 TDi-enjins aan die fakulteit se biodiesel-toetssentrum geskenk. Daardeur word dit die eerste toetssentrum in Suid-Afrika wat op biodiesel fokus.

Benewens navorsing oor die ontleding en produksie van biodiesel, word dit ook op enjins getoets. Die belang daarvan is dat dié plaasvervanger vir petroleumdiesel se verbrandingsproses skoner is.

Aanvanklik gaan slegs afvalplantoliemengsels op die Volkswagen-enjins getoets word, maar later word beplan om ook na sonneblom-, kanola-, olyf- en soja-olie uit te brei.

Een van die mikpunte van die nuwe toetssentrum is om die universiteit se intellektuele eiendom ten opsigte van biobrandstowwe te vestig en 'n evalueringsproses vir biodiesel te ontwikkel. Op die oorhandigingseremonie van die enjins het prof. Leon Lorenzen, mede-dekaan van die fakulteit, gesê benewens die toetssentrum beskik die fakulteit ook oor 'n proseslaboratorium en word gehoop om in die toekoms ook 'n analitiese fasiliteit te kan inrig.

Die behoefte aan 'n toetssentrum op die kampus het ontstaan nadat 'n onderafdeling van die departement van meganiese ingenieurswese, wat toetse op enjins gedoen het, tot so 'n mate gegroei het dat 'n aparte maatskappy – Stellenbosch Automotive Engines (CAE) – gestig is wat in 2005 na Atlantis verskuif het.

Kort daarna is die universiteit se sentrum vir hernieubare en volhoubare energiestudies tot stand gebring en onlangs ook die leerstoel in biobrandstowwe aan die ingenieursfakulteit. Albei het die behoefte aan 'n toetssentrum ter plaatse vergroot.

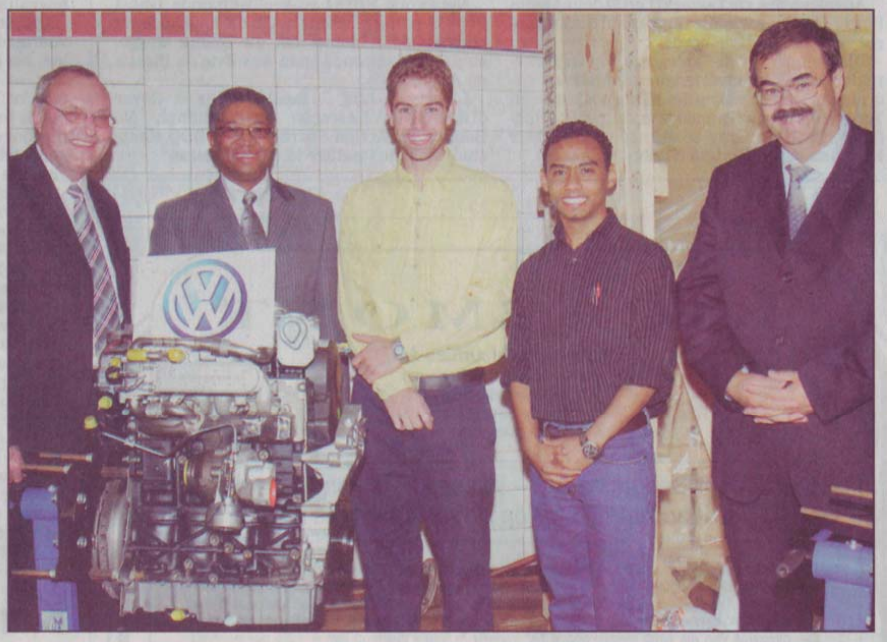

By die oorhandiging van die enjins was van links: mnr. Brian Smith (Volkswagen), prof. Russel Botman (rektor en visekanselier van die Universiteit van Stellenbosch), mnre. Duncan Palmer en Gaermo Griffin (nagraadse ingenieurstudente) en dr. Hans-Georg Kaiser (hoof van produk-ingenieurswese en -beplanning by Volkswagen SA).

Foto: ANTON JORDAAN/SSFD

Volgens Lorenzen was die grootste behoefte dié aan enjins waarop die toetse uitgevoer kon word. Hy het ook beklemtoon die doel van die toetssentrum is nie kommersieel van aard nie, maar is vir navorsingsdoeleindes.

Volgens mnr. Brian Smith, Volkswagen SA se direkteur: mensehulpbronne, is Volkswagen die grootste Duitse belegger in Suid-Afrika en het die maatskappy al 'n hele paar oud-studente van die Universiteit van Stellenbosch in diens geneem.

"Ingenieurswese bied 'n fantastiese loopbaan in Suid-Afrika en die uitdaging is om ingenieurs – veral uit voorheen benadeelde groepe – se vaardighede daarin te verhoog," het hy gesê.

Volgens hom werk Volkswagen in Duitsland nou saam met die tegniese instellings van hoër onderwys in daardie land en sou dit raadsaam wees om dié model ook in Suid-Afrika na te volg – iets wat Volkswagen SA graag wil doen.

"Daar is nie baie rolmodelle in voorheen benadeelde gemeenskappe wat ingenieurswese betref nie. Baie mense dink nog 'n ingenieur verrig laevlak-fabriekswerk," het Smith gesê.

Prof. Russel Botman, rektor van die US, het hierop gesê die universiteit se visie is om vennote te vind om hoop in Suid-Afrika te skep. Volgens hom is 'n gevoel van wanhoop een van die groot redes waarom swart mense nie die ingenieursrigting inslaan nie.

"Ons moet sorg dat mense hul potensiaal aan hul ambisie kan koppel. Volhoubaarheid is nog een van ons oogmerke. Daarom is vennootskappe soos dié met Volkswagen van kardinale belang," het Botman gesê.

Volgens hom is dit belangrik om armoede hok te slaan en terselfdertyd 'n gesonde omgewing vir die nageslag na te laat. Navorsing oor biobrandstowwe is dus 'n gebied waarop die universiteit 'n beduidende bydrae kan lewer.

Engineering News: 21-27 September 2007

AUTOMOTIVE & SYNFUELS

FUTURE FUEL

German carmaker says biofuels push is shaping its future fuel strategy

Jade Davenport
Correspondent

GERMAN automotive manufacturer Volkswagen (VW) says the much-anticipated availability of synthetic biofuels is a fundamental element of the company's future-orientated fuel strategy.

Against this background, VW is currently working in collaboration with Shell and Choren Industries – the first enterprise to produce renewable synthetic fuels – focusing on the development of both synfuels and sunfuels.

In an interview, VW South Africa's **Paul Williams** explains that, because the advance of technology in South Africa is modelled on that of the German parent company, VWSA is increasing its participation within the local biofuels research field.

The most recent evidence of this is the contribution of two VW 1.9 TDI diesel engines to the biofuel test facility at the Faculty of Engineering at Stellenbosch University for research purposes.

As the university has been designated a hub for renewable and sustainable energy by the South African National Energy Research Institute (Saneri) and has been awarded a chair in biofuels research by the Department of Science and Technology (DST), this biodiesel test facility is the first of its kind in the country.

According to the deputy dean of Stellenbosch University's faculty of engineering and head of the biofuel testing facility, Professor **Leon Lorenzen**, the research done at this test facility includes analysis and production of biodiesel as well as engine testing. "Initially, mainly waste vegetable oil blends will be analysed, optimised and produced on pilot plant scale and tested in the new VW engines," says Lorenzen.

"This research will eventually be extended to other sources of biodiesel, such as sunflower, canola, olive and soya."

The ultimate objectives of the new test facility are to evaluate the quality of biodiesel and bioethanol production in South Africa and to augment the university's intellectual property in the field of biofuels.

Williams tells *Engineering News* that the reason why VW is particularly concerned with the research process of biofuels is the lack of legislation or development strategy in place concerning renewable energy in South Africa.

"From a local perspective, there is no strategy yet regarding how biofuels will be developed in the country and, as a result, VW is concerned with the research processes at this early stage so that we may be at the forefront of technology when biofuels legislation is implemented," states Williams.

A strategy for the development of a local biofuels industry has been much anticipated; however, earlier this year, the DST announced that government will not be able to develop biofuels legislation this year owing to the fact that consultations are still taking place between the various industry stakeholders.

Ingligting: 4 October 2007

Biodiesel toetsfasiliteit twee VW diesel-enjins ryker

Matie universiteitsvoertuie wat aangedryf word deur afvalolie wat gebruik is om aartappelskyfies in die Neelsie Studentesentrum te maak? Nie onmoontlik nie! Navorsing oor biobrandstof gaan nou versnel word met die oorhandiging van twee VW 1.9 TDi-cliesel-enjins wat Volkswagen Suid-Afrika aan Universiteit Stellenbosch geskenk het. Die enjins sal in die Fakulteit Ingenieurswese se biodiesel-toetsfasiliteit benut word. Dit sal die eerste gefokusde biodiesel-toetsfasiliteit in Suid-Afrika wees.

Deesdae raak biodiesel 'n toenemend aantreklike plaasvervanger vir petroleum diesel. Die verbradingsproses daarvan is skoner, en omdat dit hemieubaar is, plaas dit nie 'n groot las op minerale oliereserwes nie. Verdere navorsing is nodig om die produksieproses van biodiesel uitvoerbaar, volhoubaar en tinansieel lewensvatbaar te maak en om die werkverrigting van enjins wat hierdie tipe brandstof gebruik, te meet.

Navorsing in die Fakulteit Ingenieurswese se biodiesel-toetsfasiliteit sluit die analise en produksie van biodiesel in sowel as die toets van enjins wat hierdie biodiesel gebruik.

Aanvanklik sal hoofsaaklik afval plantoliemengsels ontleed, optimeer en genoeg vir navorsingsdoeleindes vervaardig word om die werkverrigting van die enjins te evalueer. Die navorsing sal later kanola, olyf en soja. Gaermo Griffin (MSclng-student) sat die chemiese ontleding en vervaardiging van die biodiesel behartig en Duncan Palmer, nog 'n MSclng-student, sal die werkverrigting van die diesel-enjins evalueer. Prof Leon Lorenzen van Proses-ingenieurswese en Johan van der Spuy van Meganiese en Megatroniese Ingenieurswese is ondeskeidelik hul studieleiers.

By die oorhandiging van die diese/-enjins was van links: Dr Hans-Georg Kaiser (hoof van produkingenieurswese en produkbeplanning, VWSA), Brian Smith (direldeur: menslike hulpbronne, VWSA) en prof Russel Botman (reldor, US), Duncan Palmer (MSc/ng-student), prof Leon Lorenzen (mededekaan: navorsing) Johan van der Spuy (Meganiese en Megatroniese Ingenieurswese) en prof Arnold Schoonwinkel (dekaan: Ingenieurswese).

Die doel van die evaluering van biobrandstowwe in die nuwe toetsfasiliteit is om 'n evaluasieproses ten opsigte van biodiesel in Suid-Afrika daar te stel en die US se intellektuele eiendom rakende biobrandstowwe op te bou.

"Die nuwe toetsfasiliteit gaan vir voorgraadse en nagraadse opleiding sowel as navorsing gebruik word en nie vir kommersiele doeleindes ingespan word nie, n sa prof Leon Lorenzen, mededekaan navorsing.

Die US is reeds baie aktief op die gebied van hemieubare energienavorsing. 'n Sentrum vir Hemubare en Volhoubare Energiestudie het verlede jaar tot stand gekom en vanjaar is 'n leerstoel gevestig wat op biobrand stowwe en ander skoon altematiewe brandstowwe fokus. Die skenking van die diesel-enjins sat dus meer dryfkrag aan US se navorsingspoging op die gebied van energienavorsing verleen.

The Matie: 23 September 2007

DIESELKRAG MScIng-studente, Duncan Palmer (links) en Gaermo Griffin, by een van die Volkswagen dieselenjins wat die US se biodiesel-toetsfasiliteit onlangs ryker geword het. Foto: ANTON JORDAAN (SSFD)

Nuwe dryfkrag vir biodieselnavorsing

CYRIL PRINSLOO

DIE UNIVERSITEIT se biodiesel-toetsfasiliteit het onlangs twee dieselenjins van Volkswagen Suid-Afrika (VWSA) ontvang. Dié toetsfasiliteit is die eerste van sy soort in die land.

Op 30 Augustus 2007 het prof Russel Botman, rektor en visekanselier, die twee 1.9ℓ TDi-enjins van mnr Brian Smith, Direkteur: Menslike Hulpbronne van VWSA, ontvang. Dit is dieselfde enjins as wat in die nuwe Golf 5 GTI gebruik word.

Die biodiesel projek vorm deel van die universiteit se Sentrum vir Hernubare en Volhoubare Energiestudie. Die hoof doel van die projek is die vervaardiging en toetsing van biodiesel. Daar word ook beoog om die universiteit se intellektuele eiendom rakende biobrandstowwe uit te brei.

Twee MScIng-studente gaan aan die projek werk. Terwyl Gearmo Griffin die vervaardiging van die biodiesel gaan behartig, sal Duncan Palmer die produk op die enjins toets. Toekomstige nagraadse studente sal op hulle werk kan voortbou.

Biodiesel gebruik plantolies in plaas van minerale olies. Die voordeel hiervan is dat biodiesel nie minerale oliereserwes uitput nie. Dit brand ook baie skoner as petroleum diesel en is dus beter vir die omgewing en vir jou motor. Volgens Palmer is die hoofklem van biodiesel egter nie op omgewingsvriendelikheid nie, maar eerder om afnemende oliereserwes teen te werk.

Verder sê Palmer behoort biodiesel nie die kragvermoë van die enjins te beïnvloed nie. Die brandstofverbruik is egter hoër en dit is duurder om te vervaardig.

Die fakulteit het reeds 'n proseslaboratorium en 'n enjintoetsfasiliteit waar die biodiesel onderskeidelik vervaardig en getoets gaan word. 'n Analitiese laboratorium word egter nog benodig sodat die eienskappe van verskillende biodieselprodukte vergelyk kan word.

Alumni Ingligting: November 2007

VW skenk 2 diesel-enjins aan biodieseltoetsfasiliteit

Volkswagen SA het twee 1.9 TDi-diesel-enjins aan die Fakulteit Ingenieurswese se biodiesel-toetsfasiliteit geskenk. Dit sal die eerste gefokusde biodiesel-toetsfasiliteit in Suid-Afrika wees.

Navorsing in die Fakulteit Ingenieurswese se biodiesel-toetsfasiliteit sluit die analise en produksie van biodiesel in sowel as die toets van enjins wat hierdie biodiesel gebruik. Aanvanklik sal hoofsaaklik afval plantoliemengsels ontleed, optimeer en genoeg vir navorsingsdoeleindes vervaardig word om die werkverrigting van die enjins te evalueer. Die doel van die evaluering is om 'n evaluasie-proses ten opsigte van biodiesel in Suid-Afrika daar te stel en die US se intellektuele eiendom rakende biobrandstowwe op te bou.

Van links Brian Smith (direkteur: Menslike Hulpbronne, VWSA), prof Russel Botman (rektor, US), Duncan Palmer en Gaermo Griffin (nagraadse Matie ingenieurstudente) en dr Hans-Georg Kaiser (hoof van produkingenieurswese en produkbeplanning, VWSA).

Navorsing sal later uitgebrei word na ander bronne van biodiesel, soos sonneblom, kanola, olyf en soja. Gaermo Griffin (MScIng-student) sal die chemiese ontleding en vervaardiging van die biodiesel behartig en Duncan Palmer, nog 'n MScIng-student, sal die werkverrigting van die diesel-enjins evalueer. Prof Leon Lorenzen van Prosesingenieurswese en Johan van der Spuy van Meganiese en Megatroniese Ingenieurswese is ondeskeidelik hul studieleiers.

"Die nuwe toetsfasiliteit gaan vir voorgraadse en nagraadse opleiding sowel as navorsing gebruik word en nie vir kommersiële doeleindes ingespan word nie," sê prof Leon Lorenzen, mededekaan navorsing.

Die US is reeds baie aktief op die gebied van hernieubare energienavorsing. 'n Sentrum vir Hernubare en Volhoubare Energiestudie het verlede jaar tot stand gekom en vanjaar is 'n leerstoel gevestig wat op biobrandstowwe en ander skoon alternatiewe brandstowwe fokus. Die skenking van die diesel-enjins sal dus meer dryfkrag aan US se navorsingspoging op die gebied van energienavorsing verleen.

www.sun.ac.za/index.asp: 8 August 2007

Boost for biodiesel research. Volkswagen South Africa donated two VW 1.9 TDi-engines to the University on Thursday. At the handing over ceremony Mr Brian Smith, Director: Human Resources of VW SA handed over the engines to the Rector, Prof Russel Botman. Matie students Messrs Duncan Palmer (left) and Gaermo Griffin, will use the engines in the bidiesel testing facility in the Faculty of Engineering (article to follow). (photo: Anton Jordaan)

SACHIe Research and Development conference: 26 June 2007

1st prize won for best poster

The development of a biofuels evaluation laboratory (Production and Engine Testing) with emphasis on biodiesel

D Palmer, G Griffin, L Lorenzen, J van der Spuy*

Department of Process Engineering, University of Stellenbosch, Private Bag X 1, Matieland, 7602

*Department of Mechanical and Megatronic Engineering, University of Stellenbosch, Private Bag X1, Matieland, 7602

[duncs@sun.ac.za ; gaermo@sun.ac.za]

Background

Biodiesel is fast becoming an attractive substitute of petroleum diesel due to cleaner combustion and the depleting mineral oil reserves.

Further research is needed to make the production process feasible, sustainable and financially viable and to measure the performance characteristics of engines using the fuel.

Objectives

- The research is aimed to produce a process unit capable of handling different feedstock with varying quality whilst still maintaining the maximum yield.
- Yield properties should be similar to that of mineral diesel and meet the legal requirements and standards for South Africa.

Research Development

Labscale Production

At this level, research is done to define and optimize the process variables to:

- Accelerate the batch production process,
- Increase the yield and
- Minimise energy input into the system.

Industrial Production

At this level, research is done to define and optimize the process variables to:

- Accelerate the batch production process,
- Increase the yield and
- Minimise energy input into the system.

The outcomes of this stage is then used to:

- Improve the efficiency an existing batch production process using waste vegetable oil

Chemical Analysis

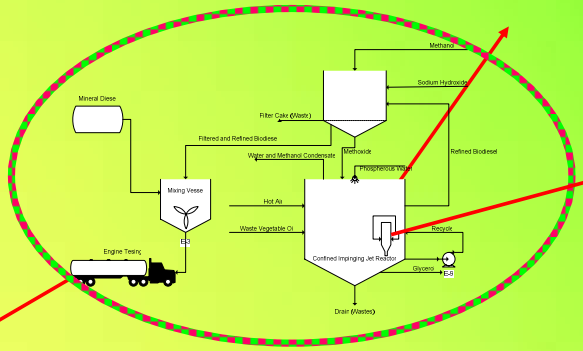

Mixing Modelling

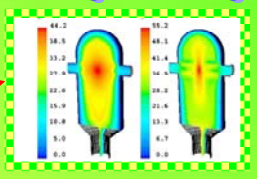

Engine Testing

Engine testing will be done in a biofuel specific facility. Biodiesel combustion properties, such as energy content and emissions data will be obtained.

The biodiesel results will then be used to refine an optimise the manufacturing process. On road tests may also be performed using a fleet vehicle.

Prospects

Who can say what the future holds?

References: [1] Gavi, E., 2007. CFD modelling and scale-up of confined impinging jet reactors. Chemical Engineering Science, pp 2228-2241.

Appendix P: BTF Corporate logo